J. Print Media Technol. Res. – Vol. 11 No. 4 (2022)
December 2022

4-2022

ISSN 2414-6250 (Online)
UDC 665

Journal of Print and Media Technology Research

Scientific contributions

Professional communication

ISSN 2414-6250

Editor-in-Chief
Gorazd Golob (Ljubljana)

Published by iarigai
www.iarigai.org

The International Association of Research Organizations for the Information, Media and Graphic Arts Industries

J. Print Media Technol. Res. – Vol. 11 No. 4 (2022)
December 2022
ISSN 2414-6250 (Online)
A print version is available on-demand
ISSN 2223-8905 (Print)

Journal of Print and Media Technology Research

A PEER-REVIEWED QUARTERLY

PUBLISHED BY

The International Association of Research Organizations
for the Information, Media and Graphic Arts Industries
Magdalenenstrasse 2, D-64288 Darmstadt, Germany
http://www.iarigai.org
journal@iarigai.org

EDITORIAL BOARD

EDITOR-IN-CHIEF

Gorazd Golob (Ljubljana, Slovenia)

EDITORS

Anne Blayo (Grenoble, France)
Timothy C. Claypole (Swansea, UK)
Edgar Dörsam (Darmstadt, Germany)
Nils Enlund (Helsinki, Finland)
Patrick Arthur C. Gane (Helsinki, Finland)
Mladen Lovreček (Zagreb, Croatia)
Scott Williams (Rochester, USA)

ASSOCIATE EDITOR

Markéta Držková (Pardubice, Czech Republic)

SCIENTIFIC ADVISORY BOARD

Ian Baitz (Toronto, Canada)
Irena Bates (Zagreb, Croatia)
Davide Deganello (Swansea, UK)
Jay Amrish Desai (Nagpur, India)
Elena Fedorovskaya (Rochester, USA)
Diana Gregor Svetec (Ljubljana, Slovenia)
Jon Yngve Hardeberg (Gjøvik, Norway)
Gunter Hübner (Stuttgart, Germany)
Dejana Javoršek (Ljubljana, Slovenia)
Igor Karlovits (Ljubljana, Slovenia)
Helmut Kipphan (Schwetzingen, Germany)
Yuri Kuznetsov (St. Petersburg, Russian Federation)
Magnus Lestelius (Karlstad, Sweden)
Igor Majnarić (Zagreb, Croatia)
Thomas Mejtoft (Umeå, Sweden)
Erzsébet Novotny (Budapest, Hungary)
Alexandra Pekarovicova (Michigan, USA)
Anastasios Politis (Athens, Greece)
Cathy Ridgway (Egerkingen, Switzerland)
Wolfgang Schmidt (Munich, Germany)
Tomáš Syrový (Pardubice, Czech Republic)
Li Yang (Stockholm, Sweden)
Werner Zapka (Stockholm, Sweden)

iarigai CC BY-NC 4.0

A mission statement

To meet the need for a high quality scientific publishing platform in its field, the International Association of Research Organizations for the Information, Media and Graphic Arts Industries is publishing a quarterly peer-reviewed research journal.

The journal is fostering multidisciplinary research and scholarly discussion on scientific and technical issues in the field of graphic arts and media communication, thereby advancing scientific research, knowledge creation, and industry development. Its aim is to be the leading international scientific journal in the field, offering publishing opportunities and serving as a forum for knowledge exchange between all those interested in contributing to or learning from research in this field.

By regularly publishing peer-reviewed, high quality research articles, position papers, surveys, and case studies as well as review articles and topical communications, the journal is promoting original research, international collaboration, and the exchange of ideas and know-how. It also provides a multidisciplinary discussion on research issues within the field and on the effects of new scientific and technical developments on society, industry, and the individual. Thus, it intends to serve the entire research community as well as the global graphic arts and media industry.

The journal is covering fundamental and applied aspects of at least, but not limited to, the following topics:

Printing technology and related processes

- Conventional and special printing
- Packaging
- Fuel cells and other printed functionality
- Printing on biomaterials
- Textile and fabric printing
- Printed decorations
- Materials science
- Process control

Premedia technology and processes

- Colour reproduction and colour management
- Image and reproduction quality
- Image carriers (physical and virtual)
- Workflow and management

Emerging media and future trends

- Media industry developments
- Developing media communications value systems
- Online and mobile media development
- Cross-media publishing

Social impact

- Media in a sustainable society
- Environmental issues and sustainability
- Consumer perception and media use
- Social trends and their impact on media

Submissions to the Journal

Submissions are invited at any time and, if meeting the criteria for publication, will be rapidly submitted to peer-review and carefully evaluated, selected and edited. Once accepted and edited, the papers will be published as soon as possible.

✉ Contact the Editorial office: journal@iarigai.org

Journal of Print and Media Technology Research

4-2022

December 2022

J. Print Media Technol. Res. – Vol. 11 No. 4 (2022), 233–304

The information published in this journal is obtained from sources believed to be reliable and the sole responsibility on the contents of the published papers lies with their authors. The publishers can accept no legal liability for the contents of the papers, nor for any information contained therein, nor for conclusions drawn by any party from it.

Journal of Print and Media Technology Research is listed in:

Emerging Sources Citation Index

Scopus

DOAJ – Directory of Open Access Journals

Index Copernicus International

NSD – Norwegian Register for Scientific Journals, Series and Publishers

Printed in Slovenia

Contents

A letter from the Editor

Gorazd Golob
Editor-in-Chief
E-mail: gorazd.golob@jpmtr.org
journal@iarigai.org

The last issue of the Journal in 2022 is in front of you. It consists of four papers covering wide scientific and research fields of our interdisciplinary periodical. Unfortunately, also the Errata section is added, after a few years. The attentive reader, a student, found an error in the published paper where the graphs with tone reproduction curves of prints were in the shape characteristic for the visual presentation of the tone value increase. Thanks to the student and his professor, the member of the Scientific Advisory Board, the wrong graphs, unfortunately, overlooked by the authors, the reviewers, and the editors, are now corrected.

The first paper of the current Journal issue deals with the study of the effectiveness and utilization of equipment in the newspaper printing house. The second paper shows the new approach to image contrast enhancement based on the bat algorithm. The added value of both original scientific papers is in the use of modern tools based on adapted algorithms and computer programs used in the research process and presentation of the results.

The third, research paper deals with markers for image registration in digital photography for correction and compensations of camera tilt for improved registration of stacked images in digital photography.

The fourth article gives the results of the research on the naturalness perception of 2.5D prints of wood images, based on the assessments and descriptions of the printed samples given by observers.

The Topicalities, edited by Markéta Držková (marketa.drzkova@jpmtr.org), begins with the news on research activities conducted by CIE and Fogra, including an overview of newly published standards by CIE, on colorimetry, color management systems and measurement of light.

The books from the Bookshelf are dedicated to additive manufacturing / 3D printing, print history, design, textile printing, and some other fields. An interesting news for experts in flexography is a publication of a new edition of FIRST 7.0, the well-known overview of specifications and tolerances in this field.

Three doctoral theses are also "on the Bookshelf". Olga Taran defended her thesis at the University of Geneva. The topic of her research was artificial intelligence and machine learning applied to the security of printed graphical codes used in anti-counterfeiting technologies. The second presented thesis was defended by Davit Gigilashvili at the Norwegian University of Science and Technology, Gjøvik. His research was oriented on the appearance of translucent objects and their perception and assessment by human observers. Liwen Zhang defended his thesis at the University of New South Wales, Sydney. With his research, he contributed to the development of reversible-deactivation radical polymerization and its application in 3D printing.

An overview of the events is a bit short but the good news is the presence of "live" symposiums and conferences. Some events are dedicated mainly to printing challenges, research, and technology; however, similar topics are included and covered also by the events that are primarily dedicated to imaging, photonics, computer graphics, and similar fields.

The tough year, impacted by the pandemic, war, economic, energy, and other crises, is behind us, and I am convinced there are some moments and events to forget for many of us. However, the new year is in front of us. I would like to express my good wishes and success to all colleagues, members of the editorial team, readers of the Journal, researchers, and supporters of our activities. The call for papers is constantly open, and I would appreciate your contributions as authors, reviewers, or members of the editorial team.

Ljubljana, December 2022

Errata

The following corrections are to be made:
J. Print Media Technol. Res. Vol. 10 No. 2 (2022), paper JPMTR-2119, pp. 99–118.

Page 111: The Figures 16 and 17 are incorrect and should be replaced with the correct figures below.

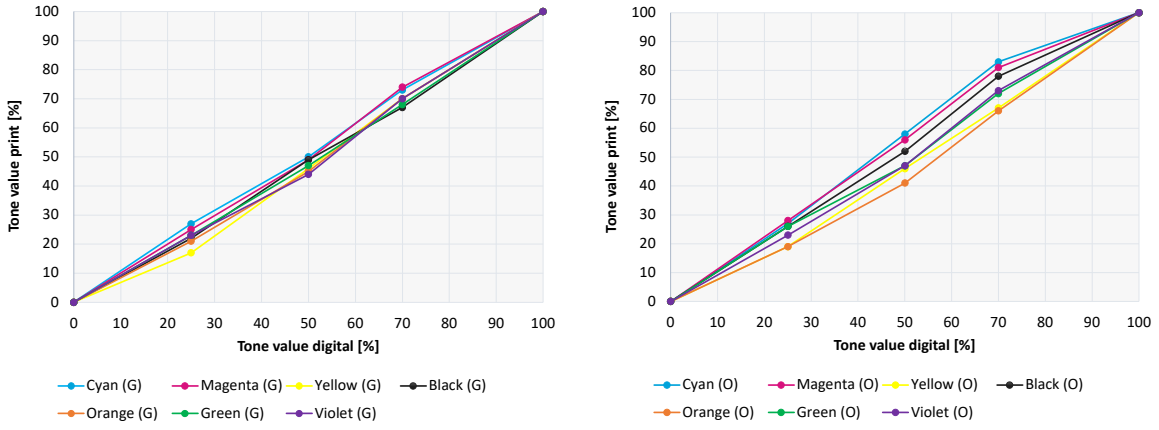

a) *b)*

Figure 16: The SCTV tone value curves from the Esko verification run for the gear (a) and operator (b) side; variation in tonal values is noticeable between the two sides

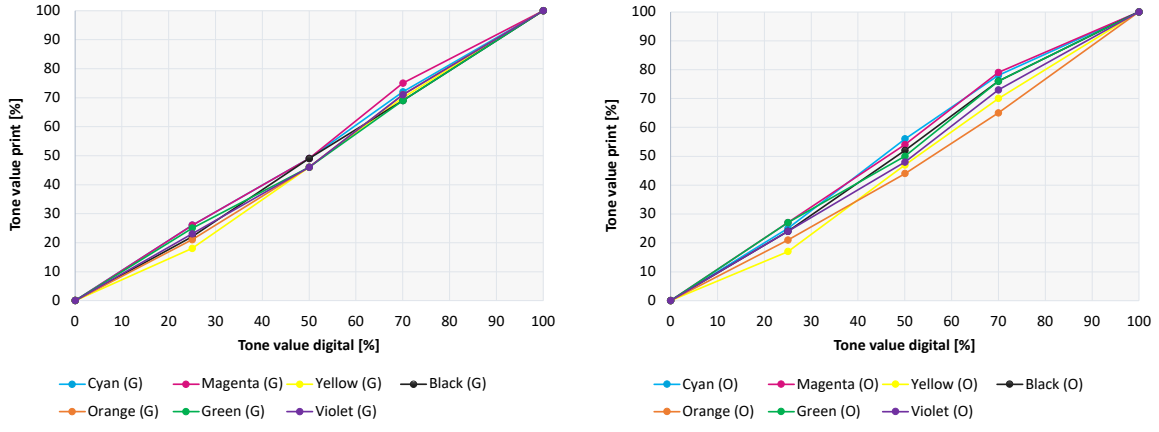

a) *b)*

Figure 17: The SCTV tone value curves from the GMG verification run for the gear (a) and operator (b) side; variation in tonal values is noticeable between the two sides

Pages 116 and 117 (Appendix): the Figures A1 to A6 are incorrect and should be replaced with the correct figures below.

Detailed SCTV curves from the Esko characterization press runs

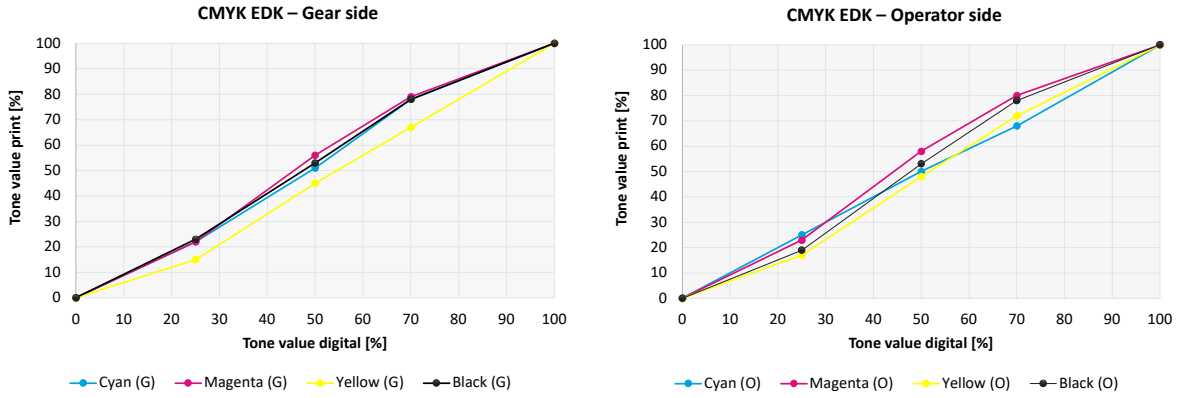

Figure A1: CMYK EDK tone value curves

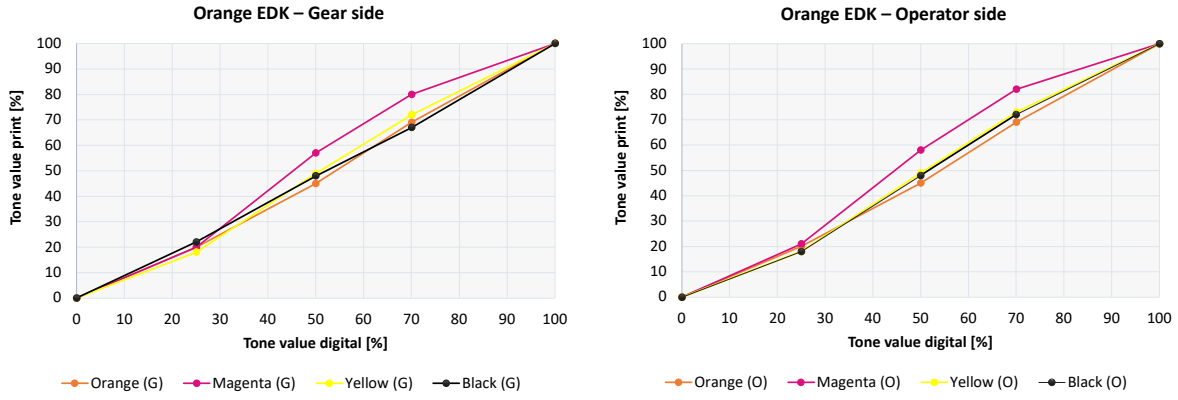

Figure A2: OMYK (Orange) EDK target tone value curves

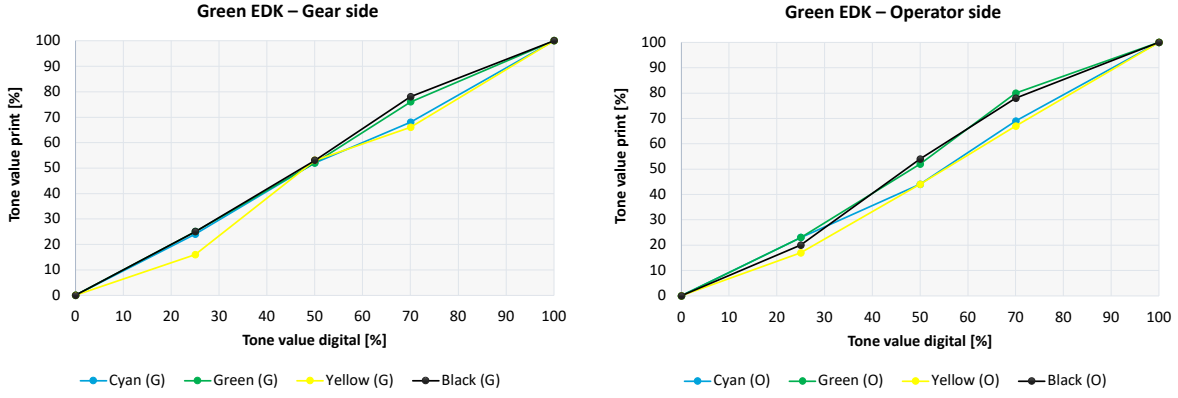

Figure A3: CGYK (Green) EDK target tone value curves

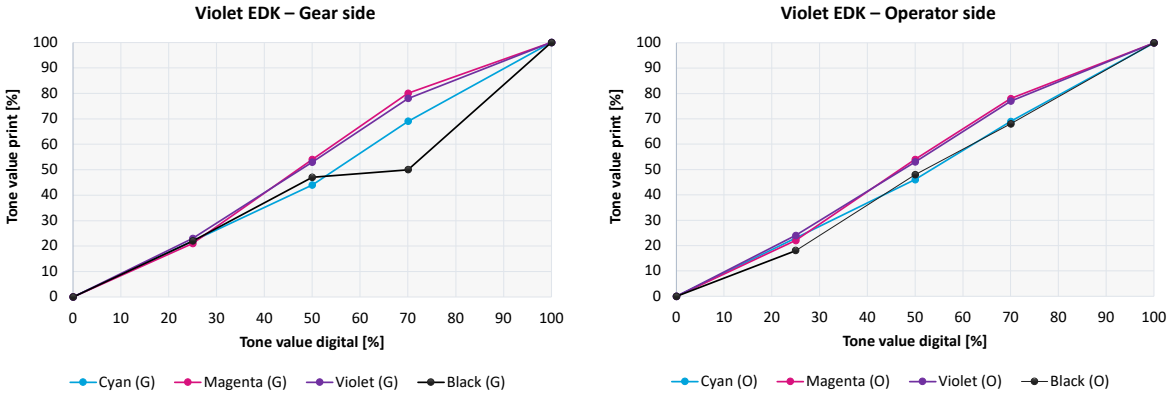

Figure A4: CMVK (Violet) EDK target tone value curves

Detailed SCTV curves from the GMG characterization press run

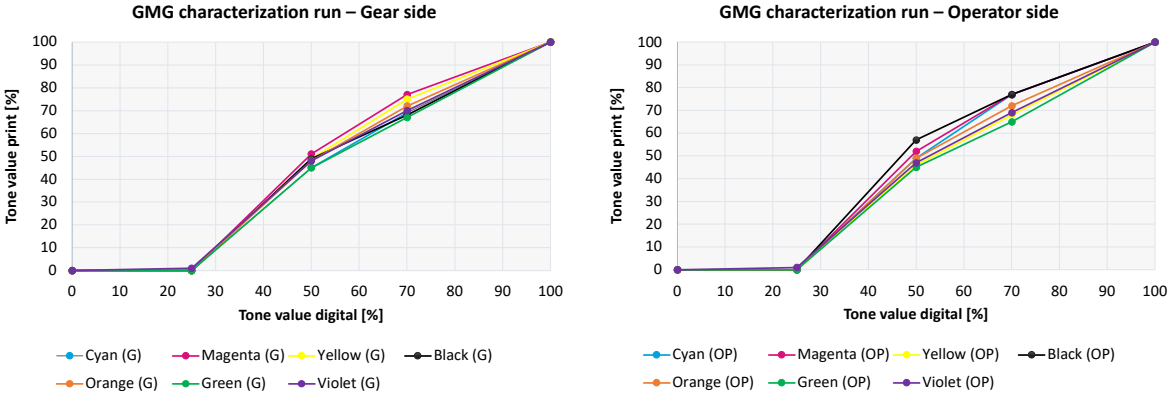

Figure A5: Tone value curves for the GMG characterization run

Detailed SCTV curves from the ISC chart characterization run

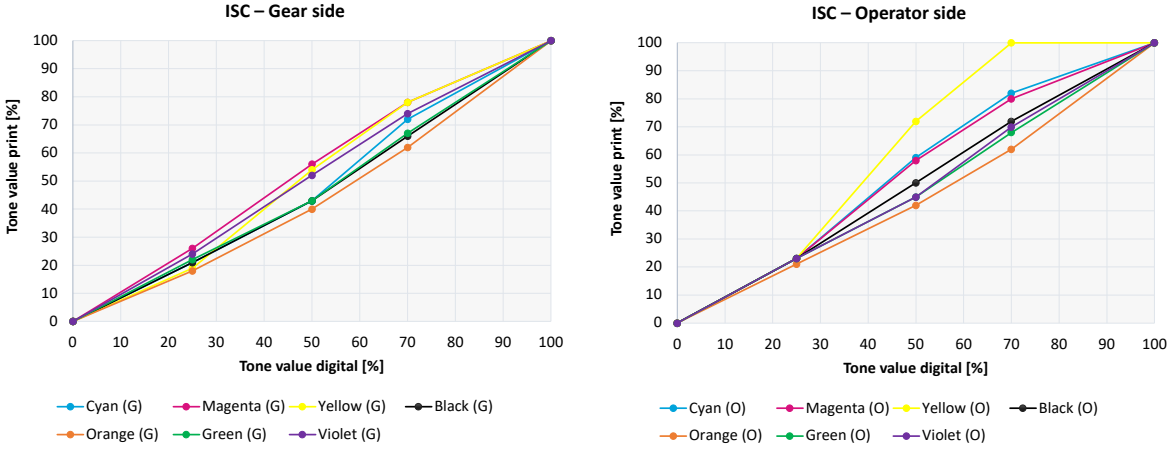

Figure A6: Tone value curves for the ISC characterization run

JPMTR-2220
DOI 10.14622/JPMTR-2220
UDC 681.6-021.4-027.3

Original scientific paper | 169
Received: 2022-09-22
Accepted: 2022-11-08

Assessment of effectiveness and utilization of printing machines

Avijit Kar and Arun Kiran Pal

Department of Printing Engineering, Jadavpur University,
Salt Lake Campus, B-73-80, Plot No. 8, Salt Lake Bypass,
LB Block, Sector III, Bidhannagar, Kolkata – 700106, West Bengal, India

avijitk.print.rs@jadavpuruniversity.in
arun.pal@jadavpuruniversity.in

Abstract

Maintenance has become increasingly important in the production planning and management strategies of some companies. Overall equipment effectiveness is widely used for performance indicator in manufacturing industries around the world. Print productions are also not apart from problems related to the effectiveness of the machines/equipment caused by the six big losses like breakdown losses, setup and adjustment losses, idle and minor stoppage losses, reduced speed losses, process defect losses and reduced yield losses. This can be seen with the frequency of failures that occurs in the machines because of several types of downtime so that the production target is not achieved. Total productive maintenance is the best method that can be used to improve the productivity and efficiency of the plant productions by using the machine effectively. Print production largely depends on the reliability, availability and maintainability of sophisticated printing machines. Aim of the present study is to determine quantitatively overall effectiveness and utilization of some printing equipment. The results of the effectiveness of web-offset printing machine and other ancillary equipment like computer-to-plate (CTP) machines and exposure unit are found to be below 'world standard' value of 85 %. The cause of low effectiveness value was due to poor performance and availability of the machines. Equipment utilization is also needed for the evaluation of printing equipment necessity, appropriateness and efficiency of the usage in print production. The proposed methodology may be able to increase the amount of working printing equipment by implementing proper maintenance planning. A significant increment of OEE (2.93 %) for web-offset printing machine is observed after implementation of proposed maintenance planning. The methodology is also validated by failure probability and reliability of the machines.

Keywords: overall equipment effectiveness (OEE), availability ratio, performance ratio, quality ratio, overall equipment losses (OEL)

1. Introduction

In manufacturing industry, production decisions and its maintenance actions are taken on the basis of daily production output, production speed, production losses, etc., to reach the maximum level of client's satisfaction. The number of failures, downtime associated with breakdown, make ready time, and loss of production are the major problem in print production house.

A common issue in modern printing press is to maintain the availability and reliability of machine. If effective management of printing equipment maintenance is applied then overall effectiveness of equipment can be increased. Overall equipment effectiveness (OEE) is a way to measure the efficiency of any costly equipment as it is the key performance indicator for implementation of total productive maintenance (TPM) philosophy. The primary stages of assessing OEE are implemented by measurement of availability loss, performance loss and quality loss.

Total effective equipment performance (TEEP) is a performance metric that takes account for both effectiveness in terms of equipment losses and utilization in terms of schedule losses. The workflow management of press is also concerned with the utilizations of printing machines, particularly with the reasons for optimizing utilization and reducing losses due to inefficient utilization. The target is the highest utilization of costly equipment for the productivity improvement and best possible return of the facilities.

Based on the existing problems on printing machines a proposed methodology has been suggested by conducting an in-depth analysis of variation of availability and utilization so that proper maintenance planning can be achieved.

2. Literature review

The theory behind TPM and OEE methodology started from 19th century. The idea of implementation of TPM is to increase the efficiency of a system or process or plant production by increasing the value of OEE metrics based on availability of a machine, performance efficiency of the process and rate of quality product (Nakajima, 1988). The purpose of TPM implementation is to increase the production equipment effectiveness, which is typically measured by the OEE to encourage the customers and merchants for investment and other important decisions (Mileham, et al., 1997). In this competitive production and process industry, managements are striving to improve customer's satisfaction and minimize production costs. Generally, production costs are reduced by the increment of the meantime between failures rate of the production equipment and minimizing maintenance costs of the equipment (Ramayah, Jantan and Hassan, 2002). But reduction of maintenance costs is not the solution as it may lead to ineffectiveness of the production equipment with time. If a company has an OEE of 85 % or above, then it is considered to be a world-class company. The commonly used maintenance performance indicators (Campbell and Jardine, 2001) are measured by equipment performance like availability, reliability and OEE, process performance and cost performance. Moynihan and Allwood (2014) in their journal paper stated how utilization can be used efficiently to determine the load of all structural steel beams in construction industry. Jagadeesh (2016) in his paper revealed how important is the CC for capacity planning in manufacturing industry to schedule proper job order to meet client's deadline in any deficit and surplus situation. In an another investigation it had been shown how capacity cushion (CC), utilization factor (UF) and OEE is influencing overall effectiveness of a plastic manufacturing unit where it was suggested the triple shift a day may increase productivity (Abu Jadayil, Khraisat and Shakoor, 2017). An assessment of utilization coefficient (UC) of dental equipment was conducted (Gupta, et al., 2017) at medical facility to generate maintenance schedule or timeline of hospital equipment. Generally overall equipment effectiveness (OEE) is a measure of total utilization of time, material and facilities in a manufacturing and process unit. It was further studied that OEE is a measuring system of effectiveness of a machine condition (Purba, Wijayanto and Aristiara, 2018). Nila Chandra Sakti has proposed a model of OEE along with six big losses to identify the root cause of failure and then suggested the probable maintenance method (Sakti, Nurjanah and Rimawan, 2019). Application of OEE model can be measured in the form of the real time performance indicator in manufacturing industry (Hwang, et al., 2017). The TPM can be introduced in a printing press on the basis of risk index to increase the OEE metrics and further failure probability reduction (Kar and Pal, 2019). In an another research paper it had been discussed two ways how simple moving average and Holt's double exponential smoothening methods were applied to determine OEE, to predict future performance and to minimize the error percentage (Anusha and Umasankar, 2020). An intensive study had been conducted on high downtime of continuous blanking machines and its six big losses (Marfinov and Pratama, 2020). After reviewing various journals related to OEE, it is seen that OEE is widely used by manufacturing industry (Atikno and Purba, 2021). Recently, a case study (Setiwan, Al Latif and Rimawan, 2022) was conducted to determine OEE and its performance pattern in PVC compound industry. Also a research approach is used by Azizah and Rinaldi (2022) to generate an in depth analysis to improve overall equipment effectiveness performance of a packaging company.

In the present investigation, a methodology has been developed on the basis of variation of effectiveness and utilization of printing machines for proper implementation of TPM philosophy in the press to avoid unexpected failures and downtime of these machines.

3. Theoretical background of the study

3.1 Overall equipment effectiveness and overall equipment loss measurement

The TPM technique focuses on availability (A), performance (P) and quality-rate (Q) that affect productivity. Availability losses are the result of breakdowns and change-over, i.e. the situation in which the line is experiencing unexpected stoppage. Deterioration of performance are due to speed losses and small stops or idling or empty positions i.e. the line may be running, but it is not producing the expected quantity. The above stated losses can be categorised with following Equation [1].

$$OEE = A \cdot P \cdot Q \quad [1]$$

where,

$$A = \frac{\text{Operating or run time}}{\text{Total planned production time}} \quad [2]$$

$$P = \frac{\dfrac{\text{Total pieces}}{\text{Operating run time}}}{\text{Ideal run rate}} \quad [3]$$

$$Q = \frac{\text{Good pieces}}{\text{Total pieces}} \quad [4]$$

The quantitative assessment of OEE is central to the formulation and execution of a TPM improvement strategy. The TPM has the standard of 90 % availability, 95 % performance efficiency and 99 % rate of quality (Nakajima, 1988). Thus, an overall 85 % of OEE is considered as worldwide performance benchmark. An OEE measure provides a strong indicator for introducing a pilot and subsequently companywide TPM program. The mathematical expression of the corresponding overall equipment loss (OEL) is given in Equation [5].

$$\text{OEL} = 1 - \text{OEE} \quad [5]$$

The alternate way to validate the equipment losses is to estimate separately all the big losses that cause low performance of machines and equipment, namely equipment failure (breakdown losses, BL), setup and adjustment losses (SAL), idling and minor stoppage losses (IMSL), reduced speed losses (RSL), process defect losses (PDL), reduced yield losses (RYL). All six losses are summarized in Equations [6] to [11].

$$\text{BL} = \frac{\text{Total breakdown or malfunction time}}{\text{Planned production time}} \quad [6]$$

$$\text{SAL} = \frac{\text{Total setup, installation or adjustment time}}{\text{Planned production time}} \quad [7]$$

$$\text{IMSL} = \frac{\text{Non-productive time}}{\text{Planned production time}} \quad [8]$$

$$\text{RSL} = \frac{\text{Actual runtime} - \text{Ideal run time}}{\text{Planned production time}} \quad [9]$$

$$\text{PDL} = \frac{\text{Ideal cycle time} \times \text{Total process defect}}{\text{Planned production time}} \quad [10]$$

$$\text{RYL} = \frac{\text{Time taken for new product development or printing after rejection or damage}}{\text{Planned production time}} \quad [11]$$

3.2 Utilization factor and capacity cushion

The UF is one of the important parameters to monitor the functional status of the equipment or it is the parameter to assess the productivity of service of equipment. An optimum utilization of the equipment will result in optimal machine handling and rapid turnover with minimum possible production and maintenance cost along with client's satisfaction. The UF (also known as utilization ratio) is the ratio of actual (or present or observed) to maximum allowable performance or production time or output or value within specific limit of timeline or capacity, which is abbreviated in Equation [12] (Gupta, et al., 2017).

$$\text{UF} = \frac{\text{Actual production time per day or week}}{\text{Maximum allowable production time per day or week}} \quad [12]$$

It is important to note that the actual production value or time consists of downtime, runtime, production delay, etc., for that particular shift or day or week whereas maximum allowable production time is the maximum available limit of time or performance that a system or plant can operate per shift or day or week or month.

The CC is the extra capacity available in the company that is left after utilizing the machines and equipment to produce the demanded quantity. It refers to the unused capacity and thus is maintained in anticipation of several requirements. Therefore, capacity cushion is defined as the amount of reserve capacity which a process uses to handle sudden increase in demand or temporary losses of production capacity; it measures the amount by which the average utilization (in term of total capacity) falls below 100 % as shown in Equation [13] (Jagadeesh, 2016; Abu Jadayil, Khraisat and Shakoor, 2017).

$$\text{CC} = 1 - \text{UF} \quad [13]$$

3.3 Failure probability and reliability

Reliability test is often carried out for both short and long span of time on a component to evaluate the failure probability, machine lifetime and its future maintenance strategies to reduce the machine breakdown and its corresponding maintenance cost. Linear regression technique is used to analyse failure pattern by the following probability Equation [14].

$$F_{x,f(x)} = \frac{p}{q} \quad [14]$$

where

$$p = [N \cdot \Sigma\{x \cdot f(x)\}] - \{\Sigma x \cdot \Sigma f(x)\} \quad [15]$$

$$q = \sqrt{[\{N \cdot \Sigma(x^2)\} - (\Sigma\, x)^2][\{N \cdot \Sigma\, f(x^2)\} - \{\Sigma\, f(x)\}^2]} \quad [16]$$

where x is breakdown time (in minutes), $f(x)$ is cumulative % of failure (calculated from number of failures per day and sum of number of failures for 91 days), N is sum of total operating time for 91 days (in minutes) and $F_{x,f(x)}$ is correlation coefficient. Failure data of the different components or sub-components of the printing press is used for determining the correlation coefficient. From the concept of probability, it is known that the value of the correlation coefficient must be between

+1.0 and –1.0. If the correlation coefficient estimates positive value, then the failure rate is increasing, otherwise the rate is decreasing. Reliability function $R(t)$ for the equipment has been calculated by using Equation [17].

$$R(t) = 1 - F(t) = 1 - \int_0^t f(t)\,dt \quad [17]$$

The cumulative density function for reliability is denoted as $F(t)$, which is also related to failure probability and in combination with the fact that area under the probability density function is always equal to 1 (Kar and Pal, 2019). Probability density function of time to failure is denoted by $f(t)$ and t is the operating time.

3.4 Detail of printing press equipment

Maintenance is the most important duty of a printing press. The machines in an old printing house are running many years and consequently OEE, utilization, availability and reliability checking is found to be a crucial task of the printing press. In a printing press if any major machine and its supporting system has got breakdowns, the operational process would be subjected to some troubles.

The present study is conducted at Ganashakti Printer's Private Limited, a daily newspaper house, situated in Kolkata, India. This house comprises of various machines such as four colour web-offset printing machine, computer-to-plate (CTP) units and plate exposure unit, etc., in its press and prepress sections.

Computer-to-plate is an imaging device, which is used to convert an image created in desktop publishing (DTP) application into a plate made of aluminium or polyester, etc. Once the plate is imaged, it is used for four colour printing in web-offset machine. In exposure unit, printing plate is exposed by the application of ultraviolet (UV) light. The proposed observation and analysis was done on the existing four equipment, the details of which are summarized in Table 1.

Table 1: Different equipment of the daily newspaper house

No.	Machine name	Make	Year of manufacturing	Model	Approx. capacity (pieces/hr)	Output
1	Web-offset printing machine	The Printers House Pvt. Ltd, India	2009	Orient Xcell, 3c-1	41 200	Daily newspaper, supplement paper, book, magazine, etc.
2	Computer to plate 1 (CTP1)	Epson	2014	Sure Colour T5270 (Ultra Colour XD ink)	20	Preparation of plate for printing
3	Computer to plate 2 (CTP2)	Epson	2009	Sure Colour T5270 (Ultra Colour XD ink)	15	Preparation of plate for printing
4	Exposure unit	Technova	2005	Proteck, Ecolux-i	30	Preparation of plate for printing

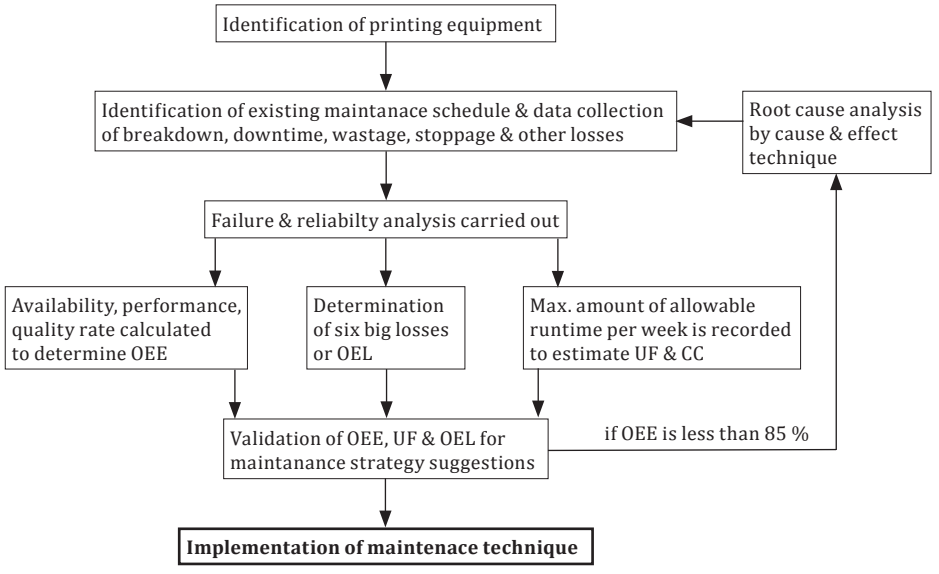

Figure 1: Framework of proposed methodology

4. Methodology

Typically, in the workflow of every print-production house, all jobs are carried out on urgent basis. Generally printing equipment works for either 12 or 24 hours a day based on the job pressure in the organization. And especially newspaper printing presses are famous for the fastest workflow process as the news of entire day needs to be covered in a predetermined and limited size of a paper roll, then that needs to undergo various approval and correction stages and then the final layout will be printed within a very short period of time as it has to be delivered to different regions and outskirts of the city. But at the same time it is very important to monitor the machine's health, production rate, breakdown, root-causes of faults and maintenance procedure in order to make appropriate performance. The present study involves the identification and documentation of all parameter leading to the estimation of overall equipment efficiency, UF and CC, failure identification and analysis of the printing machines. Apart from this, attempts have been made to examine the potential inter-relation among the parameters like OEE, OEL, six big losses and UF for each machine. Finally comparative analysis between all the factors is done on the ground of failure analysis and effectiveness of equipment to establish the suitable maintenance technique. The flowchart given in Figure 1 represents the proposed framework of the methodology.

5. Results

Basic data collected from the printing press is operating time, downtime including breakdown time, total planned production time, number of failures of the components, wastage and reworks, and total products for consecutive 13 weeks (or 91 days). The weekly collected data for web-offset printing machine and other equipment together with their ideal run rate were analysed to estimate OEE and thus OEL and are given in Appendix in Tables A1 to A4 for different machines.

Also weekly variation and analysis of UF, and thus CC and total equipment efficency are given in Table 2 and for this maximum number of available time for each machines has been recorded. Failure time of different machines has also been noted and then compiled from the daily maintenance reports for thirteen weeks. During this investigation the average temperature inside the press was 27–33 °C and average relative air humidity was 75–85 %. Moreover, as the printing job is mostly associated with newsprint thus the press uses the paper of the same grammage and printing is done mainly in night shift though 30–35 % of the printing was done in both day and night shifts. Furthermore, it is assumed that the operational conditions are the same for all the machines.

Using Tables A1 to A4 from Appendix and Table 2, variation of A, P, Q, OEE, OEL, UF and CC for different machines in the printing house with the number of weeks are shown in Figure 2. Comparative observation of different parameters of four pieces of equipment is providing valuable insights into the actual picture of the printing house. Moreover, weekly variations of UF and CC of four pieces of equipment give a clear idea for a better understanding of the machine conditions inside the printing house.

Also, basic data of the four pieces of equipment in the printing house are represented in Table 3 for a total

Table 2: Weekly analysis of UF and CC

No. of a week	wk1	wk2	wk3	wk4	wk5	wk6	wk7	wk8	wk9	wk10	wk11	wk12	wk13
Web-offset printing machine													
Max. no. of min	6210	6210	5520	5520	6900	5520	6900	8280	7590	8970	6900	4830	5520
UF	0.2283	0.2673	0.2440	0.2303	0.2832	0.2507	0.2939	0.2943	0.2791	0.3701	0.2145	0.1482	0.1862
CC	0.7717	0.7327	0.7560	0.7697	0.7168	0.7493	0.7061	0.7057	0.7209	0.6299	0.7855	0.8518	0.8138
CTP1													
Max. no. of min	4830	4830	4830	4830	4830	4830	4830	4830	4830	4830	4830	4830	4830
UF	0.0921	0.0986	0.1340	0.1054	0.0841	0.1072	0.0961	0.1559	0.1311	0.1081	0.1313	0.0855	0.1230
CC	0.9079	0.9014	0.8660	0.8946	0.9159	0.8928	0.9039	0.8441	0.8689	0.8919	0.8687	0.9145	0.8770
CTP2													
Max. no. of min	4830	4830	4830	4830	4830	4830	4830	4830	4830	4830	4830	4830	4830
UF	0.0503	0.0451	0.0532	0.0702	0.0816	0.0598	0.0642	0.0849	0.0631	0.0578	0.0600	0.0286	0.0412
CC	0.9497	0.9549	0.9468	0.9298	0.9184	0.9402	0.9358	0.9151	0.9369	0.9422	0.9400	0.9714	0.9588
Exposure unit													
Max. no. of min	4830	4830	4830	4830	4830	4830	4830	4830	4830	4830	4830	4830	4830
UF	0.1099	0.1099	0.1222	0.1304	0.1178	0.1453	0.1427	0.1909	0.1625	0.1706	0.1857	0.1126	0.1571
CC	0.8901	0.8484	0.8778	0.8696	0.8822	0.8547	0.8573	0.8091	0.8375	0.8294	0.8143	0.8874	0.8429

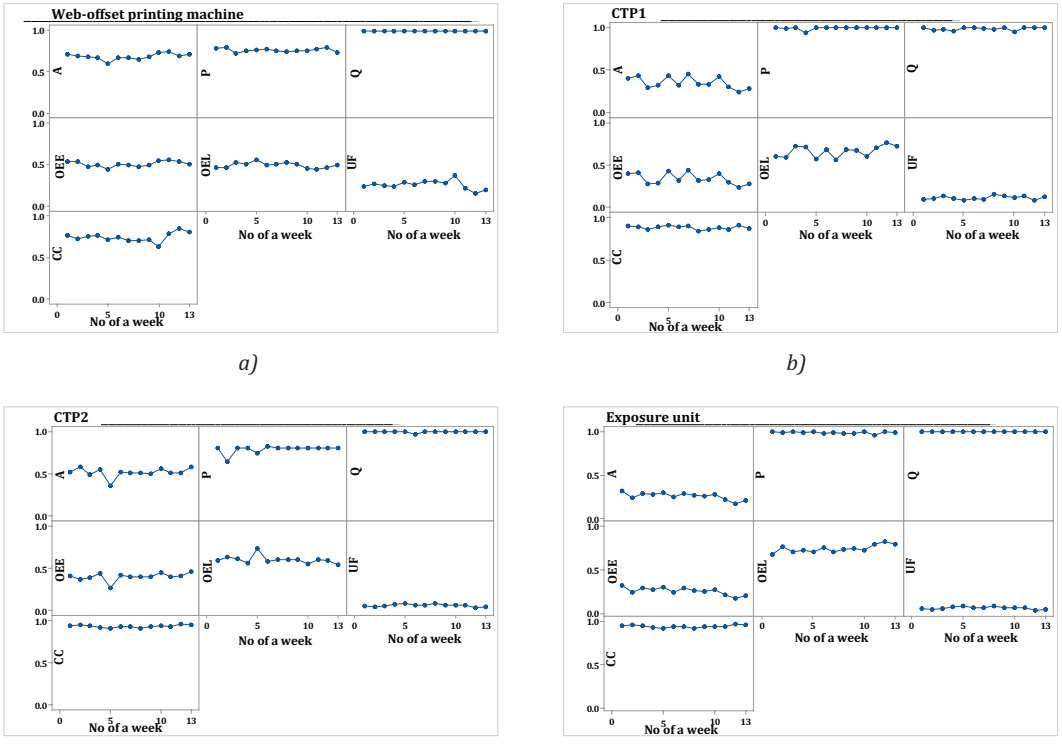

Figure 2: Scatterplot of availability, performance, quality, overall equipment effectiveness, overall equipment loss, utilization factor, and capacity cushion vs no. of weeks for (a) web-offset printing machine, (b) CTP1, (c) CTP2, and (d) exposure unit for 13 week

number of 91 days. From this table, Table 4 has been generated to re-estimate OEE, OEL, UF and CC values of the equipment for the total number of 91 days. Here failure probability and thus reliability of four machines have also been determined from Equations [14] and [17] to validate the results of the OEE and UF.

Table 3: Data of equipment in printing house for total 91 days

Name	Web-offset printing machine	CTP1	CTP2	Exposure unit
Operating time (minutes))	14 813	2 394	1 845	2 347
Downtime (minutes)	6 957	4 630	1 836	6 827
Total planned production time	21 770	7 024	3 671	9 174
No. of failure	506	711	284	1 146
Good pieces	7 600 443	781	362	1 157
Waste and reproduced	96 186	12	1	0
Total output	7 696 629	793	363	1 157
Ideal run rate	687	0.33	0.25	0.50

Table 4: The OEE, OEL, UF, CC, failure probability and reliability of the machines in printing house on the basis of total 91 days

Name	Web-offset printing machine	CTP1	CTP2	Exposure unit
A	0.68	0.34	0.50	0.26
P	0.76	1.00	0.79	0.98
Q	0.99	0.98	1.00	1.00
OEE	0.51	0.33	0.39	0.25
OEL	0.49	0.66	0.60	0.75
Max. no. of min	83 490	62 790	62 790	62 790
UF	0.26	0.11	0.06	0.15
CC	0.74	0.89	0.94	0.85
Failure probability	0.50	0.75	0.57	0.81
Reliability	0.50	0.25	0.43	0.19

6. Analysis and discussion

It is observed that web-offset printing machine has a high quality rate and medium rate of performance and availability, viz. 98.75 %, 75.63 % and 68.04 %, which

results in a medium OEE of 50.82 %. But it is seen that only 26.07 % of available time is been utilized, which is the highest value with respect to other devices though it is the extremely low value in comparison to world class standard. To get clearest picture of effectiveness value it has to increase the utilization rate from available and unused capacity of 73.93 %. For CTP1, both performance and quality factor has a standard rate of 99.79 % and 98.49 % but OEE is affected by low availability 34.08 %. Its OEE is 33.50 % and utilization rate is 11.19 %. The corresponding CC of CTP1 thus shows that it has 88.81 % of unused capacity to utilize on the basis of 12 hour shift. CTP2 possess availability rate of 49.99 % and performance rate of 79.13 % against high quality rate of 99.72 %, resulting in low overall equipment effectiveness rate of 39.44%. Also only 5.85 % is utilized and 94.15 % of time-period remains unused. Last but not the least exposure unit has the lowest OEE value among the all four equipment, i.e. 25.22 %, and utilization rate is 14.61 %, with 85.39 % capacity unused.

For validation of the analysis of effectiveness and utilization of the four printing equipment, a comparative assessment has been done with the values of failure probability and reliability of the machines. It is observed that the exposure unit with the lowest effectiveness has the highest failure probability, whereas web-offset printing machine has the highest effectiveness with the lowest failure probability. Finally it can be said that web-offset printing machines is more reliable while exposure unit is comparatively less reliable. In general, data collection for longer duration of time would give more accurate results.

6.1 Three dimensional analysis

From the previous analysis it is observed how availability, performance, and quality are varying on weekly basis, which is directly affecting the OEE and failure probability. The quality factors of all the machines are found to be high, nearly up to the level of world standard, whereas availability and performance ratios of machines are found to be much less than the standard value. It may be due to different reasons, like prepress delay, malfunction of the machines, loading–unloading delay, material arrangement delays, sudden breakdown of machine, speed loss etc.

A 3D surface plot is useful for investigating desireable response values with the operating conditions. Operating conditions as predictors are generally on the *x* and *y* axis whereas response values are on *z* axis. So, in this case it can be postulated that availability and performance ratio are the "operating conditions" and OEE is the "response value" for the surface plot. A contour plot is also generated to visualize 3D-data in a form of 2D-plot. Figure 3 represents the surface plots and contour plots of four different pieces of equipment. From these plots, it can be seen how availability along with performance is influencing OEE of all the four machines. Here it is also observed that OEE of all the machines is far below the standard value. The values are less due to high frequency of breakdown of the machines. It is important to mention that number of failure (stoppage or downtime) of printing machine consists of loading–unloading, tear down of paper, brake problem, dampening or ink problem, change of plate due to edition, angle defect, wrong installation, inappropriate pressure in pipeline, failure in bearing and gear shaft, etc. Similarly, loading–unloading of plate in CTP machine, prepress delay, editor end-correction, machine malfunction or breakdown are the causes of downtime of CTP1 and CTP2. Loading–unloading in machine, system malfunction and breakdown, delay of exposure due to malfunction of machine or exposing bulb are the reasons of downtime for exposure unit.

It is seen that availability has relatively lower values viz. 68.04 %, 34.08 %, 49.99 %, 25.58 %, for all four machines and the quality rate has high values of 98.75 %, 98.49 %, 99.72 %, 100 %. The performance value has both medium to good values, i.e. 75.63 %, 99.79 %, 79.13 %, 98.59 %. The effectiveness parameters along with the UFs of all the machines are shown in Figure 4 in the form of a bar chart to make a comparative study of all the machines. Failure probability and reliability of the machines are also compared with the effectiveness parameters; it shows that reliability functions of all the four machines are more or less matching with the corresponding OEE values.

6.2 Analysis of six big losses

From the above discussions, it is clear that OEE of all the machines under study needs to be improved. Therefore it is necessary to determine the all six big losses which will help to identify the root causes of failures. The six big losses of all the equipment are determined by using Equations [5] to [11] and given in Table 5.

Table 5: Analysis of six big losses for all four equipment

Six big losses	Web-offset printing machine	CTP1	CTP2	Exposure unit
BL	0.0544	0.0286	0.0579	0.0235
SAL	0.2651	0.1331	0.1176	0.0581
IMSL	0.0000	0.4974	0.3233	0.6625
RSL	0.1658	0.0021	0.1068	0.0036
PDL	0.0064	0.0051	0.0054	0.0000
RYL	0.0110	0.0051	0.0014	0.0000
Total loss	0.5028	0.6716	0.6123	0.7478
OEL	0.4918	0.6650	0.6056	0.7478
OEE	0.5082	0.3350	0.3944	0.2552

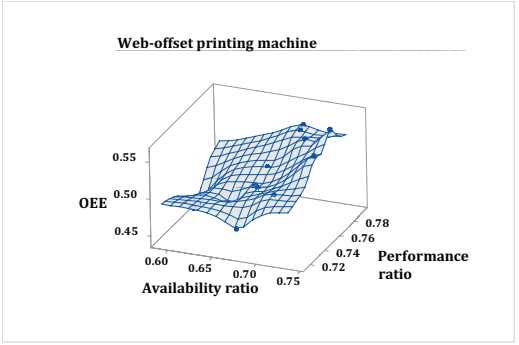

a)

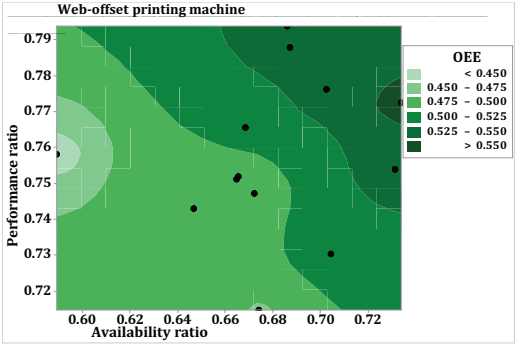

b)

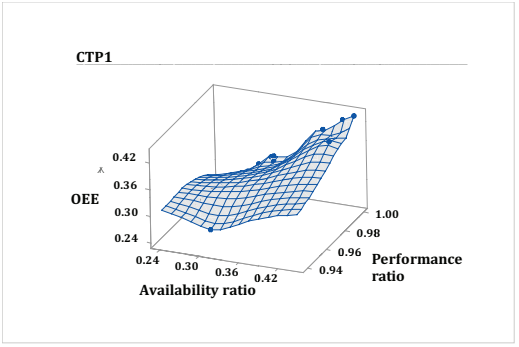

c)

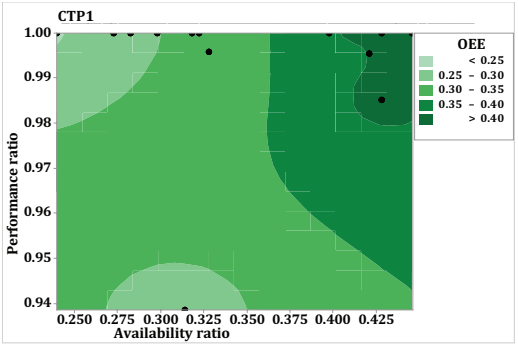

d)

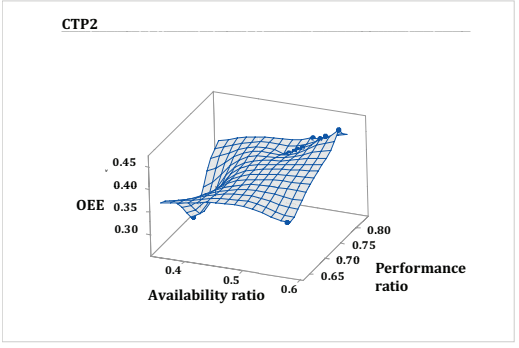

e)

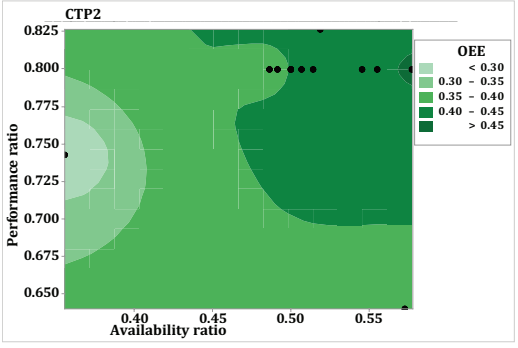

f)

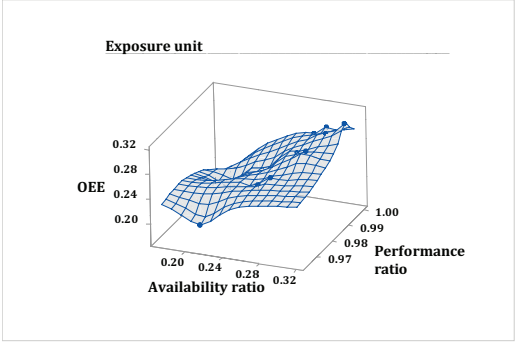

g)

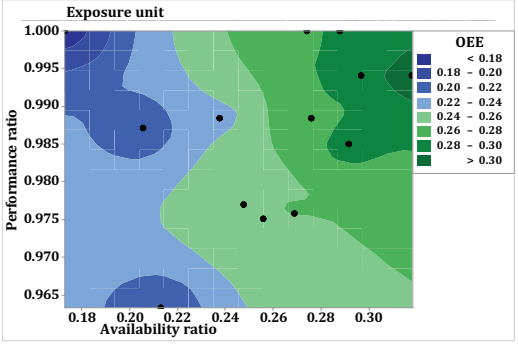

h)

Figure 3: Surface and contour plots of overall equipment effectiveness vs performance and availability for web-offset printing machine (a) and (b), for CTP1 (c) and (d), for CTP2 (e) and (f), and for exposure unit (g) and (h), respectively

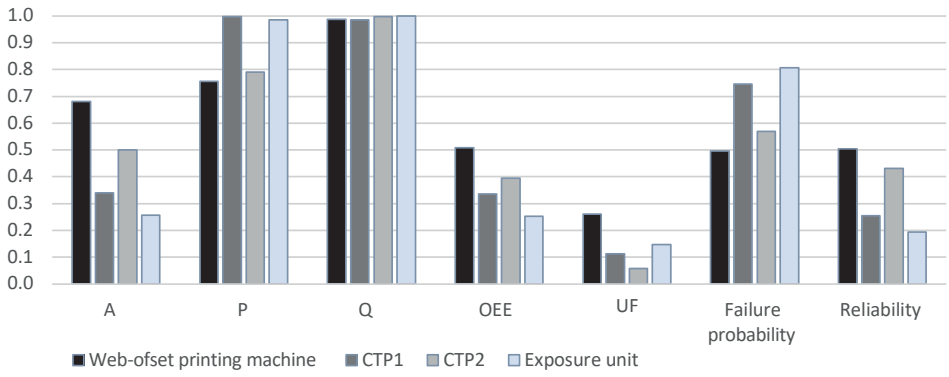

Figure 4: Comparison of effectiveness details of all four equipment

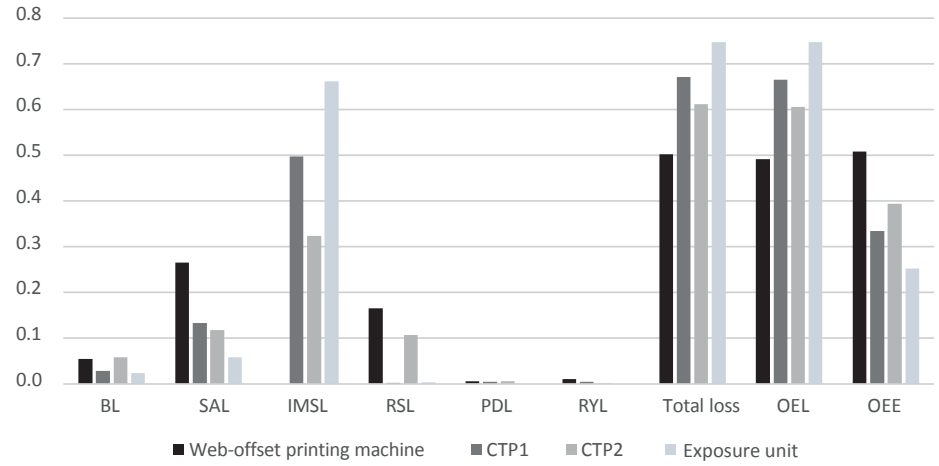

Figure 5: Comparative analysis of six big losses with OEL for four printing equipment

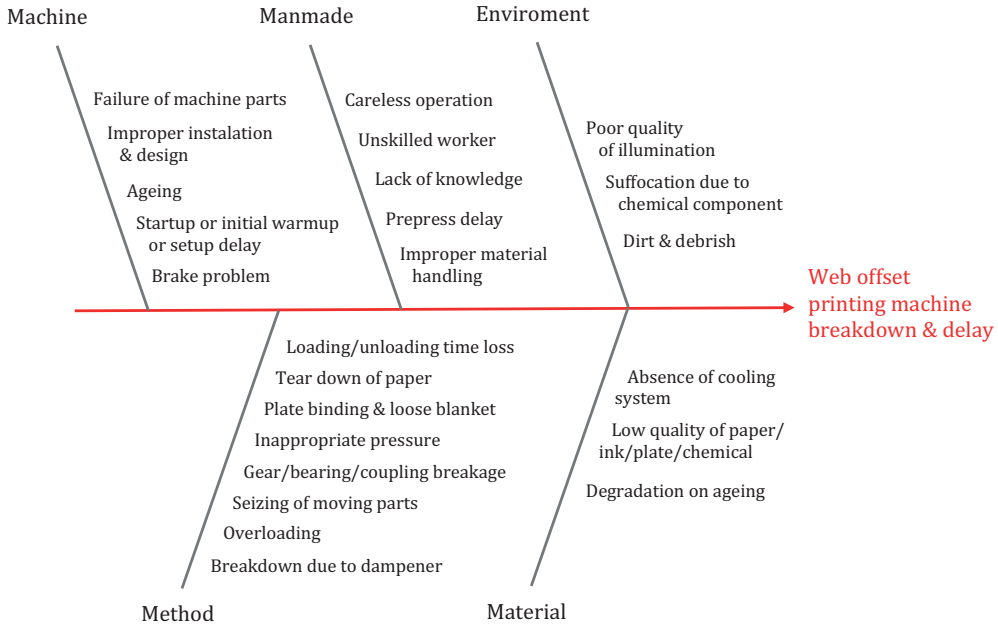

Figure 6: Fish-bone diagram (or cause and effect diagram) for web-offset printing machine breakdown

Figure 5 shows the comparative analysis of the above losses of the machines along with the OEL and OEE. Here it shows that OEL of the four machines nearly matches with the values of total losses incurred by the corresponding machines. The analysis of OEL will help to predict hidden causes of failure and probable area of improved productivity.

6.3 Ishikawa analysis

The cause and effect diagram is also known as fish-bone diagram (FBD) or Ishikawa diagram or analysis, which is composed of five main pillars namely Manmade, Machine, Method, Environment and Material. These causes lead to the main effects of failure, i.e. breakdown of a printing press. Each pillar is subdivided into different sub-branches that lead to the causes of breakdown of each component and subcomponent of the press.

Figure 6 gives the complete overview of the causes of breakdown of the web-offset printing machine. Similar diagram can also be developed for other three machines. Based on the FBD of different equipment, the causes for improper functioning and their corresponding corrective actions are listed in Table 6. The recommendations for further maintenance planning of different machines have also been suggested.

Table 7: Prediction of improved values of six big losses and OEE of the machines after implementation of TPM

Parameter Six big losses	Maximum modified parameters			
	Web-offset printing machine	CTP1	CTP2	Exposure unit
BL	0.0000	0.0000	0.0000	0.0000
SAL	0.2804	0.2809	0.1901	0.0595
IMSL	0.0000	0.0000	0.0000	0.6785
RSL	0.1775	0.0153	0.1743	0.0037
PDL	0.0046	0.0000	0.0000	0.0000
RYL	0.0068	0.0000	0.0000	0.0000
Total loss	0.4694	0.2962	0.3644	0.7417
OEL	0.4626	0.2962	0.3643	0.7417
OEE	0.5374	0.7038	0.6356	0.2525
UF	0.2466	0.0530	0.0362	0.1427
CC	0.7534	0.9470	0.9638	0.8573

Table 6: Different types of failures of the machines and corresponding recommendations

Component / subcomponent	Causes	Corrective actions	Recommendation for maintenance approach
Web-offset printing machine	Tear down of paper, dampening and ink problem, inappropriate pressure	Continuous monitoring the given task or job to immediately detect failure	Corrective maintenance
	Brake problem	Repair	Breakdown maintenance
	Bearing, rotating element or gear shaft failure	Repair	Breakdown maintenance
	Failure due to plate and blanket	If misprint occurs due to angle of plate or disorientation of plate then replace the plate. Remake the plate again. On ageing of machine, degradation or loosening of blanket observed. Pretension of blanket or incorrect installation of blanket need proper repair.	Corrective and preventive maintenance
	Loading–unloading	Need to install automatic loading system where paper reels need to rotate with same rpm of running reel	Corrective maintenance
	Prepress delay	Detection of root cause of failure	Predictive maintenance
CTP1 and CTP2	Loading–unloading	Automation	Corrective maintenance
	Delay of printing due to malfunction machine	Detection of root cause of failure	Predictive maintenance
	Prepress delay	Detection of root cause of failure	Predictive maintenance
Exposure unit	Loading–unloading	Automation	Corrective maintenance
	Delay of exposure due to malfunction of machine or exposing bulb	Replacement or repair lighting system and detection of cause of machine malfunction	Preventive or breakdown and proactive maintenance
	Prepress delay	Detection of root cause of failure	Predictive maintenance

Based on these recommendations, modified losses, effectiveness and UF have been re-estimated by considering the fact that the downtime including breakdown time can be reduced by decreasing number of failures with the help of modern technology and management system. The modified losses values for all machines are shown in Table 7 which indicates that modified effectiveness of all the machines increases with the decrease of losses (modified) in the corresponding machines.

7. Conclusion

The OEE is a powerful tool to identify previously hidden production losses and inefficiencies. Tracking OEE scores and using them to improve in production process is a vital step towards world class manufacturing. The OEE systems provide the rich functionality necessary to expose exactly what percentage of production time is truly productive and to reveal the causes of loss productivity. Even increasing the OEE score by 1% can lead to dramatic savings and turn-around lost production time into a positive contribution to profit. Based on the results and the analysis of OEE of different machines of a newspaper printing house it can be concluded that the measurement of effectiveness level of web-offset printing machine is comparatively high (50.82 %) but less than the world standard value of 85 %.

Web-offset printing machine is also found as the most frequently used machine owing to its UF of 26.07 %. Exposure unit is the comparatively limited used machine having lower UF of 14.61 % and downtime is more i.e. 6 827 minutes, hence OEE is less (25.22 %). The variations of OEE and utilization also give a clear picture of the printing house, where they are and where is the weakness point and how to improve.

The various problems due to different types of losses occurring in the printing press can be prevented from causing unwanted troubles leading to decrease in the overall efficiency of the system. The sequencing of jobs plays an important role to reduce the losses, wastes and time. The sequencing of jobs depends not only on operator but on the workflow also. Hence, sequencing of jobs needs to be improved for better results.

The proposed methodology influences not only maintenance management but also knowledge management because it is a quantitative method to estimate effectiveness and utilization validated by failure probability and reliability. These approaches ensure that reliability of equipment is increased after implementation of maintenance planning suggested, which may contribute to the availability of the machines as well as its safe operation. It is observed that for web-offset printing machine the percentage of increment of OEE is nearly 2.93 % after implementation of maintenance planning which is quite significant. The present investigation also helps to identify the critical equipment based on the root-cause analysis by using fish-bone diagram. Finally, it is suggested that this quantitative assessment needs to be implemented by top management in complying with the requirements of standard print production management for progressive output, effectivity, availability and productivity.

Reference

Abu Jadayil, W., Khraisat, W. and Shakoor, M., 2017. Different strategies to improve the production to reach the optimum capacity in plastic company. *Cogent Engineering*, 4(1): 1389831. http://doi.org/10.1080/23311916.2017.1389831.

Anusha, C.H. and Umasankar, V., 2020. Performance prediction through OEE model. *International Journal of Industrial Engineering and Management*, 11(2), pp. 93–103. http://doi.org/10.24867/IJIEM-2020-2-256.

Atikno, W. and Purba, H.H., 2021. Sistematika tinjauan literature mengenai *overall equipment effectiveness* (OEE) pada industri manufaktur dan jasa. *Journal of Industrial and Engineering System*, 2(1), pp. 29–39. https://doi.org/10.31599/jies.v2i1.401.

Azizah, F.N. and Rinaldi, D.N., 2022. Effort to improve overall equipment effectiveness performance with six big losses analysis in the packaging industry PT BMJ. *Indonesian Journal of Industrial Engineering and Management*, 3(1), pp. 26–34. http://dx.doi.org/10.22441/ijiem.v3i1.13508.

Campbell, J.D. and Jardine, A.K.S. eds., 2001. *Maintenance excellence: optimizing equipment life-cycle decisions*. New York, USA: Marcel Dekker.

Gupta, V., Gupta, N., Sarode, G.S., Sarode, S.C. and Patil, S., 2017. Assessment of equipment utilization and maintenance schedule at Dental Institution in Bengaluru, India. *World Journal of Dentistry*, 8(2), pp. 104–108. http://dx.doi.org/10.5005/jp-journals-10015-1421.

Hwang, G., Lee, J., Park, J. and Chang, T.-W., 2017. Developing performance measurement system for internet of things and smart factory environment. *International Journal of Production Research*, 55(9), pp. 2590–2602. https://doi.org/10.1080/00207543.2016.1245883.

Jagadeesh, R., 2016. Optimizing the capacity addition in a component manufacturing industry – an empirical investigation. In: N. Sengupta and M. Sengupta, eds. *Contemporary Research in Management: Volume V*. Mysore, Karnataka, India: SDM Institute for Management Development, pp. 333–366.

Kar, A. and Pal, A.K., 2019. An approach to risk-based maintenance strategy of a printing press. *Journal of Print and Media Technology Research*, 8(3), pp. 155–165. http://dx.doi.org/10.14622/JPMTR-1907.

Marfinov, B.F.P.A. and Pratama, A.J., 2020. Overall equipment effectiveness (OEE) analysis to minimize six big losses in continuous blanking machine. *Indonesian Journal of Industrial Engineering and Management*, 1(1), pp. 25–32. http://dx.doi.org/10.22441/ijiem.v1i1.8037.

Mileham, A.R., Culley, S.J., McIntosh, R.I., Gest, G.B. and Owen, G.W., 1997. Set-up reduction (SUR) beyond total productive maintenance (TPM). *Proceedings of the Institution of Mechanical Engineers, Part B: Journal of Engineering Manufacture*, 211(4), pp. 253–260. https://doi.org/10.1243/0954405971516248.

Moynihan, M.C. and Allwood, J.M., 2014. Utilization of structural steel in buildings. *Proceedings of the Royal Society A: Mathematical, Physical and Engineering Sciences*, 470(2168): 20140170. http://dx.doi.org/10.1098/rspa.2014.0170.

Nakajima, S., 1988. *Introduction to TPM: total productive maintenance*. Portland, OR, USA: Productivity Press.

Purba, H.H., Wijayanto, E. and Aristiara, N., 2018. Analysis of overall equipment effectiveness (OEE) with total productive maintenance method in jig cutting: a case study in manufacturing industry. *Journal of Scientific and Engineering Research*, 5(7), pp. 397–406.

Ramayah, T., Jantan, M. and Hassan, M.M., 2002. Change management and implementation of total productive maintenance: an exploratory study of Malaysian manufacturing companies. *Utara Management Review*, 3(1), pp. 35–49.

Sakti, N.C., Nurjanah, S. and Rimawan, E., 2019. Calculation of overall equipment effectiveness total productive maintenance in improving productivity of casting machines. *International Journal of Innovative Science and Research Technology*, 4(7), pp. 442–446.

Setiwan, B., Al Latif, F. and Rimawan, E., 2022. Overall equipment effectiveness (OEE) analysis: a case study in PVC compound industry. *Indonesian Journal of Industrial Engineering and Management*, 3(1), pp. 14–25. http://doi.org/10.22441/ijiem.v3i1.12066.

Appendix

Weekly collected data for analysed equipment are presented in Tables A1 to A4

Table A1: The OEE and OEL measurement of web-offset printing machine

No. of a week	wk1	wk2	wk3	wk4	wk5	wk6	wk7	wk8	wk9	wk10	wk11	wk12	wk13
Operating time (minutes)	996	1 139	908	846	921	925	1 348	1 576	1 424	2 428	1 086	492	724
Downtime (minutes)	422	521	439	425	642	459	680	861	694	892	394	224	304
Total planned production time (minutes)	1 418	1 660	1 347	1 271	1 563	1 384	2 028	2 437	2 118	3 320	1 480	716	1 028
No. of failure	29	38	42	32	30	29	44	61	52	93	24	13	19
Good pcs	525 437	614 045	438 000	430 938	474 151	481 039	687 410	792 991	721 027	1 239 791	571 864	263 947	359 803
Waste and reproduced	5 779	7 125	7 925	6 099	5 640	5 421	8 313	11 602	10 089	17 813	4 474	2 395	3 511
Total output	531 216	621 170	445 925	437 037	479 791	486 460	695 723	804 593	731 116	1 257 604	576 338	266 342	363 314
Ideal run rate	687	687	687	687	687	687	687	687	687	687	687	687	687
A	0.7024	0.6861	0.6741	0.6656	0.5893	0.6684	0.6647	0.6467	0.6723	0.7313	0.7338	0.6872	0.7043
P	0.7763	0.7938	0.7149	0.7520	0.7583	0.7655	0.7513	0.7431	0.7473	0.7539	0.7725	0.7880	0.7304
Q	0.9891	0.9885	0.9822	0.9860	0.9882	0.9889	0.9881	0.9856	0.9862	0.9858	0.9922	0.9910	0.9903
OEE	0.5394	0.5384	0.4733	0.4935	0.4416	0.5059	0.4934	0.4736	0.4955	0.5436	0.5624	0.5366	0.5095
OEL	0.4606	0.4616	0.5267	0.5065	0.5584	0.4941	0.5066	0.5264	0.5045	0.4564	0.4376	0.4634	0.4905

Table A2: The OEE and OEL measurement of CTP1

No. of a week	wk1	wk2	wk3	wk4	wk5	wk6	wk7	wk8	wk9	wk10	wk11	wk12	wk13
Operating time (minutes)	177	204	183	153	174	165	207	247	204	220	189	99	162
Downtime (minutes)	268	272	464	356	232	353	257	506	429	302	445	314	432
Total planned production time (minutes)	445	476	647	509	406	518	464	753	633	522	634	413	594
No. of failure	56	60	61	44	51	48	61	73	61	62	58	29	47
Good pcs	59	65	60	49	58	55	68	80	68	69	63	33	54
Waste and reproduced	0	2	1	2	0	0	1	2	0	4	0	0	0
Total output	59	67	61	51	58	55	69	82	68	73	63	33	54
Ideal run rate	0.3333	0.3333	0.3333	0.3333	0.3333	0.3333	0.3333	0.3333	0.3333	0.3333	0.3333	0.3333	0.3333
A	0.3978	0.4286	0.2828	0.3006	0.4286	0.3185	0.4461	0.3280	0.3223	0.4215	0.2981	0.2397	0.2727
P	1.0000	0.9853	1.0000	1.0000	1.0000	1.0000	1.0000	0.9960	1.0000	0.9955	1.0000	1.0000	1.0000
Q	1.0000	0.9701	0.9836	0.9608	1.0000	1.0000	0.9855	0.9756	1.0000	0.9452	1.0000	1.0000	1.0000
OEE	0.3978	0.4097	0.2782	0.2888	0.4286	0.3185	0.4397	0.3187	0.3223	0.3966	0.2981	0.2397	0.2727
OEL	0.6022	0.5903	0.7218	0.7112	0.5714	0.6815	0.5603	0.6813	0.6777	0.6034	0.7019	0.7603	0.7273

Table A3: The OEE and OEL measurement of CTP 2

No. of a week	wk1	wk2	wk3	wk4	wk5	wk6	wk7	wk8	wk9	wk10	wk11	wk12	wk13
Operating time (minutes)	125	125	125	185	140	150	155	205	150	155	145	70	115
Downtime (minutes)	118	93	132	154	264	139	155	205	155	124	145	68	84
Total planned production time (minutes)	243	218	257	339	394	289	310	410	305	279	290	138	199
No. of failure	18	14	20	30	22	23	24	34	25	24	23	11	16
Good pcs	25	20	25	37	26	30	31	41	30	31	29	14	23
Waste and reproduced	0	0	0	0	0	1	0	0	0	0	0	0	0
Total output	25	20	25	37	26	31	31	41	30	31	29	14	23
Ideal run rate	0.25	0.25	0.25	0.25	0.25	0.25	0.25	0.25	0.25	0.25	0.25	0.25	0.25
A	0.5144	0.5734	0.4864	0.5457	0.3553	0.5190	0.5000	0.5000	0.4918	0.5556	0.5000	0.5072	0.5779
P	0.8000	0.6400	0.8000	0.8000	0.7429	0.8267	0.8000	0.8000	0.8000	0.8000	0.8000	0.8000	0.8000
Q	1.0000	1.0000	1.0000	1.0000	1.0000	0.9677	1.0000	1.0000	1.0000	1.0000	1.0000	1.0000	1.0000
OEE	0.4115	0.3670	0.3891	0.4366	0.2640	0.4152	0.4000	0.4000	0.3934	0.4444	0.4000	0.4058	0.4623
OEL	0.5885	0.6330	0.6109	0.5634	0.7360	0.5848	0.6000	0.6000	0.6066	0.5556	0.6000	0.5942	0.5377

Table A4: The OEE and OEL measurement of exposure unit

No. of a week	wk1	wk2	wk3	wk4	wk5	wk6	wk7	wk8	wk9	wk10	wk11	wk12	wk13
Operating time (minutes)	169	174	170	174	169	174	201	248	201	226	191	94	156
Downtime (minutes)	362	558	420	456	400	528	488	674	584	598	706	450	603
Total planned production time (minutes)	531	732	590	630	569	702	689	922	785	824	897	544	759
No. of failure	78	84	82	83	77	78	97	120	99	125	99	52	72
Good pcs	84	86	85	86	84	85	99	121	98	113	92	47	77
Waste and reproduced	0	0	0	0	0	0	0	0	0	0	0	0	0
Total output	84	86	85	86	84	85	99	121	98	113	92	47	77
Ideal run rate	0.5	0.5	0.5	0.5	0.5	0.5	0.5	0.5	0.5	0.5	0.5	0.5	0.5
A	0.3183	0.2377	0.2881	0.2762	0.2970	0.2479	0.2917	0.2690	0.2561	0.2743	0.2129	0.1728	0.2055
P	0.9941	0.9885	1.0000	0.9885	0.9941	0.9770	0.9851	0.9758	0.9751	1.0000	0.9634	1.0000	0.9872
Q	1.0000	1.0000	1.0000	1.0000	1.0000	1.0000	1.0000	1.0000	1.0000	1.0000	1.0000	1.0000	1.0000
OEE	0.3164	0.2350	0.2881	0.2730	0.2953	0.2422	0.2874	0.2625	0.2497	0.2743	0.2051	0.1728	0.2029
OEL	0.6836	0.7650	0.7119	0.7270	0.7047	0.7578	0.7126	0.7375	0.7503	0.7257	0.7949	0.8272	0.7971

JPMTR-2217
DOI 10.14622/JPMTR-2217
UDC 778-186:004.93-021.254

Original scientific paper | 170
Received: 2022-07-03
Accepted: 2022-11-18

Image contrast enhancement by optimization of color channel difference using bat algorithm

Saorabh Kumar Mondal[1], *Arpitam Chatterjee*[2] *and Bipan Tudu*[3]

[1]Department of Applied Electronics and Instrumentation Engineering, Haldia Institute of Technology, Haldia, India
[2]Department of Printing Engineering, Jadavpur University, Kolkata, India
[3]Department of Instrumentation and Electronics Engineering, Jadavpur University, Kolkata, India

arpitam.chatterjee@jadavpuruniversity.in

Abstract

Contrast enhancement is a popular image processing technique across different applications. Despite simplicity, many of the reported techniques lack in retention of original image features and cause different artifacts due to over or under enhancement. Such limitations cause problems in cases when the contrast enhancement is used prior to computer vision tasks. This paper presents a new approach of contrast enhancement where the color channel difference has been optimized using bat algorithm to obtain better contrast, improved naturalness and original image feature retention. The potential of the presented method has been assessed with the low contrast images from standard databases and found to be competitive to established models. At the same time the use of device independent color space provides more versatility of the presented method across different applications.

Keywords: image processing technique, image enhancement, color difference estimation, color space dynamics

1. Introduction

Image contrast is an important characteristic that drives the visual appearance as well as the feature detection tasks for many computer vision applications. several natural and hardware limitations of the image capturing devices cause low image contrast. Therefore, image contrast enhancement is a prominent research topic. Broadly, the different algorithms for contrast enhancement can be divided into two categories, spatial domain and frequency domain operations. The various techniques under spatial domain have been consolidated in the works of Mustafa and Kader (2018), and Vijayalakshmi, Nath and Acharja (2020). According to Das, Gulati and Mittal (2015), some of the major developments are global histogram equalization (GHE), brightness preserving bi-histogram equalization (BBHE), dualistic sub-image histogram equalization (DSIHE), minimum mean brightness error bi-histogram equalization (MMBEBHE), adaptive histogram equalization (AHE), contrast limited adaptive histogram equalization (CLAHE), adaptive gamma correction (AGC) and adaptive gamma correction weighted distribution (AGCWD); in addition, Sheet, et al. (2010) mention dynamic histogram equalization (DHE) and dynamic fuzzy histogram equalization (DFHE). Some of the later developments in this paradigm includes contrast enhancement using feature preservation bi-histogram equalization (CEFPBHE) (Wang and Chen, 2018), variance-based brightness preserved dynamic histogram equalization for image contrast enhancement (VBBPDHE) (Dhal, et al., 2018), and recursive median and mean partitioned one-to-one grey level mapping transformations for image enhancement (RMMGHT) (Eswar Reddy and Ramachandra Reddy, 2019), two-dimensional histogram equalization (2DHE) (Celik, 2012) and residual spatial entropy based contrast enhancement using discrete cosine transform (RESECEDCT) (Celik and Li, 2016), which provide superior visual contrast. Single scale Retinex (SSR), and multi scale Retinex (MSR) (Zhang, et al., 2017; Petro, Sbert and Morel, 2014) and adaptive MSR (AMSR) models (Lee, Lien and Han, 2014) are some of the Retinex model based developments that have also shown significant improvement over conventional techniques. Contrast-limited adaptive histogram equalization with dual gamma correction (CLAHE-DGC) (Chang, et al., 2018), adaptive gamma correction with weighted histogram distribution (AGCWHD)

(Veluchamy and Subramani, 2019), fuzzy dissimilarity adaptive histogram equalization with gamma correction (FDAHE-GC) (Veluchamy and Subramani, 2020), and fuzzy dissimilarity histogram (FDH) (Sheet, et al., 2010) are some of the techniques that employ gamma correction. Frequency domain algorithms have shown better performance over spatial domain approaches in many cases since transform domains provide better control over local image characteristics, which in turn provides improved feature retention. Discrete cosine transform (DCT) coefficient scaling (DCTCS) (Samani, Panetta and Agaian, 2016), DCT coefficient histogram (DCTCH) (Panetta, Xia and Agaian, 2012), and DCT pyramid and singular value decomposition (DCT-SVD) (Atta and Ghanbari., 2013) are some of the noted works in this paradigm. Spatial entropy-based contrast enhancement in DCT (SECEDCT) (Celik, 2014) is one of the recent image enhancement techniques, which is the modification of SECE technique in DCT domain. The survey reveals that the scope of improvement is still open, especially, in terms of higher degree of naturalness and image feature retention in enhanced images, which are commonly lacking due to either over- or under-enhancements. At the same time, many of these algorithms provide compromised results in case the contrast distortion is in higher extent.

The applications of different soft computing techniques have as well been reported for image enhancement. Swarm intelligence techniques are one of the subsets of soft computing techniques where the algorithms mimic the behaviors of natural swarms. Particle swarm optimization (PSO), artificial bee colony optimization (ABC), and ant colony optimization (ACO) (Gad, 2022) are popular algorithms that have been employed for contrast enhancement. The elimination of pixel groups based on their contribution towards image detailing has been performed by mean-shift algorithm and then moth swarm algorithm has been employed to maximize the Kullback–Leibler entropy towards contrast enhancement (Luque-Chang, et al., 2021). A novel krill herd based optimization has also been applied in plateau limited histogram clipping for contrast enhancement of medical images (Kandhway, Bhandari and Singh, 2020). To improve the contrast of industrial images a novel ant lion optimization algorithm has been applied and found competitive results over other metaheuristics of swarm intelligence (Yue and Zhang, 2021). Bat algorithm (BA) was developed mimicking the food searching behavior of bat. It has shown promising potential in diverse applications (Asokan, et al., 2020) including feature preserving contrast enhancement.

This paper presents a more general and versatile approach for contrast enhancement. The contribution of the paper is two-fold; a new color channel difference based estimation of lightness that influences the image contrast to a great extent and application of BA to minimize the statistical moment of the stated lightness estimation. The lightness estimation is motivated by the dark channel priory (DCP) (Tsai, Lin and Guo, 2019) concept but it is computationally less expensive. The motivation of difference channel estimation (DCE) was towards better representation of the lightness distribution in the low contrast images.

2. Presented method

2.1 Difference channel estimation

There are many obstructions through which reflected light passes before it is captured by camera lenses. Hence, it is a very difficult task to assess the lightness distortion exactly. At the same point in time based on the transmission media (air or water), there are some frequencies of light that can travel more while some cannot because of their wavelength. Color channel can be a possible indicator for the deficiencies in the lightness distribution, which in-turn causes image quality degradation in many aspects including contrast. To address this, difference color channel was estimated. It can be noted here that all color space conversions used in this work were realized through standard conversion formulae (Nishad and Chezian, 2013).

The native color space of the color images is RGB, which was converted to YCbCr using standard conversion formulae for better interpretation of perceived color. In YCbCr color space *Cr* and *Cb* channels provide the chrominance distribution in blue and red spectrum, respectively. It can be assessed that the difference between *Cr* and *Cb* is indicative to the light receiving characteristics. For instance, in air blue light travels less distance; hence, the foggy images will have higher energy content in *Cr* than in *Cb* while in case of underwater image the energy content of *Cb* will be higher. To measure the energy difference between *Cr* and *Cb* both the channel information were converted to the frequency domain using DCT (Xu, Wang and Lu, 2011). The selection of DCT over Fourier transform is motivated by its simplicity and absence of imaginary component.

The distance between the object and the camera lens also contributes towards distortion. For instance, the light needs to travel more if the object is far, which will subject the waveforms to a higher degree of natural distortions. The luminance representation in Y channel of YCbCr can be a possible interpretation of this distance aspect. The closer objects can appear brighter than the far objects. Considering these two factors the difference channel (D) was calculated by Equation [1].

$$D = \overline{Y} - \mathrm{abs}\left(\overline{Cb} - \overline{Cr}\right) \quad [1]$$

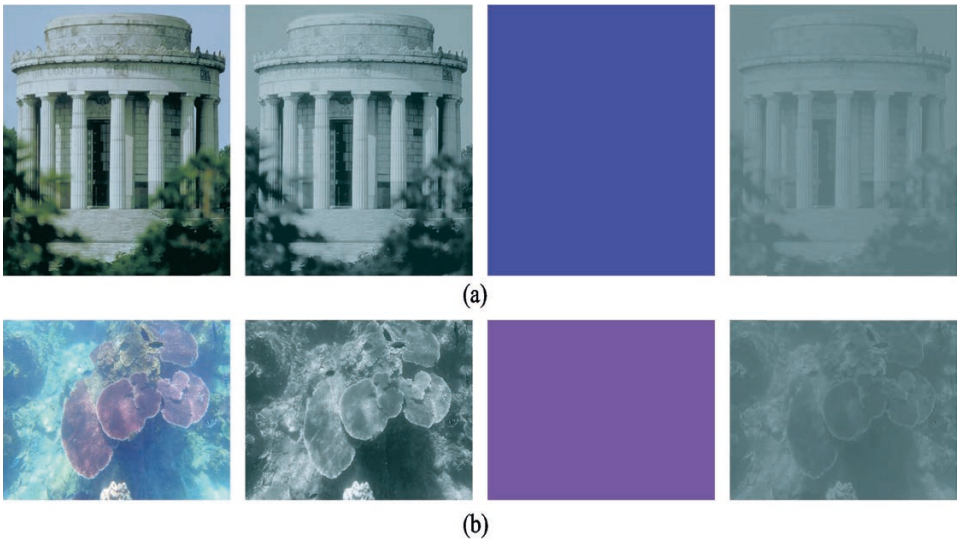

Figure 1: (From left to right) the input images, corresponding difference channel, background light estimation and transmittance for (a) atmospheric and (b) underwater image

where calculation of YCbCr has been done using standard conversion formulae (Fashandi, Peters and Ramanna, 2009) and $\overline{Y}$, $\overline{Cb}$, $\overline{Cr}$ are the DCT of *Y*, *Cb*, *Cr* channels, respectively. Further, *d* is the spatial domain representation of difference channel transform *D.*

The transmittance (*T*) was then estimated using this difference channel transform on the background light weighted input as shown in Equation [2]. The *Bg* in Equation [2] corresponds to the background light estimation where *k*-means clustering (Oyelade, Oladipupo and Obagbuwa, 2010) has been used in this work. The centroid of 10 % highest values in *d* was considered for *Bg*. Figure 1 shows examples of the difference channel and transmittance assessment that resulted from the presented method; η is the assumed effective wideband attenuation coefficient (Akkaynak, et al., 2017), which depends on the light scattering media (surface/underwater) under consideration.

$$T = 1 - \eta d(M) \qquad [2]$$

where

$$M = \underset{c \in \text{YCbCr}}{(I/Bg)}$$

2.2 Optimization using bat algorithm

The transmittance was subjected to optimization using BA. The BA has some major advantages over other popular metaheuristics in terms of simplicity, lesser parameter tuning requirements and robustness (Wang and Li, 2019). It initiates optimization with random solutions generated in the problem space. This generation can be guided towards faster convergence. The algorithm is driven using the echolocation characteristics of bats that they use to search for food. Each bat updates their position and velocity at every iteration based on their best position and velocity information at each iteration. As the bat approaches closer to the prey the loudness of the emitted sound decreases while the pulse emission rate increases. The BA algorithm can be presented as pseudo code presented in Appendix.

2.2.1 Objective function formulation

To achieve the well distributed histogram in transmittance image it was converted to device independent HSV color space from its YCbCr color space using standard conversion formulae. The *V* channel was extracted from the resulting HSV image, which was further subjected to calculation of the L2 norm of the input and enhanced image feature vector as shown in Equation [3], where *dh* and *eh* represent the DCT of *V* channel histogram information. The feature vector in this work is the DCT of *V* channel histogram. This L2 norm based similarity measurement can address the feature similarity (Fashandi, Peters and Ramanna, 2009) and has been used as one of the parameters (φ_1) in the objective function φ.

$$\varphi_1 = \left(\sum_{i=1}^{n} (dh_i - eh_i)^2 \right)^{1/2} \qquad [3]$$

The second parameter of the objective function has been developed based on the skewness and kurtosis of *dh* and *eh*. The plot of original *V* channel histogram is negatively or positively skewed (as it can be seen in Figure 3 in the Results section). The target was to reduce the skewness towards zero and maintain the kurtosis near the value of 3 considering the standard

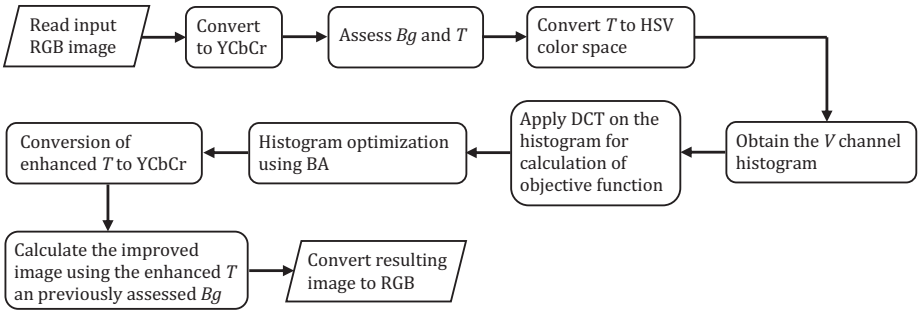

Figure 2: Overview of the proposed contrast enhancement method

normal distribution (Kallner, 2018). Therefore, the second parameter of φ (φ_2) has been formulated as expressed in Equation [4].

$$\varphi_2 = \text{skewness}(eh) + (3 - \text{kurtosis}(eh)) \quad [4]$$

Combining the above two parameters the objective function has been formulated as Equation [5]. In the presented work both parameters have been equally weighted ($w_1 = w_2 = 0.5$). However, depending on the applications or modeling requirements they can be modulated maintaining their sum to unity, i.e., $w_1 + w_2 = 1$.

$$\varphi = w_1\varphi_1 + w_2\varphi_2 \quad [5]$$

Apart from contrast the low quality images lack colorfulness as well. Though the primary goal of this work is towards contrast enhancement, a simple gamma scaling of the saturation channel has also been included to address the colorfulness issue. A global gamma based scaling can cause unnaturalness in enhanced image, which may result in over-enhancement. To avoid that the DCE has been used to assess the pixels to which the scaling has been applied. The pixels with insufficient color information have been identified by a thresholding operation. The thresholding operation generates a mask, which has been used upon the S channel and further subjected to a gamma scaling as shown in Equation [6].

$$\hat{S} = \left(S \times \hat{d}\right)^{\gamma} \quad [6]$$

where $\hat{S}$ is the gamma scaled S channel, γ is the scaling value and $\hat{d}$ is the thresholded difference channel mask. The value of γ varies depending on the image information and in this work $\gamma = -\log_2(\sigma)$ (Rahman, et al., 2016) has been used to calculate γ value of individual image, where σ is the standard deviation of S.

The enhanced transmittance in HSV domain was then reverted back to YCbCr color space and has been used to assess the distortion free image using the estimated Bg, T and a constant 1×3 vector t_0 as shown in Equation [7] (Hou, et al., 2020) where J is the contrast enhanced image in YCbCr color space. It can be noted here that values of t_0 in this work were set as [0.8 0.8 0.5] and it was arrived by trial and error with about 200 image samples from different image databases. Finally, the image was converted back to its native RGB format using standard conversion formulae. The proposed method is consolidated as a flowchart in Figure 2.

$$\underset{c \in \text{YCbCr}}{J} = \left(\underset{c \in \text{YCbCr}}{Bg} - \left(\underset{c \in \text{YCbCr}}{I} - \left(Bg - \max_{c \in \text{YCbCr}}(T, t_0) \right) \right) \right) \quad [7]$$

In this work the initial population of 10 bats (initial solutions) found to be optimal through trial and error with different number of bats. The length of the solution was 256 since the DCT domain histogram was the initial position of individual bat. The initialization of individual bat position was random but generated within the range of frequencies present in the image under consideration. The values of initial pulse frequencies $f_{\min}$ and $f_{\max}$ were set as 0 and 1, respectively. The values for both the constants α and β were set as 0.92. The maximum number of iterations was set as 100. Similarly, the loudness parameter A was initiated randomly with $A_{\min}$ and $A_{\max}$ and values as 0 and 1, respectively, where resulting $A_{\min}$ interprets the bat has reached the prey and not emitting any sound. The presented method has been realized using Matlab® in Windows® platform.

2.3 Image quality evaluation

Objective evaluations were performed against five popular image quality assessment metrics; image entropy (Wang and Ye, 2005), patch-based contrast quality index (PCQI) (Wang, et al., 2015), natural image quality evaluator (NIQE) (Mittal, Soundararajan and Bovik, 2013), contrast enhancement factor (CEF) and colorfulness (Veluchamy and Subramani, 2020). The choice of these metrics among many others was towards covering different aspects of the image quality. For instance, entropy provides measure of information fidelity while PCQI is towards contrast distortion. Similarly, NIQE is

a blind technique where no reference image is presented to the evaluation. In combination, these metrics can provide information about an overall quality of the image. During evaluation the performance is judged by their values, in paticular, for entropy, PCQI, CEF and colorfulness higher values indicate better results while for NIQE lower values indicate better results.

3. Results

The test of performance has been performed with images from standard databases (Ponomarenko, et al., 2009; Larson and Chandler, 2010; SIPI, n.d.). Figure 3 shows the histogram of the transmittance estimations of the input images, narrowness and biased nature to either side of the histogram. After the optimization the histograms of the resulting transmittance estimation are visibly well distributed in the available tonal levels, which undoubtedly improves the contrast as shown in Figure 3.

Figure 4 shows a test image and resulting contrast enhanced output along with the original and enhanced *V* channel with their corresponding histograms in spatial domain. It can be seen that the image contrast has been visibly improved. The improvement is further evident from the *V* channel presentation where each element of the image is clearly visible due to improvement in contrast. For instance, the number '21' that is

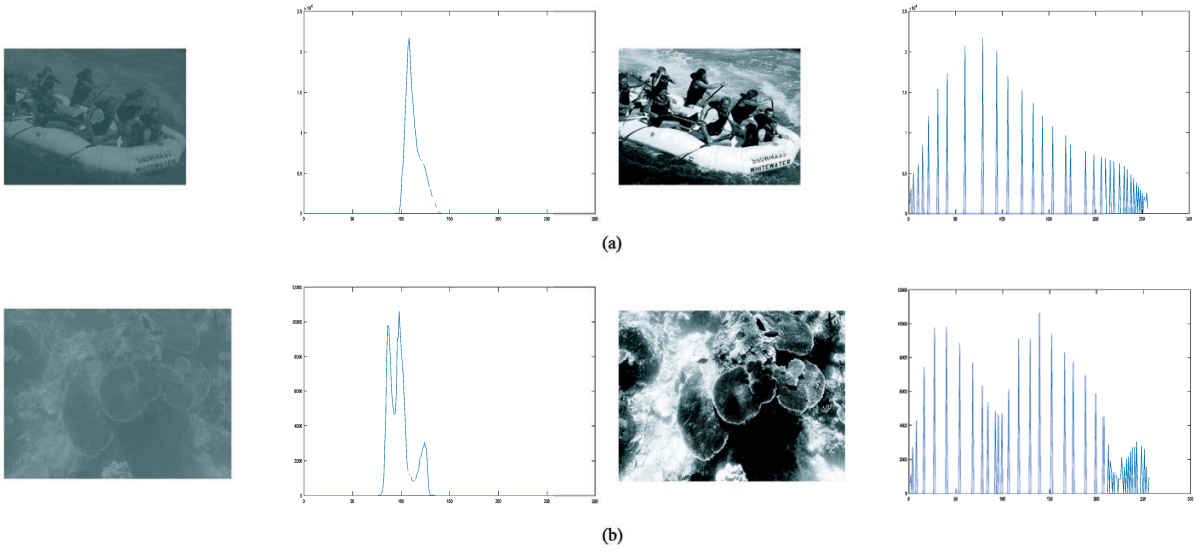

Figure 3: (Left to right) the original transmittance estimation, with corresponding histogram and enhanced transmittance with corresponding histogram for (a) atmospheric and (b) underwater images

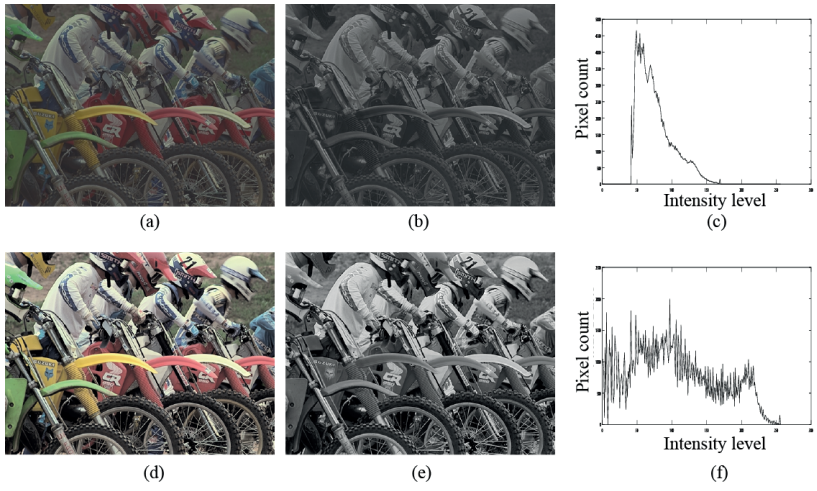

Figure 4: Result of proposed technique with 'motorcycle' image; (a) input low contrast image, (b) V channel of input image, (c) histogram of (b), (d) enhanced image, (e) V channel of enhanced image and (f) histogram of (e)

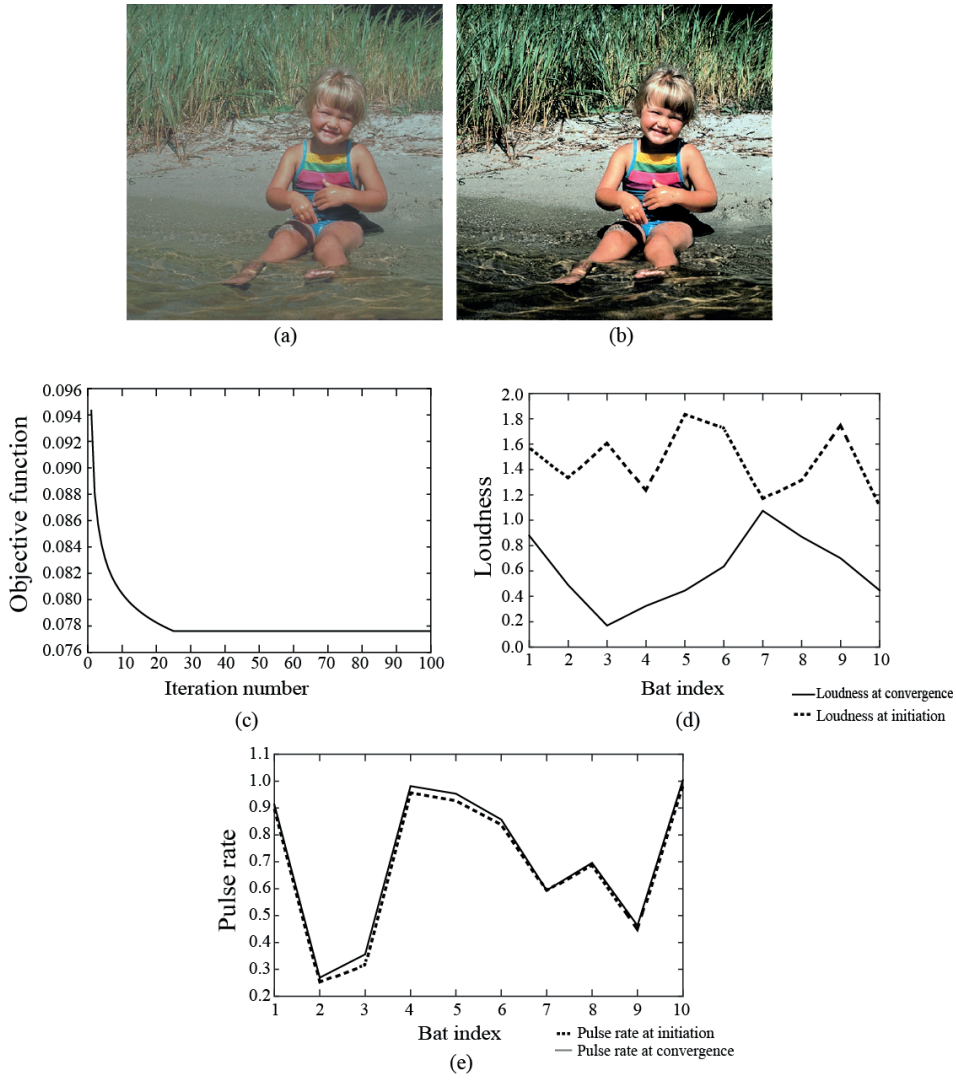

Figure 5: Result of presented method with 'child' image and BA dynamics; (a) input low contrast image, (b) enhanced image, (c) convergence curve, (d) loudness reduction and (e) pulse rate increment for each bat at the start and end of the BA

appearing on one of the helmets is not clearly visible in the input image as it is getting mixed with the background. But, as the contrast increases it becomes clearly visible in enhanced image. Such improvements can be crucial in case contrast enhancement is employed prior computer vision tasks for text or object identification. In the respective histogram plot it can also be observed that the enhancement causes substantial expansion of the histogram, which in turn provides better utilization of the entire intensity range instead of a narrow range like in original image.

In Figure 5 the BA dynamics have been presented, that are important for observing the performance of the algorithm and nature of convergence. Figure 5 clearly shows that the algorithm optimizes quickly and comes to a stable state. Also, the reduction of loudness and increase in pulse rate confirms the desired movement of BA. It also shows that the reported parameter setting can work well for the problem under consideration.

Figure 6 shows the results of proposed method with different contrast distortion levels with test images from CSIQ database. It can be seen that the performance of the proposed method is consistent across different distortion levels.

The colorfulness in the enhancement achieved with the presented method also confirms the naturalness. For instance, the results shown in Figure 6b show the sun ray feature prominently while not introducing excessive whiteness. The preservation of image features is also evident from results of Figure 6c where sharpness and edge retention is clearly visible.

Figure 6: Visual comparison of four pairs of test images at different levels of contrast

4. Discussions

In Figure 7a detailed retention analysis has been presented. It can be seen that in the image enhanced by presented technique the original image details are well retained. Also, the enlarged areas shown in Figures 7b and 7d portray that the presented method can avoid any visual artifacts due to over- or under-enhancement. The method can also provide good lightness distribution while retaining the white color.

To assess the suitability of the presented method across different types of applications, example of results obtained for low contrast underwater image has been shown in Figure 8. It can be seen that most of the techniques under consideration fail to enhance the image quality and suffer from black patches (GHE and CLAHE-DGC), over color effect and failing to produce a natural effect (MSR), degradation of sharpness (SECEDCT), etc. The AGCWHD, FDAHE-GC and proposed technique perform well for maintain the color and enhance the contrast. But among all techniques mentioned here, the proposed methodology performs much better in terms of contrast enhancement, preserving the brightness, balanced sharpness, and retention of image information.

The mean and standard deviation values for different metrics for 1000 images under consideration have been consolidated in Table 1. In this table the performance of the proposed method has been highlighted in bold font. It clearly shows competitive potential of the presented method against all the metrics under consideration. This also vouches the generosity of the presented method as other techniques have performed well against either of the metrics but not for all the metrics. However, room of improvement in terms of standard deviation values is open in the proposed method.

The PCQI maps shown in Figure 9 are binary images where black patches show the areas of contrast distortions. In this figure SECEDCT shows lots of black

Figure 7: Local improvement analysis with 'statue' image; (a) original low contrast image, (b) the region to focus, (c) enhanced image and (d) the corresponding region shown in (b)

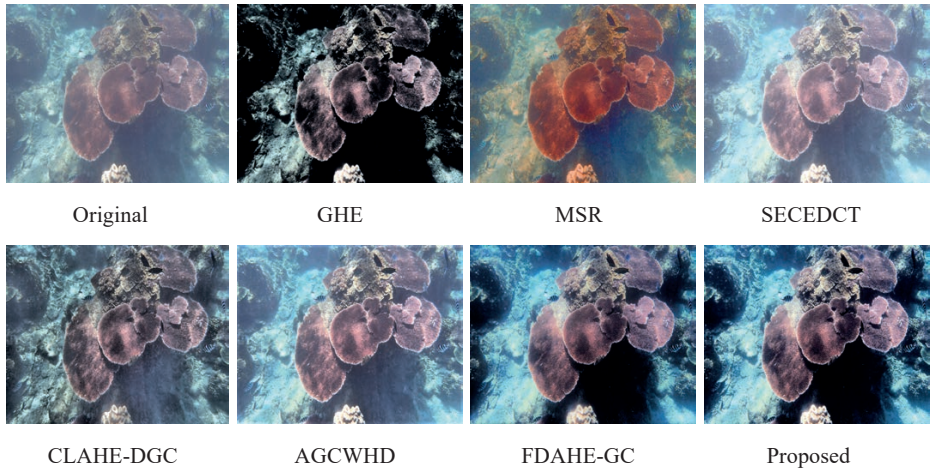

Figure 8: Results of different algorithms with 'underwater' image

Table 1: Objective evaluation of results using the proposed BA method (μ stands for mean value, and σ for standard deviation)

	Methods													
	GHE		**MSR**		**SECDCT**		**CLAHE-DGC**		**AGCWHD**		**FDAHE-GC**		**Proposed**	
Images	***μ***	***σ***	***μ***	***σ***	***μ***	***σ***	***μ***	***σ***	***μ***	***σ***	***μ***	***σ***	***μ***	***σ***
Entropy	7.36	0.66	7.48	0.68	7.34	0.62	7.42	0.52	7.53	0.62	7.62	0.82	**7.61**	**0.60**
PCQI	1.11	0.10	1.02	0.09	1.06	0.10	1.16	0.10	1.15	0.08	1.07	0.10	**1.18**	**0.12**
NIQE	3.64	1.41	3.51	1.14	3.55	1.60	3.65	1.24	3.58	1.20	3.63	1.33	**3.53**	**1.01**
CEF	1.15	0.08	0.98	0.06	0.82	0.05	0.96	0.06	0.86	0.05	1.06	0.06	**1.25**	**0.06**
Colorfulness	11.30	1.11	20.72	1.20	13.90	1.02	12.24	1.09	14.68	1.05	17.81	1.07	**21.40**	**1.10**

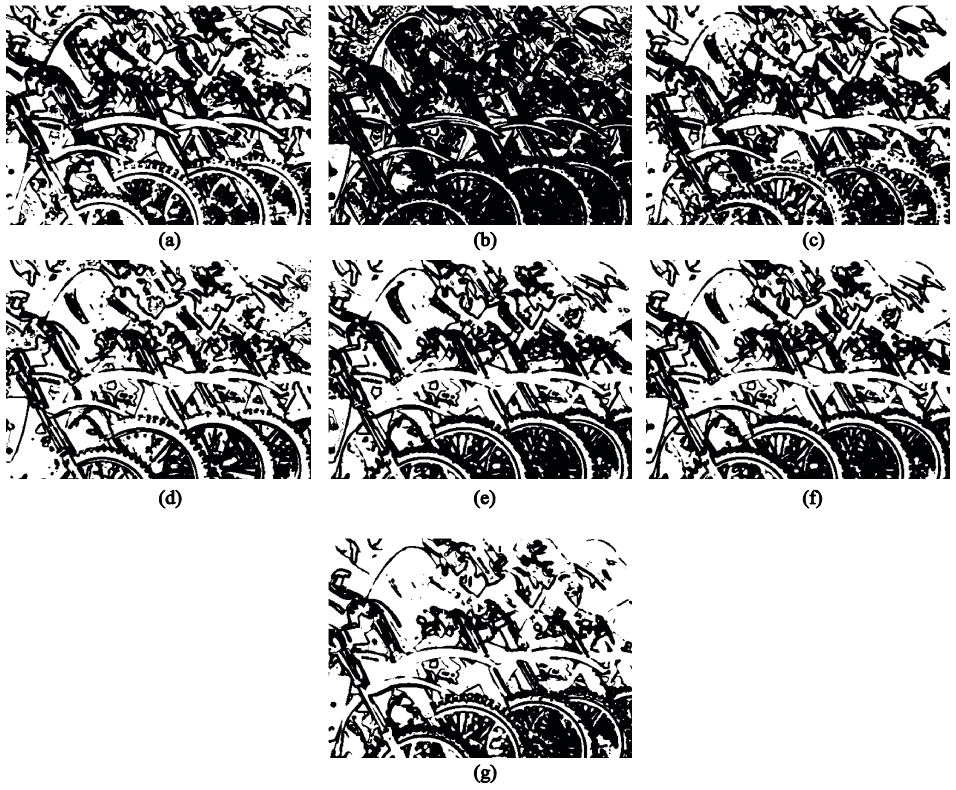

Figure 9: PCQI map (black pixels indicate PCQI < 1); (a) MSR, (b) SECEDCT, (c) FDAHE-GC, (d) AGCWHD, (e) GHE, (f) CLAHE-DGC, and (g) proposed BA method

patches representing PCQI < 1 and contrast distortion causing artificial appearance in the resulting image. Similarly, AGCWHD shows a considerably lower amount of black patches causing better output in terms of resulting contrast distortions. Proposed technique provides much lower distortions in most of the areas, which causes a higher mean-PCQI value. The MSR and FDAHE-GC show almost similar amount of distortion, whereas CLAHE-DGC and GHE perform little bit better in the tires of the motorcycles.

5. Conclusion

A new concept called DCE has been presented in the paper towards estimation of transmittance assessment. The transmittance enhancement has been proposed in HSV color space and optimization of DCT of the histogram using BA. The fast convergence of the BA provides acceptable processing time and the model based dynamics imparts higher possibility of generalization across different imaging media with the presented model.

The work can be further extended to application in contrast enhancement of medical images where the imaging model is different from the reported ones. The possibilities of improvement can be explored with other bio-inspired optimization algorithms, a more robust fitness or objective function and inclusion of multiple objective paradigms. Considering the possible future scopes the competitive results of the presented method vouch for its potential as a possible addition to the existing standard contrast enhancement method.

Data availability statement

Used images from databases freely available in public domain.

Conflict of interest statement

There is no conflict of interest identified for this article.

References

Akkaynak, D., Treibitz, T., Shlesinger, T., Loya, Y., Tamir, R. and Iluz, D., 2017. What is the space of attenuation coefficients in underwater computer vision? In: *2017 IEEE Conference on Computer Vision and Pattern Recognition (CVPR)*. Honolulu, HI, USA, 21–26 July 2017, pp. 568–577. https://doi.org/10.1109/CVPR.2017.68.

Asokan, A., Popescu, D.E., Anitha, J. and Hemanth, D.J., 2020. Bat algorithm based non-linear contrast stretching for satellite image enhancement. *Geosciences*, 10(2): 78. https://doi.org/10.3390/geosciences10020078.

Atta, R. and Ghanbari, M., 2013. Low-contrast satellite images enhancement using discrete cosine transform pyramid and singular value decomposition. *IET Image Processing,* 7(5), pp. 472–483. https://doi.org/10.1049/iet-ipr.2013.0083.

Celik, T., 2012. Two-dimensional histogram equalization and contrast enhancement. *Pattern Recognition*, 45(10), pp. 3810–3824. https://doi.org/10.1016/j.patcog.2012.03.019.

Celik, T., 2014. Spatial entropy-based global and local image contrast enhancement. *IEEE transactions on image processing*, 23(12), pp. 5298–5308. https://doi.org/10.1109/TIP.2014.2364537.

Celik, T. and Li, H.-C., 2016. Residual spatial entropy-based image contrast enhancement and gradient-based relative contrast measurement. *Journal of Modern Optics*, 63(16), pp. 1600–1617. https://doi.org/10.1080/09500340.2016.1163427.

Chang, Y., Jung, C., Ke, P., Song, H. and Hwang, J., 2018. Automatic contrast-limited adaptive histogram equalization with dual gamma correction. *IEEE Access*, 6, pp. 11782–11792. https://doi.org/10.1109/ACCESS.2018.2797872.

Das, S., Gulati, T. and Mittal, V., 2015. Image contrast enhancement using AGCWD with region based enhancement. *International Journal of Applied Engineering Research*, 10(11), pp. 30109–30119.

Dhal, K.G., Das, A., Ghoshal, N. and Das, S., 2018. Variance based brightness preserved dynamic histogram equalization for image contrast enhancement. *Pattern Recognition and Image Analysis*, 28(4), pp. 747–757. https://doi.org/10.1134/S1054661818040211.

Eswar Reddy, M. and Ramachandra Reddy, G., 2019. Recursive median and mean partitioned one-to-one gray level mapping transformations for image enhancement. *Circuits, Systems, and Signal Processing,* 38(7), pp. 3227–3250. https://doi.org/10.1007/s00034-018-1013-3.

Fashandi, H., Peters, J. and Ramanna, S., 2009. L2 norm length-based image similarity measures: concrescence of image feature histogram distances. In: *Proceedings of the 11th IASTED International Conference on Signal and Image Processing (SIP 2009)*. Honolulu, HI, USA, 17–19 August 2009. ACTA Press, pp. 178–185.

Gad, A.G., 2022. Particle swarm optimization algorithm and its applications: a systematic review. *Archives of Computational Methods in Engineering*, 29(5), pp. 2531–2561. https://doi.org/10.1007/s11831-021-09694-4.

Hou, G., Zhao, X., Pan, Z., Yang, H., Tan, L. and Li, J., 2020. Benchmarking underwater image enhancement and restoration, and beyond. *IEEE Access*, 8, pp. 122078–122091. https://doi.org/10.1109/ACCESS.2020.3006359.

Kallner, A., 2018. Laboratory statistics: methods in chemistry and health sciences. 2nd ed. Amsterdam, Oxford, Cambridge: Elsevier. https://doi.org/10.1016/B978-0-12-814348-3.00001-0.

Kandhway, P., Bhandari, A.K. and Singh, A., 2020. A novel reformed histogram equalization based medical image contrast enhancement using krill herd optimization. *Biomedical Signal Processing and Control*, 56: 101677. https://doi.org/10.1016/j.bspc.2019.101677.

Larson, E.C. and Chandler, D.M., 2010. Most apparent distortion: full-reference image quality assessment and the role of strategy. *Journal of Electronic Imaging*, 19(1): 011006. https://doi.org/10.1117/1.3267105.

Lee, C.-H., Lien, C.-C. and Han, C.-C., 2014. Color image enhancement using multiscale Retinex and image fusion techniques. *World Academy of Science, Engineering and Technology International Journal of Computer and Information Engineering*, 8(10), pp. 1796–1802. https://doi.org/10.5281/zenodo.1096355.

Luque-Chang, A., Cuevas, E., Pérez-Cisneros, M., Fausto, F., Valdivia-González, A. and Sarkar, R., 2021. Moth swarm algorithm for image contrast enhancement. *Knowledge-Based Systems,* 212: 106607. https://doi.org/10.1016/j.knosys.2020.106607.

Mittal, A., Soundararajan, R. and Bovik, A.C., 2013. Making a "completely blind" image quality analyzer. *IEEE Signal Processing Letters,* 20(3). pp. 209–212. https://doi.org/10.1109/LSP.2012.2227726.

Mustafa, W.A. and Kader, M.M.M.A., 2018. A review of histogram equalization techniques in image enhancement application. *Journal of Physics: Conference Series*, 1019: 012026. https://doi.org/10.1088/1742-6596/1019/1/012026.

Nishad, PM. and Chezian, R.M., 2013. Various colour spaces and colour space conversion algorithms. *Journal of Global Research in Computer Science*, 4(1), pp. 44–48.

Oyelade, O.J., Oladipupo, O.O. and Obagbuwa, I.C., 2010. Application of k-means clustering algorithm for prediction of students' academic performance. *International Journal of Computer Science and Information Security*, 7(1), pp. 292–295 (arXiv:1002.2425 abs/1002.2425). https://doi.org/10.48550/arXiv.1002.2425.

Panetta, K.A., Xia, J. and Agaian, S.S., 2012. Color image enhancement based on the discrete cosine transform coefficient histogram. *Journal of Electronic Imaging*, 21(2): 021117. https://doi.org/10.1117/1.JEI.21.2.021117.

Petro, A.B., Sbert, C. and Morel, J.-M., 2014. Multiscale Retinex. *Image Processing On Line,* 4, pp. 71–88. https://doi.org/10.5201/ipol.2014.107.

Ponomarenko, N., Lukin, V., Zelensky, A., Egiazarian, K., Astola, J., Carli, M. and Battisti, F., 2009. TID2008 – a database for evaluation of full-reference visual quality assessment metrics. *Advances of Modern Radioelectronics*, 10(4), pp. 30–45.

Rahman, S., Rahman, M.M., Abdullah-Al-Wadud, M., Al-Quaderi, G.D. and Shoyaib, M., 2016. An adaptive gamma correction for image enhancement. *EURASIP Journal on Image and Video Processing,* 35. https://doi.org/10.1186/s13640-016-0138-1.

Samani, A., Panetta, K. and Agaian, S., 2016. Contrast enhancement for color images using discrete cosine transform coefficient scaling. In: *2016 IEEE Symposium on Technologies for Homeland Security (HST)*. Waltham, MA, USA, 10–11 May 2016. IEEE. https://doi.org/10.1109/THS.2016.7568968.

Sheet, D., Garud, H., Suveer, A., Mahadevappa, M. and Chatterjee, J., 2010. Brightness preserving dynamic fuzzy histogram equalization. *IEEE Transactions on Consumer Electronics*, 56(4), pp. 2475–2480. https://doi.org/10.1109/TCE.2010.5681130.

SIPI, n.d. The USC-SIPI image database. [online] Available at: <http://sipi.usc.edu/database/> [Accessed March 2021].

Tsai, C.-C., Lin, C.-Y. and Guo, J.-I., 2019. Dark channel prior based video dehazing algorithm with sky preservation and its embedded system realization for ADAS applications. *Optics Express*, 27(9), pp. 11877–11901. https://doi.org/10.1364/OE.27.011877.

Veluchamy, M. and Subramani, B., 2019. Image contrast and color enhancement using adaptive gamma correction and histogram equalization. *Optik*, 183, pp. 329–337. https://doi.org/10.1016/j.ijleo.2019.02.054.

Veluchamy, M. and Subramani, B., 2020. Fuzzy dissimilarity color histogram equalization for contrast enhancement and color correction. *Applied Soft Computing*, 89: 106077. https://doi.org/10.1016/j.asoc.2020.106077.

Vijayalakshmi, D., Nath, K.N. and Acharja, O.P., 2020. A comprehensive survey on image contrast enhancement techniques in spatial domain*. Sensing and Imaging*, 21(1): 40. https://doi.org/10.1007/s11220-020-00305-3.

Wang, X. and Chen, L., 2018. Contrast enhancement using feature-preserving bi-histogram equalization. *Signal, Image and Video Processing,* 12(4), pp. 685–692. https://doi.org/10.1007/s11760-017-1208-2.

Wang, J.-S. and Li, S.-X., 2019. An improved grey wolf optimizer based on differential evolution and elimination mechanism. *Scientific Reports,* 9: 7181. https://doi.org/10.1038/s41598-019-43546-3.

Wang, S., Ma, K., Yeganeh, H., Wang, Z. and Lin, W., 2015. A patch-structure representation method for quality assessment of contrast changed images. *IEEE Signal Processing Letters,* 22(12), pp. 2387–2390. https://doi.org/10.1109/LSP.2015.2487369.

Wang, C. and Ye, Z., 2005. Brightness preserving histogram equalization with maximum entropy: a variational perspective. *IEEE Transactions on Consumer Electronics,* 51(4), pp. 1326–1334. https://doi.org/10.1109/TCE.2005.1561863.

Xu, Z.J., Wang, Z.Z. and Lu, Q., 2011. Research on image watermarking algorithm based on DCT. *Procedia Environmental Sciences*, 10, Part B, pp. 1129–1135. https://doi.org/10.1016/j.proenv.2011.09.180.

Yue, X. and Zhang, H., 2021. A novel industrial image contrast enhancement technique based on an improved ant lion optimizer. *Arabian Journal for Science and Engineering*, 46(4), pp. 3235–3246. https://doi.org/10.1007/s13369-020-05148-4.

Zhang, S., Wang, T., Dong, J. and Yu, H., 2017. Underwater image enhancement via extended multi-scale Retinex. *Neurocomputing*, 245, pp. 1–9. https://doi.org/10.1016/j.neucom.2017.03.029.

Appendix: Pseudo code of BA

Initial population of bat X (x_1, x_2, …, x_n) and associated initial velocity of each bat (v_1, v_2, …, v_n)
Generation
Fitness calculation of each bat using the objective function φ (as described in section 2.2.1)
and finding the best solution (x_{best})
Initializing initial pulse frequencies (f_i), pulse rate (r_i), loudness (A_i)
and a set of random numbers ($rn \in [-1,1]$) with normal distribution
while (number of iteration (i) < maximum number of iteration or stopping criteria met)
    Update velocity of bat using $v_i^t = v_i^{t-1} + (x_i^{t-1} - x_{best})f_i$
    where, $f_i = f_{\min} + (f_{\max} - f_{\min})\beta$; ($\beta \in [0,1]$)
    Update location of bat using $x_i^t = x_i^{t-1} + v_i^t$
    if $\left(r_i < rand(0,1)\right)$
    Generate a local solution around the existing solution using
    $x_i^t(new) = x_i^t(old) + \varepsilon\overline{A_t}$ where, ($\varepsilon \in rand[-1,1]$) and $\overline{A_t}$ is the mean of all A at iteration t
    end if
    Generate a new solution by random flying
    if $\left(rn_1 < A_i \; and \; fit(x_i^t) < fit(x_{best}^t)\right)$
    Accept new solution
    Increase pulse rate of the bat using $r_i^{t+1} = r_i^t\left(1 - \exp(-\gamma t)\right)$ where, $\gamma > 0$ is a constant
    value that controls the movement of bat
    Decrease loudness using
    $A_1^{t+1} = \alpha A_1^t$ where $\alpha > 0$ is a constant value controls the movement of bat
    end if
    Find the new best location of the bat (x_{best}^{t+1})
end while

List of abbreviations

2DHE	Two-dimensonal histogram equalization
ABC	Artificial bee colony optimization
ACO	Ant colony optimization
AGC	Adaptive gamma correction
AGCWD	Adaptive gamma correction weighted distribution
AGCWHD	Adaptive gamma correction with weighted histogram distribution
AHE	Adaptive histogram equalization
AMSR	Adaptive multi scale Retinex
BA	Bat algorithm
BBHE	Brightness preserving bi-histogram equalization
CEF	contrast enhancement factor
CEFPBHE	Contrast enhancement using feature preservation bi-histogram equalization
CLAHE	Contrast limited adaptive histogram equalization
CLAHE-DGC	Contrast-limited adaptive histogram equalization with dual gamma correction
CSIQ	Categorical image quality database
DCE	Difference channel estimation
DCP	Dark channel priory
DCT	Discrete cosine transform
DCTCH	Discrete cosine transform coefficient histogram
DCTCS	Discrete cosine transform coefficient scaling
DCT-SVD	Discrete cosine transform pyramid and singular value decomposition
DFHE	Dynamic fuzzy histogram equalization
DHE	Dynamic histogram equalization
DSIHE	Dualistic sub-image histogram equalization
FDAHE-GC	Fuzzy dissimilarity adaptive histogram equalization with gamma correction
FDH	Fuzzy dissimilarity histogram
GHE	Global histogram equalization
HSV	Hue, saturation, value
MMBEBHE	Minimum mean brightness error bi-histogram equalization
MSR	Multi scale Retinex
NIQE	Natural image quality evaluator
PCQI	Patch-based contrast quality index
PSO	Particle swarm optimization
RESECEDCT	Residual spatial entropy based contrast enhancement using discrete cosine transform
RMMGHT	Recursive median and mean partitioned one-to-one grey level mapping transformations for image enhancement
SECEDCT	Spatial entropy-based contrast enhancement in discrete cosine transform
SSR	Single scale Retinex
VBBPDHE	Variance-based brightness preserved dynamic histogram equalization for image contrast enhancement

JPMTR-2216
DOI 10.14622/JPMTR-2216
UDC 004.93|77.05|7.02

Research paper | 171
Received: 2022-06-29
Accepted: 2022-12-27

Use of ArUco markers for image registration of photographs and influence of camera tilt on process performance

Veronika Štampfl and Jure Ahtik

Chair of Information and Graphic Arts Technology,
Department of Textiles, Graphic Arts and Design,
Faculty of Natural Sciences and Engineering, Ljubljana, Slovenia

veronika.stampfl@ntf.uni-lj.si
jure.ahtik@ntf.uni-lj.si

Abstract

Image registration is widely used in the field of graphic technology, from printing processes to research. In order to successfully align two images, image sections must be recognized. In printing, simple linear markers can be used for alignment, while advanced visual systems use fiducial markers, such as ArUco markers, for specific position recognition. These can be applied to any surface and are quickly recognized by open-source algorithms. This gives us the ability to recognize any visually perceived surface and align it with the target image. This research focuses on the applicability of ArUco markers as reference points for image registration of photographs of flat, uniform surfaces. The camera tilt position was adjusted in four combinations to mimic the imperfect positioning of the camera relative to the observed surface. Twelve marker combinations were tested, varying in size, number, and positioning. Research has shown that ArUco markers are suitable as reference points for image registration, but in specific combination of size and position. General guidelines for their use have been established.

Keywords: position registration, photo-alignment, pattern recognition, fiducial markers

1. Introduction

Image registration is an important part of various processes in graphic technology. Most commonly, it is used to align separations during the printing process, where the operator interacts with the press to achieve perfect alignment of the separations and thus sharp colour reproduction (Kipphan, 2001). During print quality control, certain visual systems can monitor the quality of prints or even the press itself. Image registration is later on used to combine data from different cameras or overlap the acquired data with intended result (Villalba-Diez, et al., 2019). In postpress, for example in packaging, the technician checks the alignment of printed sheet according to the positioning marker and sets the CNC cutting device accordingly (Esko-Graphics Kongsberg AS, 2018).

Another important example of the use of image alignment in graphic technology is any type of research where data acquisition is done with imaging systems such as cameras and microscopes (Štampfl and Ahtik, 2022; Leskovšek, et al., 2019). Consumer-based cameras are often used in research purposes since photography is an approachable technique for capturing visual data. While performing image analysis of captured data, a comparison of two images is often needed to extract different data between two stages within the research. If maintaining camera position in relation to observed scene is not possible, image registration is mandatory, since it enables image alignment and further comparison of sequential images. Captured images can be manually aligned based on our visual perception, but in cases with a large number of images, automatic alignment methods are applicable. Image registration in these cases is based on certain image features or predefined areas, such as fiducial markers (Zakiev, et al., 2020).

With camera equipment evolving, integrated software takes care of the most critical settings to get an appropriately exposed image. This often eliminates the necessary understanding of ISO, white balance, aperture, and shutter speed settings, and even having the ability to focus on the desired point. However, influences of spherical and chromatic aberrations, colour profiles of the device, properties of lighting, its position, and the position of the camera are often overlooked or are not given enough attention (Ray, 2002; Opaka, et al., 2013; Kim, et al., 2011; Jackman, 2010; Keskinen, et al., 2019).

In this research, we determine the performance of ArUco markers as orientation points for image registration of photographs of flat surfaces, and the influence of camera inclination on the performance of open-source image registration algorithm when using ArUco markers as reference points. Different combinations of markers' positions, their amount and size are tested under different camera inclinations and guidelines are proposed.

2. Image registration and markers

Alignment of images is present in all research areas that deal with image processing in some way. When registering images, we always need a reference image to serve as a target for aligning the test image. Through registration, we can compose images into larger images, which we call mosaicing, we can overlay images taken at different times and thus monitor changes, we can overlay them with reference models and ensure that the product matches the desired values, or we can overlay images taken with different devices, i.e., sensors (Cosman, 2012).

The images are written as a function of two values, $f(x,y)$, where the x and y coordinates are in 2D space and f is the intensity or pixel intensity. The pixel intensity of a greyscale image is also called the greyscale value, while colour images consist of as many images as there are channels. Thus, the RGB colour image consists of three images, each representing one of the colour channels R, G, and B, and represented as a greyscale image. Numerically, images are written as matrices of the values of the individual pixels. By calculating the transformation matrix of the test image, it is aligned with the reference image (Gonzales, Woods and Eddins, 2004).

There are several types of image deformation (Figure 1). Translation moves an area so that a straight line is mapped into a straight line with the same orientation and distance between the same pairs of points. Rotation rotates the area, changing the direction of the lines while keeping the distance the same. Scaling changes the distance between two points on the surface while the direction remains the same. The affine transformation includes all three of the above deformations as well as the directional deformation of the shape. The lines remain parallel, but the shape is no longer the same. One such example is a rectangle that transforms into a parallelogram. To align such a deformation, we need at least three markers in each image. In the bilinear transformation, the straight lines are preserved, but the image is mapped conically. We need four points on each image to align them. This type of mapping is also called homography (Hladnik and Muck, 2010; Kamoun and Joslove, 2019).

Methods for registering images in the image domain are, in general, divided into sparse and dense methods (Zhang, et al., 2019), also found under feature-based methods and area-based methods (Zitová and Flusser, 2003). In sparse methods, the main points, i.e., the features, are extracted from the reference and test images and the transformation matrix is determined based on the detected coordinates. Lines, such as edges, are most commonly used to align images, as are point features, such as corners, line cross sections, and the centroids of larger surfaces. Deshmukh and Bhosle (2011) therefore name these methods as point-mapping methods. The most common are corners, which can be selected manually or detected automatically via various algorithms, such as features from accelerated segment test (FAST), scale-invariant feature transform (SIFT), speeded-up robust features (SURF), and ORB, which is a combination of oriented FAST and rotated binary robust independent elementary features (BRIEF) (Zhang, et al., 2019).

Dense methods, unlike sparse, do not first search for points common to the reference and test images, but check the degree of similarity of each pixel of the reference and test images using methods to describe similarities or differences across the image. Therefore, they are also named area-based methods. After calculating the similarity of the image pairs, a transformation matrix is created, and the similarity indices are recalculated. Various similarity evaluation methods have been proposed, such as mutual information (MI), normalized cross-correlation coefficient (NCC), root-

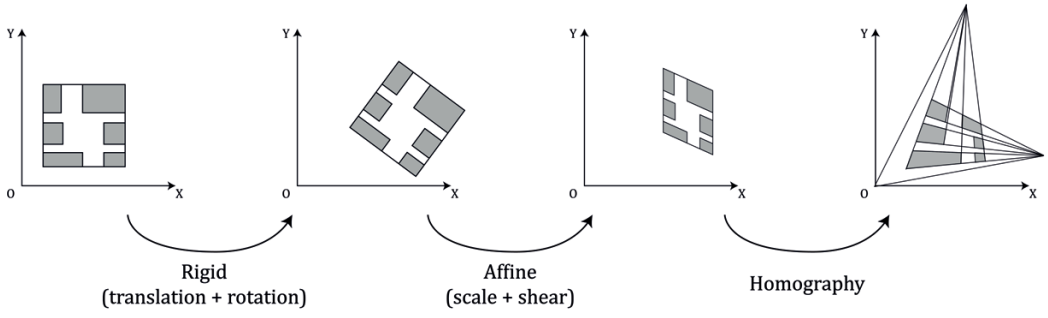

Figure 1: Types of image deformations (Kamoun and Joslove, 2019)

Figure 2: Fiducial marker types: Intersense (a), CyberCode (b), VisualCode (c), ReacTIVision (d), ARToolKit (e), Matrix (f), ARTag (g), ARToolKit Plus (h), AprilTags (i), ArUco (j) (Garrido-Jurado, et al., 2016)

mean-square-error (RMSE), and peak signal to noise ratio (PSNR). However, it should be noted that the latter two methods are highly dependent on the uniformity of illumination and may provide unusable results for unevenly illuminated test surfaces. The final transformation matrix is difficult to determine precisely, so artificial intelligence methods are used for this purpose (Zitová and Flusser, 2003; Zhang, et al., 2019).

In some cases, histogram equalisation can be used to increase image contrast and allow better detection of key elements for image registration and further analysis. In their study, Kumar Mondal, Chatterjee and Tudu (2021) demonstrate the quality of histogram equalisation methods and algorithms using Fourier spectrum analysis of greyscale test images and their binarization.

Fiducial markers were originally developed for augmented reality, where systems are used to identify and track visual areas. The use of markers has expanded to other areas, particularly robotics and drones, where markers must be robust and detectable by visual systems, economically accessible, and capable of accurate detection in 3D space (Lightbody, Krajník and Hanheide, 2017). They consist of unique patterns that, in combination with the associated algorithm, enable the identification of individual marks. The algorithms are adapted to each type of label as they differ in size, resolution, and shape (Fiala, 2010). The most common is the use of square markers with a black border, which improves the quality and speed of their recognition. Their greatest advantage is the four corner points, which allow their position to be determined quickly and easily, and often a single marker is sufficient for identification. Some types of the most common markers are shown in Figure 2 (Garrido-Jurado, et al., 2016).

3. Methods

This experiment was designed to evaluate whether ArUco markers are an appropriate tool to set up as registration markers on the surfaces of our research lab, which is often used as testing environment for capturing visual data where image registration is needed for further image analysis. Twelve combinations of markers' size, position and quantity were tested along with four camera inclinations, in order to determine the influence of inaccurate sensor position on the performance of image registration with ArUco markers.

3.1 Markers and reference images

ArUco markers allow their fast generation and detection via already established algorithms, which a user can control with code written in Python programming language. It is also possible to determine the dimensions of the markers and the size of the matrix containing them (OpenCV, 2022). In the experiment we used markers from the already existing *aruco.DICT_6x6_250* dictionary, which is available in open-source library OpenCV. We used the first six markers, labelled with IDs 0, 1, 2, 3, 4, and 5, with an internal marker matrix of 6 × 6 bits and 700 pixels per side, generated using Python.

Generated ArUco markers in various combinations of size, number, and position, as shown in Table 1, were arranged on A4 faces, the centre points of markers being 3 cm away from the edge of the paper sheet, 24 cm apart in *x* direction and 16 cm apart in *y* direction. The layouts were exported as PNG images, which were used as reference images for image registration in this experiment. A set of reference images can be seen in Figure 3.

Figure 3: Reference images for image registration; first row large markers: 2L_DIAG (a), 2L_LEFT (b), 2L_TOP (c), 4L (d), 5L(e), and 6L (f); in second row small markers (marked S instead L as in Table 1)

Table 1: Marker combinations

Label	Size [mm]	Number of markers	Position
2L_DIAG	22	2	diagonally
2L_LEFT	22	2	left corners
2L_TOP	22	2	upper corners
4L	22	4	all corners
5L	22	5	all corners and centre
6L	22	6	all corners and additional marker on top and bottom
2S_DIAG	15	2	diagonally
2S_LEFT	15	2	left corners
2S_TOP	15	2	upper corners
4S	15	4	all corners
5S	15	5	all corners and centre
6S	15	6	all corners and additional marker on top and bottom

3.2 Test surfaces and image capture

To determine the success of aligning the test photographs with the reference images, we added a grid of dark squares to the latter. The comparison can be seen in Figures 4a and 4b. The files were exported to PDF formats, which were printed on A4 office paper using a Canon imageRUNNER 2530i printer. This produced a series of test surfaces, which were placed on a platform that allowed for tilt adjustment. We tested four inclination combinations of the platform by 10° along the *x*- axis (long edge) and *y*-axis (short edge). The combinations are listed in Table 2.

To calculate the differences between the aligned images and the reference surfaces, we reduced the saturation of the print files (Figure 4c) and saved them as PNG files. This was necessary because the printed files did not reach the same level of saturation as it was set in the print file.

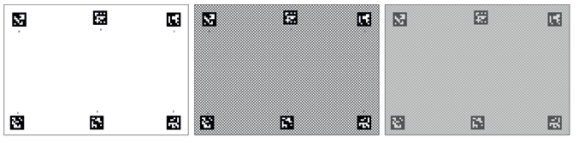

Figure 4: Reference image for image alignment (a), printing pattern (b), and reference image for calculating the degree of registration (c)

To illuminate the test areas, we used an LED strip with a colour temperature of 2700 K. Its shape corresponded to the shape of the test surface, and it was positioned 10 cm above the surface, which provided uniform illumination of the surface from above. Four series of photographs of 12 marker combinations were photographed with a Nikon D850 camera and a Nikkor 50 mm 1:1.4G lens at the same settings and a distance of 82 cm from the centre of the surface.

Table 2: Platform inclination combinations

Label extension	Inclination on *x* axis	Inclination on *y* axis
_REG	0°	0°
_X	10°	0°
_Y	0°	10°
_XY	10°	10°

3.3 Image processing and analysis

We wanted to perform the entire image processing process in one program, which we achieved using the Python programming language and the open-source libraries OpenCV, a collection of various functions and commands in the field of visual perception, the NumPy library, which allows array conversion, RawPy, which as part of the LibRaw libraries allows working with raw photo formats, and Pillow, an abbreviation for Python Imaging Library, which allows editing images.

We generated code that requires RAW photos of test areas, reference images for alignment, and reference images for calculating differences between input data. When we run the program code, it automatically saves intermediate results: generated ArUco markers, images with highlighted detected markers, aligned images, aligned images with equalised histogram, and final difference images. The entire code is divided into separate parts so that individual steps can be executed separately from the others. The individual parts are presented below with key components of the open-source Python code.

The first section of the code consists of import commands for used libraries. It also defines a matrix of strings, which are image names within one folder on a local disk. This enables the code use even with additional test images. In our case, those were strings found in Table 1 under Label.

The second section imports a dictionary of ArUco markers. They are defined, along with their size and quantity, and saved into a local folder. Key code components:

```
aruco.Dictionary_get()
aruco.drawMarker()
```

The third section ensures image registration. Reference image is imported and ArUco markers recognised. Test photographs are converted from RAW format to JPG,

taking into account the white balance setting. On each imported test image, ArUco markers are detected, marked, and saved as separate images, enabling intermediate control of the process. Detected ArUco markers on test images provide reference points, which are aligned to the reference points on the reference image. Transformation matrix is calculated based on reference points alignment and used to align test image to reference image. The aligned image is saved as a new JPG file. Key code components:

```
rawpy.imread()
aruco.detectMarkers()
aruco.drawDetectedMarkers()
cv2.findHomography()
cv2.warpPerspective()
```

The fourth section equalizes histograms of aligned images from the previous section and reference images for difference calculations (Figure 4c). This ensures comparability of images, since the brightest and the darkest part of the image is always found in ArUco marker, which serves as top and bottom threshold. Contrast limited adaptive histogram equalization (CLAHE) algorithm is used. Equalised images are saved for further processing as separate files. Key code components:

```
cv2.createCLAHE()
clahe.apply()
```

Fifth, and the last section of the code, subtracts the aligned images from their reference images, generating image differences. The function compares each pixel of the aligned image with its position on the reference image and returns the absolute difference. Difference images are saved as separate files and the quantities of pixels for each grey value are saved into a CSV file. Key code component:

```
ImageChops.difference
```

Pixel count for each grey value was plotted for every difference image, along with average pixel count values for each grey level, averaged for ArUco markers combinations and platform inclinations.

4. Results and discussion

The success rate of the tested photo-alignment method was observed by the number of pixels of each value. Black pixels (grey value is 0) indicate a 100 % match between the reference image and the photographed image, while white pixels with a value of 255 indicate a 0 % match. Grey values in between represent partial matches depending on the value.

In Table 3 black pixel counts of the averaged histograms are presented along with the calculated coverage percentage over entire image.

Table 3: Average values of black pixel count and percentage of black pixels

	Black pixels	
Averaged over	**Count**	**Percentage [%]**
REG	222 960	3.41
X	185 945	2.85
Y	196 220	3.00
XY	178 677	2.73
S	194 472	2.98
L	197 370	3.02
6	219 122	3.35
5	221 433	3.39
4	211 779	3.24
2_TOP	168 920	2.59
2_LEFT	171 607	2.63
2_DIAG	182 900	2.80

Figure 5 shows the histograms of the difference images for all test photographs. Similar trends can be observed in the histogram shapes, but there are differences in

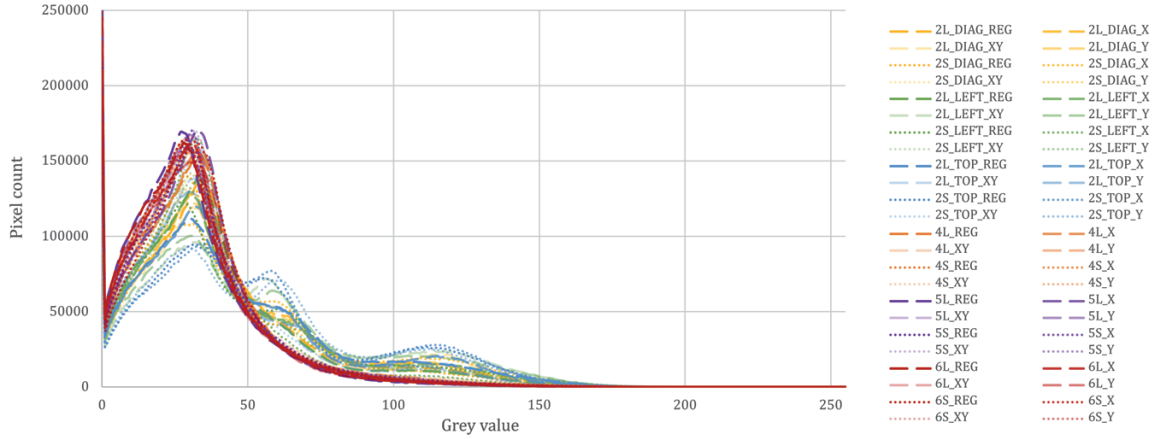

Figure 5: Histograms of difference images

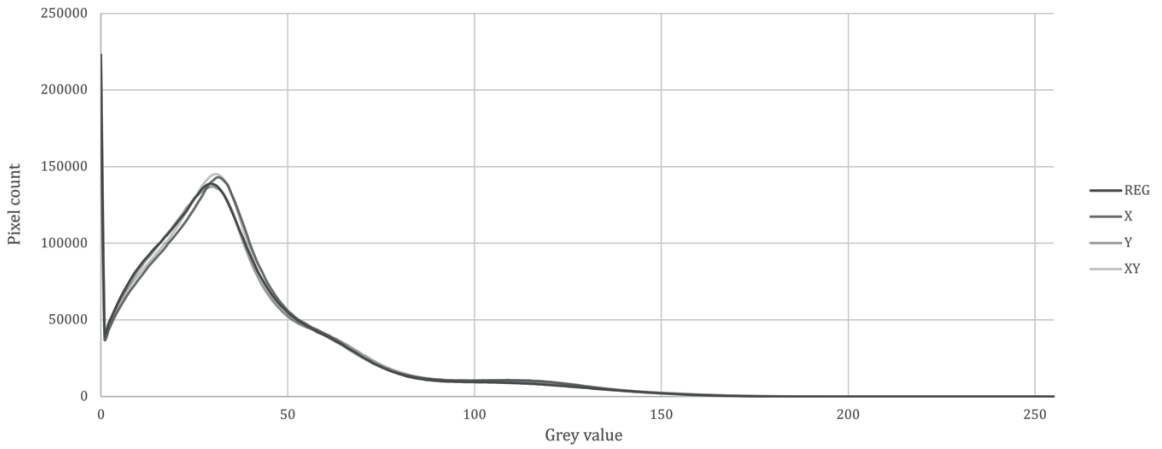

Figure 6: Histograms of averaged values at each grey value for platform inclination combinations

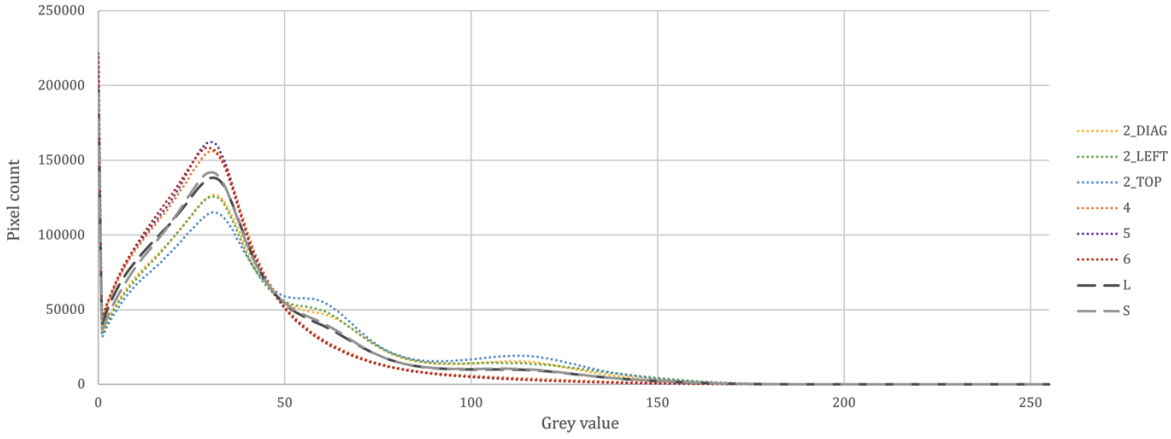

Figure 7: Histograms of averaged values at each grey value for individual marker combinations

the ranges of the function maxima. To better interpret the results, we calculated the average values of the histograms with respect to the observation angle of the photographed area (Figure 6) and individual marker patterns (Figure 7). Further, the number of dark and light pixels was calculated for the images, using the grey value of 50 as the threshold. Coefficient values are numerically presented in Table 4.

Table 4: Slope coefficient of the line between normalised values of pixel sum from grey level 0 to 50 and 51 to 255

	REG	**X**	**Y**	**XY**
S	−0.614	−0.568	−0.574	−0.636
L	−0.655	−0.572	−0.591	−0.569
6	−0.823	−0.798	−0.803	−0.649
5	−0.814	−0.789	−0.793	−0.797
4	−0.683	−0.762	−0.784	−0.726
2_TOP	−0.246	−0.250	−0.292	−0.560
2_LEFT	−0.476	−0.555	−0.348	−0.306
2_DIAG	−0.517	−0.349	−0.476	−0.443

The sums of pixel values for light (grey values 51–255) and dark pixels (grey value 0–50) was normalized and averaged for platform inclination and marker combination. The results are shown in Figure 8a, while in Figure 8b the slope coefficients of the line between normalized values for light and dark pixels are shown.

Figure 6 shows that there is not much difference between four combinations of platform inclinations, i.e., the parallelism of the camera to the photographed surface. This shows that the image registration method used is suitable for image registration of images taken with a camera tilted up to 10° in any plane. The larger number of black pixels (grey value 0) in the difference images corresponds to the lower second peaks of the histograms. Although the trends of all four histograms are similar, we can evaluate the results based only on the number of black pixels. The histograms averaged as REG have 3.41 % black pixels relative to the whole image, while X has 2.85 %, Y has 3.00 %, and XY has 2.73 %. This shows that images without tilt achieve better image registration levels, as the percentage is highest for REG. Instances with tilt across the *y*-axis (Y) have

0.15 % more black pixels than across the *x*-axis (X), indicating that image registration is more effective in instances averaged across Y. This is partly due to the different distances of the ArUco markers from the rotation axis. If you compare the coefficients for X and Y from Figure 8b, you can see that more accurate image registration is performed when the markers are further apart in the perpendicular direction to the tilt axis. This is most obvious in the cases with two markers, where 2_TOP and 2_DIAG give better results under condition Y, as one marker is 3 cm away from the tilt axis and the second 27 cm. Under condition X, the markers are 3 cm and 19 cm away from the tilt axis, giving less favourable results. This observation is also confirmed in the measurements for 2_LEFT, where for instance X, where the markers are 3 cm and 19 cm from the tilt axis, the image registration is better than in case Y, where both markers are 3 cm from the tilt axis and their relative distance is zero.

Figure 7 shows the averaged histograms of the difference images with respect to the size, amount, and position of the ArUco markers. Here, S and L represent the average histograms of the small and large markers, respectively. The shape of the histograms shows no obvious differences in the success of image registration as a function of marker size, and the same is true for the number of black pixels. However, a comparison of the coefficients from Figure 8b shows that large markers behave better in cases without tilt, as the coefficient is 0.041 lower than for the combination REG–S, while small markers behave better with tilt in both axes, with XY–S having a coefficient of −0.636 and XY–L −0.569, a difference of 0.067. With tilt in only one axis, *x* or *y*, there is not much difference between the results, in X only 0.004 in favour of the large markers and 0.017 in Y, again in favour of the same markers.

The averaged histograms from Figure 7 show large differences between the marker combinations with four, five, and six markers and those with only two. Differences can also be seen in the number of black pixels, with 4, 5 and 6 being closer together and forming one group, while 2_TOP, 2_LEFT and 2_DIAG form the second group, with the difference between 4 as the last in its group and 2_DIAG as the first in the other group being 0.44 %. The same trend of differences can be seen in the second peak of the averaged histograms, where the plots for 4, 5 and 6 are almost identical and the remaining three with two markers are much lower. Histograms for 4, 5 and 6 are decreasing gradually after grey level 50, while histograms for 2_TOP, 2_LEFT and 2_DIAG fluctuate. This suggests that image registration is less successful when two markers are used. The reasons for this have already been described in one of the previous sections and show how the position of the markers is also important.

As can be seen from the histograms in Figure 7 and the low coefficient values in Figure 8b, combinations with four, five, and six markers provide the best results regardless of platform tilt, but combinations with five markers provide the most consistent results even with platform tilt in both axes.

Combinations with six markers give the best results when the platform is not tilted or only tilted over one axis, while combinations with four markers show less

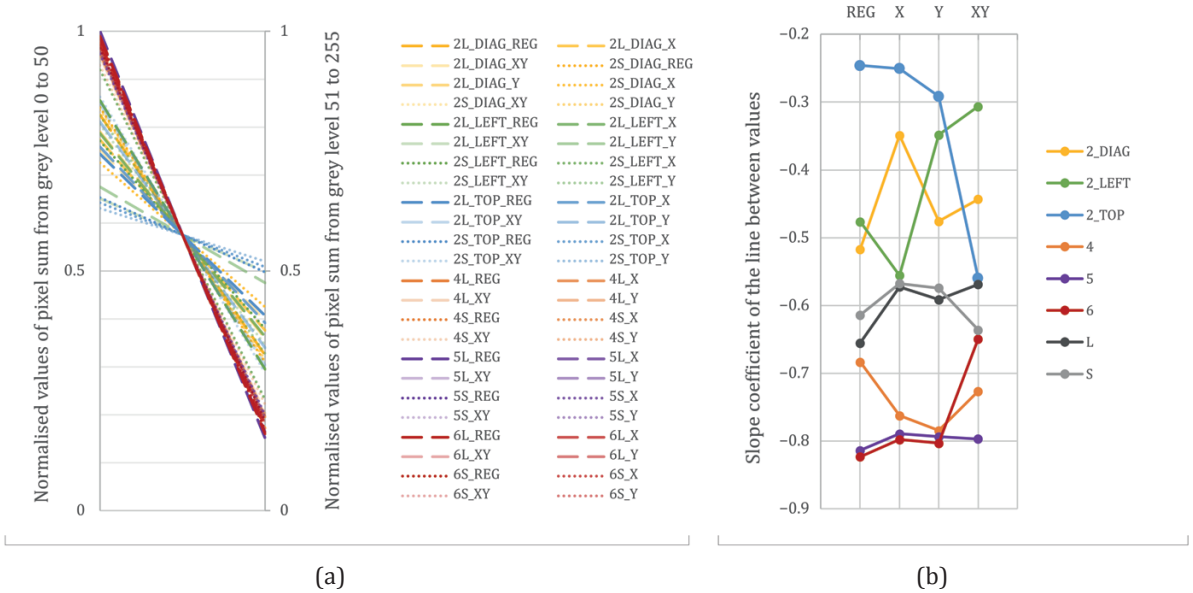

(a) (b)

Figure 8: Correlation of normalised values of pixel sums for grey levels 0 to 50 and 51 to 255, respectively (a), and slope coefficient of the line between values (b)

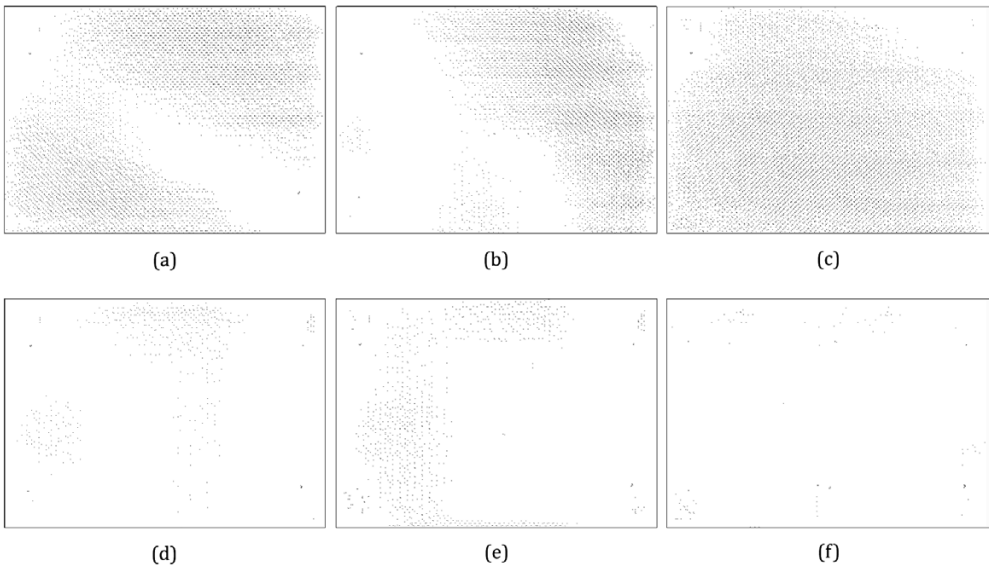

Figure 9: Inverted binarized difference images between reference images and test photos for series REG with large markers: 2L_DIAG (a), 2L_LEFT (b), 2L_TOP (c), 4L (d), 5L (e), and 6L (f)

successful image registration even in cases without platform tilt. This may be related to the fact that we did not use camera calibration methods. Therefore, spherical aberrations may still be present even though we used a lens with settings that ensure minimal aberrations of this type. An additional marker in the centre for marker combinations 5 and two additional markers on the long edges for marker combinations 6 provide intermediate control points that minimise the effect of spherical aberration.

These quantitative results can also be confirmed visually. Figure 9 shows difference images for test photos taken without the platform tilt (REG), using only large ArUco markers (L) for registration. The presented images were binarized at a threshold of 128 and inverted, to illustrate the areas of best image alignment. The black passages show the areas where image registration was less successful, which is especially visible in cases with two markers (Figures 9a, 9b, and 9c). In the 2_DIAG case, a brighter diagonal passage can be seen between the markers, indicating successful registration in that area, while the opposite corners of the image show a lower level of accurate registration. At 2_LEFT, registration is more successful on the left side of the image where the markers are located, while at 2_TOP it is more successful in the upper part of the image, again in the area of the markers, with the registration success rate decreasing with distance from the markers. Four markers provide much more uniform registration of the images, while five markers provide uniform alignment even in the centre of the image. Six markers increase the density of marker surface coverage and produce the most visually aligned image.

5. Conclusion

The study provided quantitative results on the success of the method of using ArUco tags to match photographs with prepared reference images. We found that two ArUco markers were insufficient for high-quality image alignment, regardless of their position on the test surface. Four, five and six markers on the test surface provide more consistent alignment, and the degree of success of the method depends on the position of the markers.

When using four markers, there are some deviations, which is due to the fact that the method is not able to eliminate spherical distortions caused by the photographic system. For this purpose, we suggest either calibrating the camera and including calibration profiles in the method or using a larger number of control points, i.e., markers. The five-marker method shows good results at all angles of image capture, while the most uniform image registration is provided by six ArUco markers, but not when tilted about both axes. Depending on the quantitative results and their confirmation by visual observation of the final images of the differences, we recommend the use of six markers on the observed surface, placed at regular intervals. We also recommend the use of larger markers, as they proved to be more reliable in most of the tested cases.

This method has proven to be efficient in image registration of two samples equipped with a specific array of ArUco markers. It allows the user to easily equip the observed surface with the markers, which can be quickly recognized by an open-source code available to any user.

Acknowledgements

This work was supported by the Slovenian Research Agency (Infrastructural Centre RIC UL-NTF).

References

Cosman, P., 2012. *Image registration*. [pdf] San Diego, University of California. Available at: <http://code.ucsd.edu/pcosman/regis2012.pdf> [Accessed 8 April 2022].

Deshmukh, M.P. and Bhosle, U., 2011. A survey of image registration. *International Journal od Image Processing*, 5(3), pp. 245–269.

Esko-Graphics Kongsberg AS, 2018. *User manual for Kongsberg XPA systems*. [pdf] Available at: <https://docs.esko.com/docs/en-us/Kongsberg_XPA/1.1/referenceguide/3168_User_Manual_XPA_us.pdf> [Accessed 24 November 2022].

Fiala, M., 2010. Designing highly reliable fiducial markers. *IEEE Transactions on Pattern Analysis and Machine Intelligence,* 32(7), pp. 1317–1324. https://doi.org/10.1109/TPAMI.2009.146.

Garrido-Jurado, S., Muñoz-Salinas, R., Madrid-Cuevas, F.J. and Medinca-Carnicer, R., 2016. Generation of fiducial marker dictionaries using mixed integer linear programming. *Pattern Recognition,* (51), pp. 481–491. https://doi.org/10.1016/j.patcog.2015.09.023.

Gonzales, R.C., Woods, R.E. and Eddins, S.L., 2004. *Digital image processing using MATLAB*. New Jersey: Pearson Education.

Hladnik, A. and Muck, T., 2010. *Obdelava digitalnih slik v grafiki, prvi del: osnove*. Ljubljana: Naravoslovnotehniška fakulteta, Oddelek za tekstilstvo.

Jackman, J., 2010. *Lighting for digital video and television.* 3rd ed. Oxford: Focal press, pp. 96–101.

Kamoun, E., and Joslove, J., 2019. Image registration: from SIFT to deep learning. *Sicara, Computer vision*, [blog] 16 July. Available at: <https://www.sicara.ai/blog/2019-07-16-image-registration-deep-learning> [Accessed 8 April 2022].

Keskinen, T., Mäkelä, V., Kallioniemi, P., Hakulinen, J., Karhu, J., Ronkainen, K., Mäkelä, J. and Turunen, M., 2019. The effect of camera height, actor behavior, and viewer position on the user experience of 360° videos. In: *IEEE Conference on Virtual Reality and 3D User Interfaces (VR).* Osaka, Japan, 23–27 March 2019. IEEE, pp. 423–430. https://doi.org/10.1109/VR.2019.8797843.

Kim, U.S., Lee, J.M., Kim, Y.M., Park, K.T. and Moon, Y.S., 2011. Photographic color reproduction based on color variation characteristics of digital camera. *KSII Transactions on Internet and Information Systems,* 5(11), pp. 2160–2174. https://doi.org/10.3837/tiis.2011.11.016.

Kipphan, H. ed., 2001. *Handbook of print media: technologies and production methods*. New York: Springer.

Kumar Mondal, S., Chatterjee, A. and Tudu, B., 2021. Image contrast enhancement using histogram equalization: a bacteria colony optimization approach. *Journal of Print and Media Technology Research,* 10(2), pp. 95–118. https://doi.org/10.14622/JPMTR-2103.

Leskovšek, M., Stankovič Elesini, U., Škerjanc, A., Vrabec, M., and Gabrijelčič Tomc, H., 2019. Making a 3D model of merino wool fibre with photogrammetric processing of SEM images. In: *MCM2019: proceedings from the 14th Multinational Congress on Microscopy*. Belgrade, Serbia, 15–20 September 2019. Belgrade, Serbia: University of Belgrade, Institute for Biological Research "Siniša Stanković", National Institute of Republic of Serbia, Serbian Society for Microscopy, pp. 53–55.

Lightbody, P., Krajník, T. and Hanheide, M., 2017. A versatile high-performance visual fiducial marker detection system with scalable identity encoding. In: *SAC '17: Proceedings of the Symposium on Applied Computing*. Marrakech, Morocco, 3–7 April 2017. New York, NY, USA: Association for Computing Machinery, pp. 376–282. https://doi.org/10.1145/3019612.3019709.

Opaka, U., Javoršek, A., Starešinič, M. and Javoršek, D., 2013. Analysis of colour profile quality for digital camera Nikon D50. *Tekstilec*, 56(2), pp. 123–128. https://doi.org/10.14502/Tekstilec2013.56.123-128.

OpenCV, 2022. *ArUco marker detection*. [online] OpenCV: Open Source Computer Vision. Available at: <https://docs.opencv.org/4.x/d9/d6a/group__aruco.html> [Accessed 24 November 2022].

Ray, S.F., 2002. *Applied photographic optics: lenses and optical systems for photography, film, video, electronic and digital imaging.* 3rd ed. Routledge.

Štampfl, V. and Ahtik, J., 2022. The influence of the surrounding space on the lighting conditions in a photographic scene. In: *Proceedings of the 11th International Symposium on Graphic Engineering and Design GRID*. Novi Sad, Serbia, 3–5 November 2022. Novi Sad: University of Novi Sad. pp. 863–871. https://doi.org/10.24867/GRID-2022-p95.

Villalba-Diez, J., Schmidt, D., Gevers, R., Ordieres-Meré, J., Buchwitz, M., and Wellbrock, W., 2019. Deep learning for industrial computer vision quality control in the printing industry 4.0. *Sensors*, 19(18): 3987. https://doi.org/10.3390/s19183987.

Zakiev, A., Tsoy, T., Shabalina, K., Magid, E. and Saha, S.K., 2020. Virtual experiments on ArUco and AprilTag systems comparison for fiducial marker rotation resistance under noisy sensory data. In: *2020 International Joint Conference on Neural Networks*. Glasgow, UK, 19–24 July 2020. IEEE. https://doi.org/10.1109/IJCNN48605.2020.9207701.

Zitová, B. and Flusser, J., 2003. Image registration methods: a survey. *Image and Vision Computing,* 21(11), pp. 977–1000. https://doi.org/10.1016/S0262-8856(03)00137-9.

Zhang, Z., Han, D., Dezert, J. and Yang, Y., 2019. A new image registration algorithm based on evidential reasoning. *Sensors,* 19(5): 1091. https://doi.org/10.3390/s19051091.

Professional communication

JPMTR-2215
DOI 10.14622/JPMTR-2215
UDC 531.3-028.25:159.937-035.67

Professional communication | 172
Received: 2022-06-20
Accepted: 2022-10-14

Effect of various ink types on naturalness perception of 2.5D prints

Altynay Kadyrova[1], *Marius Pedersen*[1], *Stephen Westland*[2] *and Clemens Weijkamp*[3]

[1]Department of Computer Science, Norwegian University of Science and Technology, 2802, Gjøvik, Norway — altynay.kadyrova@ntnu.no, marius.pedersen@ntnu.no
[2]School of Design, University of Leeds, LS2 9JT, Leeds, UK — s.westland@leeds.ac.uk
[3]Canon Production Printing Netherlands B.V., 5914 HH, Venlo, The Netherlands — clemens.weijkamp@cpp.canon

Abstract

Naturalness perception of 2.5D prints is content dependent and varies depending on the level of elevation used for reproduction. Moreover, various factors can influence the naturalness perception of 2.5D prints such as ink types, viewing angle, and illumination, to name a few. In this work, we focus on the effect of various ink types on the naturalness perception of 2.5D prints of wood images fabricated at 0.5 mm elevation. We found that the naturalness perception of 2.5D prints is influenced by the type of ink used. In particular, we found that 2.5D prints of wood images with matt inks were perceived by observers as more natural than with glossy inks. There were differences between the observers based on their level of expertise. The acquired findings can help to reproduce wooden content to be perceived as natural by using a specific type of ink.

Keywords: elevation, 2.5D printing, ink

1. Introduction

Ink used for printing is a colored liquid and its visual characteristics are color, transparency or opacity, intensity, and gloss (Leach, 2012). Gloss can attract attention to the product/print and glossier print might look more chromatic and darker to some extent (Kipphan, 2001). Samadzadegan, Blahová and Urban (2014) explained that darker samples were perceived more glossy than lighter ones due to the large contrast effect of specular gloss highlights on dark samples in their experiment.

There are various ink types on the market with various levels of gloss/matt. Ink types along with other parameters (e.g., print mode, substrate type) might affect the glossiness of the print (Samadzadegan, et al., 2015). Existing works have studied glossiness aspect of 2.5D prints (i.e., with surface elevation) via experimenting with inks (Baar, et al., 2014; Samadzadegan, Blahová and Urban, 2014). For example, Baar, et al. (2014) created two print modes, glossy and matt, that give almost constant gloss/matt appearance in the prints regardless of the ink coverage because, in standard print mode, an increase in ink coverage gives increase in glossiness. Nonetheless, limited research has been carried out on the perception of naturalness of 2.5D prints (Kadyrova, Pedersen and Westland, 2022a; 2022b). The effects of different parameters on naturalness perception of 2.5D prints were investigated in terms of elevation (Kadyrova, Pedersen and Westland, 2022b) and elevation and surface roughness (Kadyrova, Pedersen and Westland, 2022a). To the best of our knowledge, the naturalness perception of 2.5D prints fabricated with various ink types (i.e., with various glossiness) has not been investigated. Thus, this is the first work to look into the effect of various ink types on the naturalness perception of 2.5D prints.

According to industrial feedback, customers found 2.5D prints too glossy to look natural. Therefore, it is valuable to investigate the effect of various ink types with various glossiness on the naturalness perception of 2.5D prints because glossiness of the prints can be influenced by both the ink types and additional varnish layers. The elevation level affects the naturalness perception of 2.5D prints and it is content dependent (Kadyrova, Pedersen and Westland, 2022a). Based on the results of our previous work (Kadyrova, Pedersen and Westland, 2022b), observers found it natural when

2.5D prints of wood images were fabricated at 0.5 mm elevation. As a result, we work with 2.5D prints of wood images at 0.5 mm elevation fabricated with various ink types and assess effect of ink types on the naturalness perception of 2.5D prints at a given illumination and viewing distance. Based on the obtained results, we can recommend the use of a specific type of ink with a specific glossiness for the reproduction of natural-looking wooden content. For simplicity, by prints we mean 2.5D prints of wood images hereafter in the text.

2. Methodology

We used the term realistic to mean naturalness following the methodology of our previous work (Kadyrova, Pedersen and Westland, 2022b). We worked with 20 wood images that represent various wood content such as wooden floor (4 images), roof (2 images), wall (6 images), and wicker (8 images). The original color images and their height maps were reproduced from 3D textures retrieved from a copyright-free website (3D textures, 2021). To reduce black edges and reach the intended maximum elevation, the height maps were Gaussian filtered (with $\sigma = 4$ being a standard deviation of the Gaussian distribution) and intensity adjusted, respectively. The color images and the processed height maps had a dimension of 782 × 782 pixels prior to being inputted for printing.

The optimal elevation that makes 2.5D prints of wood images (regardless of the wood content) perceptually natural was found to be 0.5 mm (Kadyrova, Pedersen and Westland, 2022b). Therefore, we used 0.5 mm elevation for all prints and varied ink types.

Table 1 shows the ink types used in our work. We used commercially available inks (Canon IJC UV-curable inks) with various coatings. For example, IJC 255a is IJC 255 ink with gloss coating – Royal Talens Amsterdam Acrylic Varnish (RTAAV) applied with 2 layers with brush, fabricated with Arizona flatbed printer – AZ480 with mercury curing lamps. Glossy/matt distribution was done based on industrial information and gloss measurements.

The gloss of flat color patches (light and dark brown which represent most of the colors in our prints) for six groups of inks was measured with a Konica Minolta multi gloss 268 plus glossmeter at 20°, 60°, and 85° (Table 2) in Gloss Units (GU) following ISO standard (International Organization for Standardization, 2014). These angles were chosen due to their common use in the printing industry (Ng, et al., 2003), where 20° geometry is recommended for measurement of high-gloss surfaces, 60° for semigloss surfaces, and 85° for matt surfaces. In Table 2, we can observe that dark colors have higher gloss than light colors within glossy inks (i.e., IJC 255a, IJC 255b, IJC 357).

We used a Forex substrate (PVC foam board with 3 mm thickness) and Arizona flatbed printers for the fabrication of the prints. Files for printing were prepared with Canon Touchstone Elevated Printing software and processed with Canon Advanced Layering Processing System (ALPS) engine that includes a raster imaging processor and uses a specific color profile. Canon optimized the ALPS engine for the best color and elevation output of the used inks. The prints were made in the quality mode at a print resolution of 450 × 450 dpi. The print size was 66.2 mm × 66.2 mm with an additional 3 mm on each side of the substrate to allow observers to hold the prints without touching the edges. There were 6 reproductions per image and 120 of 2.5D prints in total for the experiment.

A ranking experiment was carried out to assess the naturalness perception of the 2.5D prints. If we were to use, for example, the pair comparison method, then the experiment would have become long for observers due to the number of reproductions. Following the experiment design of our previous work (Kadyrova, Pedersen and Westland, 2022b), first, consent from the observers was acquired; second, the observers adapted to the illumination while reading the instruction followed by a training session with some representative prints. We presented the prints in a random order to the observer and they were placed on a table in a viewing room with D50 illumination (around 1900 lux). The instruction was to rank the 2.5D prints from the most to the least realistic representation of wooden floor/roof/wall/wicker and explain why. The keyword (i.e., wooden floor/roof/wall/wicker) was given as a reference, and we allowed observers to move and tilt the prints with gloves without touching the surface. The distance between the eyes of the observer and the prints was approximately 50 cm. We informed the observers that there was no time restriction. The average experiment duration was 41 minutes per observer, excluding the time of the training session which was around 3 to 4 minutes per observer on average. The experiment was carried out in English. The audio explanations given by the observers on their rankings were recorded for analysis purposes.

In total, we had 22 observers (20 males and 2 females) with an average age of around 46 years and a standard deviation of around 11 years, where 6 of them were with high-level expertise, 4 with low-level expertise, and the remaining were with medium-level expertise with backgrounds from chemistry, physics, electronics, and mechanics. Color vision and visual acuity were checked by using Ishihara plates and a Snellen chart, respectively. All observers had normal color

Table 1: Ink types used in our work with coating, printer, curing lamp, and glossy/matt information

Label	Ink name	Coating	Printer	Curing lamp	Glossy/ matt
IJC 255a	IJC 255	Gloss coating (RTAAV) applied with 2 layers with brush	AZ480	Mercury	Glossy
IJC 255b	IJC 255	Gloss coating (RTAAV) applied with 1 layer with spray can	AZ480	Mercury	Glossy
IJC 357	IJC 357	Without coating	AZ2380XTF	LED	Glossy
IJC 255c	IJC 255	Canon IJC 257 varnish printed on top	AZ480	Mercury	Matt
IJC 255d	IJC 255	Matt coating (RTAAV) applied with 1 layer with spray can	AZ480	Mercury	Matt
IJC 358	IJC 358	Without coating	AZ1380XT	LED	Matt

Table 2: Measured gloss values of patches of ink types at 20°, 60°, and 85°, given in GU

Degrees	Patches	IJC 255a	IJC 255b	IJC 357	IJC 255c	IJC 255d	IJC 358
20°	Dark brown	4.0	4.0	3.5	0.6	0.3	0.3
	Light brown	3.7	3.5	2.3	1.2	1.0	0.9
60°	Dark brown	27.4	27.9	22.5	6.0	4.2	3.5
	Light brown	24.8	23.8	16.0	6.3	4.9	3.8
85°	Dark brown	36.0	37.0	21.3	4.5	8.8	3.9
	Light brown	31.8	30.0	17.0	4.7	7.5	3.4

vision except one observer, who was color deficient. The recruited observers were from Canon Production Printing Netherlands and the majority of them were Europeans.

3. Results and discussion

We present *Z*-scores (Engeldrum, 2000) (calculated from raw ranked data) of all wood images by all observers, of images in each wood content by all observers, and of high-medium-low level expertise observers for all images to find the effects of various ink types on the naturalness perception of 2.5D prints. An error bar plot was used to visualize *Z*-scores. Mean *Z*-scores are shown by a circle in the centre of the vertical lines. We calculated confidence intervals (CI) via Equation [1] (Green and MacDonald, 2011).

$$\mathrm{CI} = 1.96\frac{\sigma}{\sqrt{N}} \qquad [1]$$

where N is the number of observations, and σ is the standard deviation which in the case of *Z*-score can be computed as $1/\sqrt{2}$ (Bertalmío, 2019). The 95 % CI is the mean *Z*-scores ± CI. In Figures 1 to 8, we provide ink labels and average gloss values for 60° that were computed as average gloss values of two colors in GU from Table 2.

In Figure 1, we can observe that the observers perceived prints with matt inks as more natural compared to prints with glossy inks. In particular, they perceived prints with IJC 255d ink as the most natural. Generally, wood represents natural material. The natural materials are matt and have rough surface (Karana, 2012). Therefore, it is logical that the observers perceived prints of wood images with matt inks as natural. In addition, matt appearance preference over glossy might be application dependent. For example, matt food packaging might enhance naturalness perception of food (Marckhgott and Kamleitner, 2019).

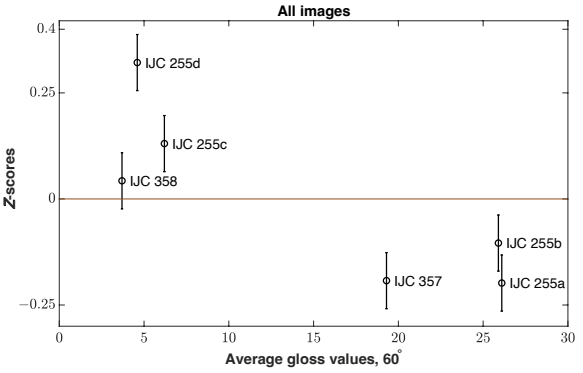

Figure 1: Z-scores of all wood images by all observers: mean Z-score values are given with 95 % CIs and average gloss values are given in GU

Based on audio data of the observers, the prints with IJC 255d ink were perceived as the most natural because the prints seemed to have the right contrast, more fine details, less elevation, and they seemed to be easy for the eyes and not blurry. A binomial sign test was applied on raw data with Bonferroni correction with a significance level of α / n (where $\alpha = 0.05$ is the desired alpha value and n is the number of comparisons: 0.05/15) (Bonferroni, 1936) to determine whether

there are statistically significant differences between ink types. According to the *p*-values (Table 3), there were no statistically significant differences between glossy inks (i.e., IJC 255a, IJC 255b, and IJC 357).

The observers perceived prints with glossy inks as less natural in all wooden floor (Figure 2), roof (Figure 3), and wicker (Figure 4) images. In the case of all wooden wall images (Figure 5), the observers perceived prints with both glossy and matt inks as less natural except with IJC 255d ink (i.e., matt ink) which were perceived as the most natural. The observers perceived prints with at least one matt ink as more natural for wooden floor, roof, wicker, and wall images. Wooden floor and wall can be considered for an indoor applications whereas wooden roof and wicker (can be used also for indoor) for an outdoor applications. Matt (i.e., low gloss) values can be preferred for indoor applications

Table 3: The p-values obtained by a sign test for all wood images, where green cells are those that have a statistically significant difference whereas red cells are those that do not have a statistically significant difference; the threshold used in the Bonferroni correction is 0.05/15 = 0.0033

	IJC 255a	IJC 255b	IJC 357	IJC 255c	IJC 255d	IJC 358
IJC 255a	–	0.0115	0.7386	9.2672×10^{-6}	1.2117×10^{-7}	3.4958×10^{-4}
IJC 255b		–	0.4177	1.1268×10^{-4}	9.0922×10^{-7}	0.0019
IJC 357			–	2.0322×10^{-7}	1.2277×10^{-10}	3.4958×10^{-4}
IJC 255c				–	1.1268×10^{-4}	0.3168
IJC 255d					–	1.4023×10^{-8}
IJC 358						–

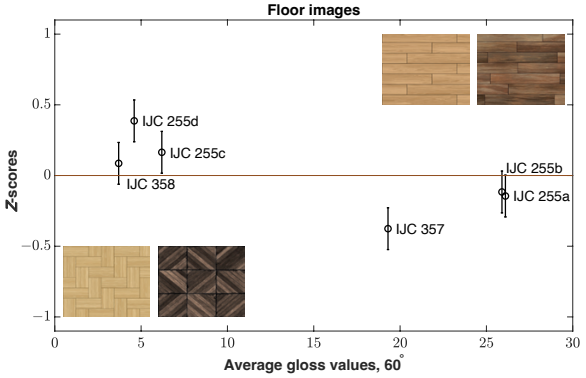

Figure 2: Z-scores of all wooden floor images by all observers: mean Z-score values are given with 95 % CIs and average gloss values are given in GU

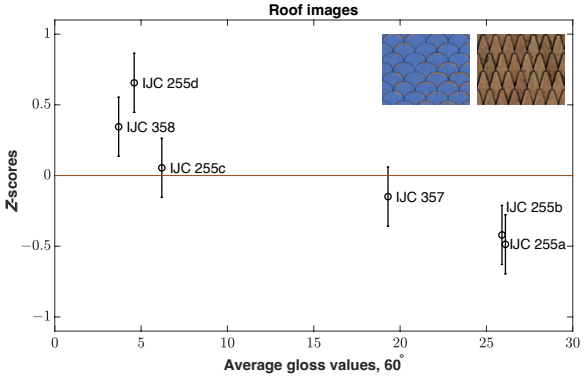

Figure 3: Z-scores of all wooden roof images by all observers: mean Z-score values are given with 95 % CIs and average gloss values are given in GU

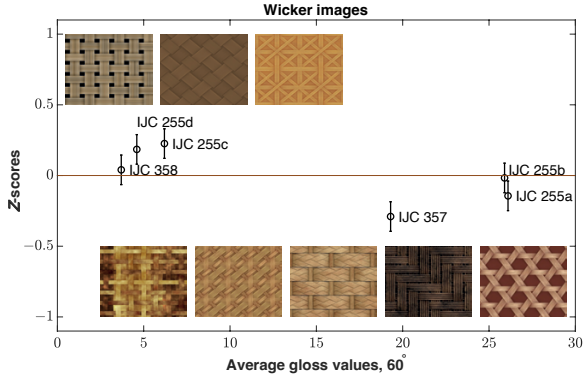

Figure 4: Z-scores of all wooden wicker images by all observers: mean Z-score values are given with 95 % CIs and average gloss values are given in GU

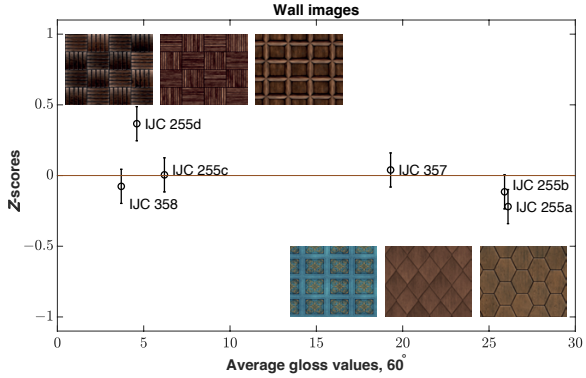

Figure 5: Z-scores of all wooden wall images by all observers: mean Z-score values are given with 95 % CIs and average gloss values are given in GU

and high-gloss values for outdoor applications (Leek, et al., 2022). The reason of selecting prints with matt ink as more natural for wooden roof by the observers was due to weather considerations. Some observers explained that wooden roof tends to be influenced by weather and time, and therefore matt look is more appropriate than glossy look for wooden roof to be perceived as natural. For wooden wicker, some observers commented that some level of gloss is needed but not too much or too less. Thus, wooden wicker should not be completely matt to be perceived as natural.

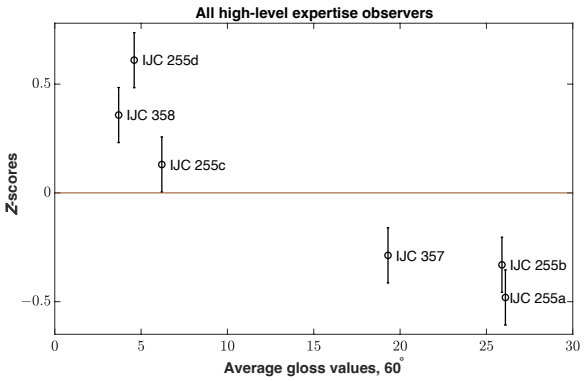

Figure 6: Z-scores of all high-level expertise observers for all images: mean Z-score values are given with 95 % CIs and average gloss values are given in GU

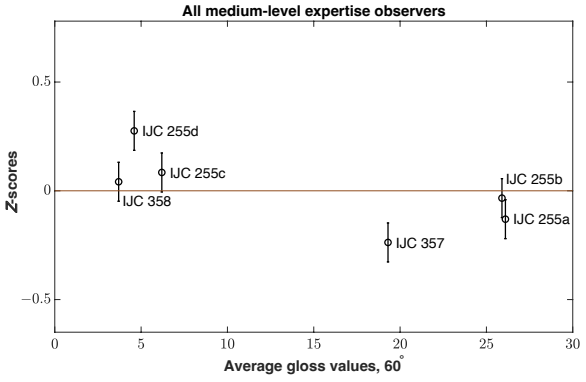

Figure 7: Z-scores of all medium-level expertise observers for all images: mean Z-score values are given with 95 % CIs and average gloss values are given in GU

There were differences in the naturalness perception of 2.5D prints within the observers with various level of expertise based on their *Z*-scores for all images. Both high-level (Figure 6) and medium-level (Figure 7) expertise observers perceived prints with matt inks as more natural than with glossy inks. More specifically, they perceived prints with IJC 255d ink (i.e., matt ink) as the most natural. Low-level expertise observers perceived prints with IJC 358 ink (i.e., matt ink) as the least natural while they perceived prints with IJC 255c ink (i.e., matt ink) as the most natural (Figure 8). In other words, low-level expertise observers perceived prints with matt inks as both natural and unnatural depending on type of matt inks. When these observers ranked prints with IJC 358 ink as the least natural, they commented that those prints with IJC 358 ink were perceived as having less 2.5D effect and a cartoonish look.

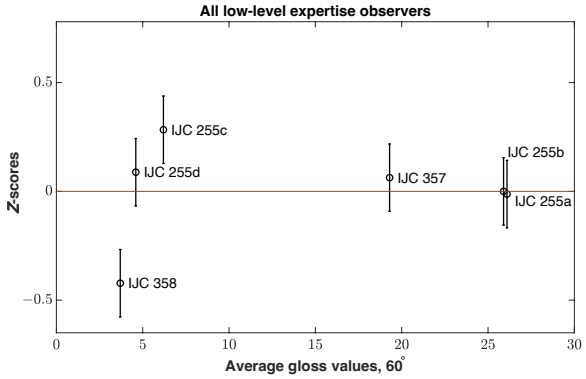

Figure 8: Z-scores of all low-level expertise observers for all images: mean Z-score values are given with 95 % CIs and average gloss values are given in GU

When the observers did ranking, they assigned each ink type (i.e., six reproductions per image) to six ranks: the most, second most, third most, third least, second least, and the least realistic for each image. We calculated standard deviation values of each rank across all images per observer. Afterwards, we calculated average of standard deviation values across ranks per observer. Based on acquired average standard deviation values, four observers were below 1.00 with minimum of 0.52, ten observers were higher than 1.50 with maximum of 1.70, and the remaining observers were in between. Those observers who were more consistent, they probably ranked based on glossiness of the inks in the prints while others probably considered content. Thus, some observers for some images probably included the content in their rankings and that could be the reason for them having larger standard deviation. For instance, in the case of prints of wooden floor images, some observers mentioned that they should be matt to be perceived as natural because too much gloss makes the prints look like plastic whereas some other observers mentioned that wooden floor should be glossy as it gives feeling of new floor. Additionally, we checked inter-observer variability by Spearman correlation coefficient and, on average for all images, it showed that the correlation varies between the observers. For gloss measurement values (Table 2), we assigned ranking and then we considered average of ranking of all measurements for 20°, 60°, and 85° for two colors (dark and light brown) which resulted in the following gloss measurement rank for the inks from glossy to matt: IJC 255a (being the glossiest),

IJC 255b, IJC 357, IJC 255c, IJC 255d, and IJC 358 (being the least glossy). Then we checked whether observer ranking correlated with the gloss measurement rank by Spearman correlation coefficient which is illustrated in Figure 9. If the correlation value is one, it means that the observers ranked the prints with the glossiest ink as the most natural. Similarly, if the correlation value is minus one, it means that the observers ranked the prints with the most matt ink as the most natural. The correlation value around zero means that the observers did not rank based on the gloss level. In Figure 9, we can observe that some observers ranked based on the gloss level while the others ranked, most probably, based on content.

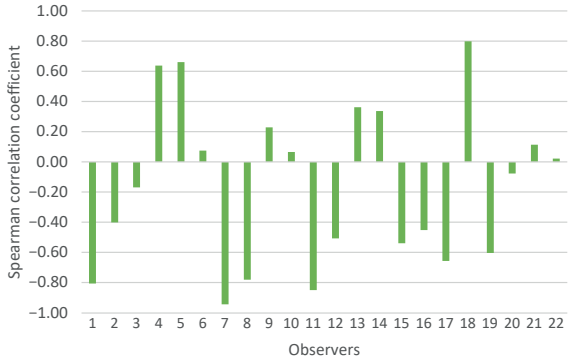

Figure 9: The correlation of observer ranking with gloss measurement rank

Figure 10 shows frequency of each ink type selection through all images for each rank by the observers (presented frequency count values are sum across all observers). We can observe that prints with IJC 255a ink were selected mostly as the least then second least, with IJC 255b ink as second least then second most, with IJC 357 ink as third least then third most, with IJC 255c ink as third most then second most, with IJC 255d ink as the most then second most, and with IJC 358 ink as the least then the most realistic representation of wooden images. Those observers who mostly ranked the prints with IJC 358 ink as the most realistic commented that the prints were perceived as being less grainy while those who ranked as the least realistic commented that the prints were perceived having less 2.5D effect, cartoonish look, and not wood color.

From audio data of observers where they provided their explanations on their rankings, we derived the most used attributes through frequency analysis. We observed that the observers were able to find that the prints had various gloss/matt levels (Figure 11).

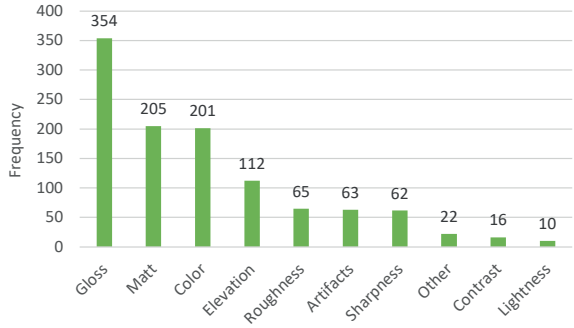

Figure 11: The most used attributes by the observers

Therefore, the two most used attributes were gloss and matt. Gloss attribute included gloss, shiny, and reflection sub-attributes. Color, bright color, saturated color, warm color, brown, yellow, and similar sub-attributes were grouped into color attribute. Elevation attribute included sub-attributes such as relief, height, elevation, 2.5D, and similar. Texture, coarseness, granularity, and smoothness were grouped into roughness attribute while noise, graininess, dots, defects, and artifacts were grouped into the artifacts attribute. Roughness was mentioned quite often in terms of coarseness and texture, and it is expected because the surface pro-

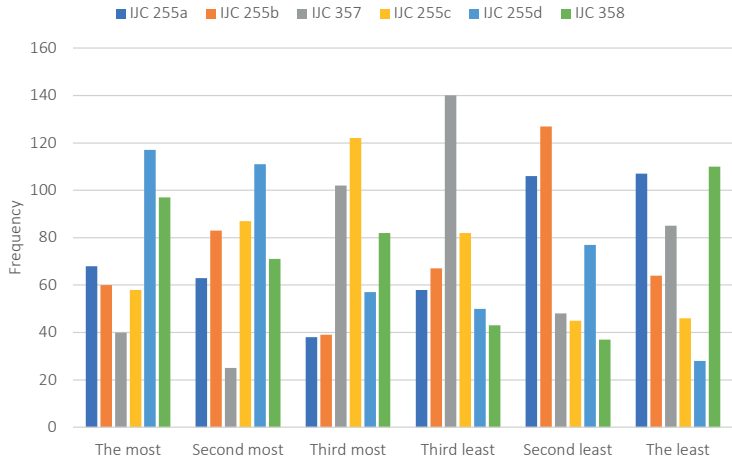

Figure 10: Each ink type selection frequency through all images in each rank

duced by UV-curable ink has a tendency to be granular (Arita, et al., 2017). Sharpness attribute included details, blurry, sharpness, and similar sub-attributes. Other attribute group included words such as plastic and cartoonish. Some observers mentioned that glossiness seems to emphasize 2.5D effect (i.e., elevation) in the prints while matt seems to make the prints look less elevated. They also mentioned that too much gloss is not preferred because it might make eyes to blink and it might make the prints look like plastic. Lightness attribute included darker and lighter sub-attributes.

Because we worked with wood images only, we assume that results might vary when considering other material images with respect to the effect of ink types on the naturalness perception of 2.5D prints. Thus, content and application might affect the results.

To conclude, the prints with matt inks were perceived as natural by the observers. Moreover, low-level expertise observers perceived the naturalness of the prints differently than other observers to some degree. Frequency analysis of the most used attributes showed that the prints had sufficient level of gloss because the observers were able to differentiate the prints based on the glossiness. We assume that the observers ranked the prints, most likely, based on the gloss level and content.

4. Conclusions and future works

We investigated the effect of various ink types on the naturalness perception of 2.5D prints of wood images fabricated at 0.5 mm elevation. We found that the gloss level of the ink affects the naturalness perception of 2.5D prints. Based on the results, the observers perceived prints with matt inks as more natural than with glossy inks. Moreover, prints with IJC 255d ink were perceived as the most natural by the observers. While high-level and medium-level expertise observers perceived prints with matt inks as more natural, low-level expertise observers perceived prints with matt inks as both natural and unnatural depending on matt ink types. Thus, there was a difference between high-medium levels and low-level expertise observers in the naturalness perception of the prints.

Our results might help industry in selection of appropriate ink types to reproduce natural-looking 2.5D prints of wood images at 0.5 mm elevation. Potential future work can be to conduct visual experiment with real wood surface and its reproduction and check whether observers can differentiate reproduction from the real wood in terms of naturalness. In addition, increasing the size of prints for the experiment can be considered.

Funding

This research was funded by the ApPEARS project from the European Union's Horizon 2020 research and innovation programme under the Marie Sklodowska-Curie grant agreement No 814158.

Acknowledgments

We would like to thank observers for participation in the experiment.

References

3D textures, 2021. *3D textures*. [online] Available at: <https://3dtextures.me> [Accessed 6 July 2021].

Arita, M., Yoshino, M., Hatanaka, S. and Kamei, T., 2017. 2.5-dimensional inkjet fabrication using UV curable ink. In: *33rd International Conference on Digital Printing Technologies: Printing for Fabrication 2017*. Denver, CO, USA, 5–9 November 2017. Springfield, VA, USA: Society for Imaging Science and Technology, pp. 175–180.

Baar, T., Samadzadegan, S., Brettel, H., Urban, P. and Ortiz Segovia, M.V., 2014. Printing gloss effects in a 2.5D system. In: M.V. Ortiz Segovia, P. Urban and J.P. Allebach, eds. *Proceedings of SPIE 2018, Measuring, Modeling, and Reproducing Material Appearance*. San Francisco, CA, USA, 11 March 2014. SPIE, pp. 160–167. https://doi.org/10.1117/12.2039792.

Bertalmío, M., 2019. *Vision models for high dynamic range and wide colour gamut imaging: techniques and applications*. London, UK: Academic Press.

Bonferroni, C.E., 1936. Teoria statistica delle classi e calcolo delle probabilità. *Pubblicazioni del R. Istituto superiore di scienze economiche e commericiali di Firenze*, 8.

Engeldrum, P.G., 2000. *Psychometric scaling: a toolkit for imaging systems development*. Winchester, MA, USA: Imcotek Press.

Green, P. and MacDonald, L. eds., 2011. *Colour engineering: achieving device independent colour*. Chichester, West Sussex, UK: John Wiley & Sons.

International Organization for Standardization, 2014. *ISO 2813:2014 Paints and varnishes – Determination of gloss value at 20 degrees, 60 degrees and 85 degrees*. Geneva: ISO.

Kadyrova, A., Pedersen, M. and Westland, S., 2022a. Effect of elevation and surface roughness on naturalness perception of 2.5D decor prints. *Materials*, 15(9): 3372. https://doi.org/10.3390/ma15093372.

Kadyrova, A., Pedersen, M. and Westland, S., 2022b. What elevation makes 2.5D prints perceptually natural? *Materials*, 15(10): 3573. https://doi.org/10.3390/ma15103573.

Karana, E., 2012. Characterization of 'natural' and 'high-quality' materials to improve perception of bio-plastics. *Journal of Cleaner Production*, 37, pp. 316–325. https://doi.org/10.1016/j.jclepro.2012.07.034.

Kipphan, H. ed., 2001. *Handbook of print media: technologies and production methods*. Berlin, Germany: Springer.

Leach, R.H. ed., 2012. *The printing ink manual*. 4th ed. Dordrecht: Springer Science & Business Media.

Leek, K.M., Weijkamp, C.T., Van Der Asdonk, P. and Van Keulen, L., Canon Production Printing Holding B.V., 2022. *Method for applying an image*. U.S. Pat. 11,458,741 B2.

Marckhgott, E. and Kamleitner, B., 2019. Matte matters: when matte packaging increases perceptions of food naturalness. *Marketing Letters*, 30(2), pp. 167–178. https://doi.org/10.1007/s11002-019-09488-6.

Ng, Y., Zeise, E., Mashtare, D., Kessler, J., Wang, J., Kuo, C., Maggard, E. and Mehta, P., 2003. Standardization of perceptual based gloss and gloss uniformity for printing systems. In: *PICS 2003: Image Processing, Image Quality; Image Capture Systems Conference, Including MCS/05 Fifth International Symposium on Multispectral Color Science*. Rochester, NY, USA, 13–16 May 2003. Society for Imaging Science and Technology, pp. 88–93.

Samadzadegan, S., Blahová, J. and Urban, P., 2014. Color-printed gloss: relating measurements to perception. In: *22nd Color and Imaging Conference*. Boston, MA, USA, 3–7 November 2014. Society for Imaging Science and Technology, pp. 207–211.

Samadzadegan, S., Baar, T., Urban, P., Ortiz Segovia, M.V. and Blahová, J., 2015. Controlling colour-printed gloss by varnish-halftones. In: *Proceedings Volume 9398, Measuring, Modeling, and Reproducing Material Appearance 2015*. San Francisco, CA, USA, 13 March 2015. Society of Photo-Optical Instrumentation Engineers. https://doi.org/10.1117/12.2080805.

TOPICALITIES

Edited by Markéta Držková

CONTENTS

News & more

The activities of CIE in 2022

In the first weeks of 2022, the International Commission on Illumination established its new Research Forum CIE RF-04 Lighting in the Usage of Augmented, Virtual, and Mixed Reality Devices. During the following months, four Technical Committees (TCs) were newly formed: two under Division 2, Physical Measurement of Light and Radiation, and the other two as a part of Division 3, Interior Environment and Lighting Design. The task of CIE TC 2-97 is to prepare a revision of CIE S 025/E:2015 Test Method for LED Lamps, LED Luminaires and LED Modules and its supplement CIE S 025-SP1/E:2019 that were both introduced quite recently, whereas CIE TC 2-98 will revise an older technical report CIE 130-1998 Practical Methods for the Measurement of Reflectance and Transmittance. The aim of CIE TC 3-61 is to review regional daylight requirements and assess the feasibility of global harmonisation. The last one, CIE TC 3-62 Resilient Lighting, should develop lighting requirements and plans for disaster lighting.

Besides several events held in the year 2022 by the CIE National Committees, the one-day CIE Symposium on Advances in Measurement of Temporal Light Modulation took place in October in Athens, Greece. The proceedings with 9 of the 13 papers were published as CIE x049:2022. All papers are also available individually, six of them with open access. Their topics include, for example, implementing lock-in detection in photometry and spectroradiometry using temporal light modulation and minimising the uncertainties in the calculation of stroboscopic effect visibility measure.

Since the end of 2021, the requirements to perform reproducible photometric and colorimetric measurements of devices used in road vehicles for road illumination, light-signalling, and retroreflection are available as a draft international standard CIE DIS 027:2021. The document was prepared by the corresponding committee of Division 2 and is still subject to changes. Among other recent publications, the Technical Report CIE 249:2022 Visual aspects of time-modulated lighting systems deals with distortions in the perception of the environment that are caused by the fast change in luminous output. These effects are mostly undesired and bring the risk of negative impact not only on the experience of the illumination quality but also on performance and health. The report was prepared under Division 1, Vision and Colour, and builds on the Technical Note CIE TN 006:2016, which defined the perceptual effects modulated light can produce, the methods for quantifying these temporal light artefacts and the parameters that influence their visibility. The effects of light on human health, performance and well-being are also presented in the joint ISO/CIE TR 21783:2022 Light and lighting – Integrative lighting – Non-visual effects, published in September 2022. This document reviews the relevant scientific background on the non-visual responses to light and discusses beneficial aims, avoidance of risks and implementation considerations. Another joint ISO/CIE document, which revises ISO 23539:2005 Photometry – The CIE system of physical photometry to bring the standard up to date with recent developments, is under publication. Five recently published documents most relevant to the scope of JPMTR are presented on the next page in more detail.

Fogra research projects and new tools in 2022

Recently, two projects of Fogra were completed by dedicated research teams, both from the field of prepress technology. DeepQuality, the joint project of Fogra and the Institute of Imaging and Computer Vision at the RWTH Aachen University, applied machine learning for dynamic image style evaluation to increase automation of image retouching. Besides the report, the output of this project includes a publicly available WebApp where users can test trained artificial intelligence systems on their images. The second project, TextileRGB, was concerned with colour communication in digital textile printing. The work employed the colour appearance assessment of 110 textile samples with disperse dyes, sublimation dyes, reactive dyes, pigment inks and acid dyes. The research was also focused on the suitable ICC RGB exchange colour spaces and production of paper proofs where it is important to consider the relevant paper characteristics, i.e. its shade, the content of optical brightening agents, gloss and texture. The tools developed within the project include an RGB-based test form for RGB process control and quality assurance and a spreadsheet for instrumental evaluation, both available for free. The test form serves for the characterisation of digital textile printing processes, enabling analysis of their output, as well as for the validation of the accuracy of profiling and proof printing. The proposed RGB workflow makes use of the exchange colour space FOGRA58, further developed within this project, and enables accurate colour reproduction of D65/10°-based textile originals. For OBA-rich substrates, it is recommended to use the M2 measurement mode. The new MediaWedge Textile RGB, a subset of the established chart TC 9.18 RGB, is available in the Fogra shop.

The ongoing Fogra research projects include those started in 2021 (see JPMTR Vol. 10, No. 4), which are to be completed now or in the coming months. Among the projects started in 2022, two are worked on by the Printing Techniques Department. The first one explores the use of LED UV lamps instead of the hot-air units for ink drying in web offset presses to increase the economic efficiency and sustainability of print production through independence from natural gas, a topic which gained even more importance due to the present energy crisis. The approach is based on developing a cost and CO_2 calculator and obtaining the required data through extensive research. Also, the suitability of papers for the proposed process needs to be investigated. The second project concerns the visual and metrological characterisation of metallic effects to increase process reliability in packaging printing. The solution comprises the production and measurement of different metallised prints and defining an appropriate scale for the metallic effect using pairwise visual comparisons under different lighting conditions to determine a functional relationship between the strength of the metallic effect and the metrological parameters. In the area of prepress technology, two new projects were started as well. One builds on a past project focused on modelling colour appearance for full-colour 3D printers (see also JPMTR Vol. 10, No. 4) and deals with 3D soft proof for an accurate simulation of volumetric light transport effects and geometric errors in 3D prints. It aims to develop and validate two renderers, one device-independent and one device-specific, using deep-learning approaches. Further, a new 3D printing exchange colour space should be created and integrated into the iccMax framework. Another project is dedicated to the development of a cross-process print quality assessment procedure and the corresponding indicator, the so-called ISO index. Finally, the new project in the area of security applications investigates electrostatic discharge methods for integrated biometric sensors in smart cards.

ISO/CIE 11664-2:2022 and ISO/CIE 11664-6:2022 Colorimetry Part 2: CIE standard illuminants Part 6: CIEDE2000 colour-difference formula

The current versions of these two parts of the ISO/CIE 11664 series on colorimetry were published in August 2022. The first edition of Part 2 cancels and replaces ISO 11664-2:2007 (CIE S 014-2:2006). The CIE illuminant D50, commonly used in graphic arts and printing, is now defined as a CIE standard illuminant, representing the main change in this revision. Values for D50 relative spectral power distribution at 1 nm intervals from 300 to 830 nm are included in Annex B. The second edition of Part 6 is a minor revision of its first edition from 2014. First editions of Part 1: CIE standard colorimetric observers, Part 3: CIE tristimulus values, and Part 4: CIE 1976 L*a*b* colour space were published in June 2019, see JPMTR Vol. 8, No. 4 (2019). Part 5: CIE 1976 L*u*v* colour space and u′, v′ uniform chromaticity scale diagram was published in 2016, and its second edition is under development.

CIE TN 013:2022 – Terms related to Planckian radiation temperature for light sources

This Technical Note defines the terms thermodynamic temperature, Planckian radiator (blackbody) temperature, radiance temperature, colour temperature, correlated colour temperature, distribution temperature and ratio temperature, highlighting their relationships. For each term, it provides relevant details and information on the applicability, for example, limited by chromaticity. For correlated colour temperature and distribution temperature, it also describes the sources of uncertainties. This document supersedes CIE 114-1994 CIE Collection in photometry and radiometry, Part 4 Distribution temperature and ratio temperature, and is available for free.

CIE 248:2022 – The CIE 2016 colour appearance model for colour management systems: CIECAM16

This document was prepared under Division 1 and Division 8, Image Technology, and supersedes CIE 159:2004 A colour appearance model for colour management systems: CIECAM02. The report describes the evolution and application of the CIECAM16 colour appearance model, including its use in practical applications. It provides a chromatic adaptation transform and equations to calculate a set of perceptual attribute correlates using the CIE 1931 standard colorimetric observer. The revised model maintains the same prediction performance for visual data as the previous model but is simpler. It may be helpful for colour management systems that involve related colours, especially for evaluating photographic prints and self-luminous displays.

CIE 250:2022 – Spectroradiometric measurement of optical radiation sources

With 94 pages, this report is the most extensive one among those published in 2022. It was prepared under Division 2 and, after almost 40 years, supersedes CIE 063-1984 The spectroradiometric measurement of light sources. The document explains the basic measurement principles and measured quantities and provides instructions for measurement in the wavelength range of 200–2 500 nm. It describes optics, measurement geometries for irradiance, radiant intensity, radiant flux and radiance, lamps and source spectra determination. Also, it presents in detail different aspects contributing to measurement uncertainty, from wavelength scale to coherence.

Bookshelf

Smart Materials in Additive Manufacturing
Volume 1: 4D Printing Principles and Fabrication
Volume 2: 4D Printing Mechanics, Modeling, and Advanced Engineering Applications

These two new volumes were contributed by almost 80 experts from across the globe and bring a comprehensive account of current advances in a rapidly evolving field of 4D printing where 3D-printed smart materials form dynamic objects responding in a controlled way to external stimuli. The first volume is intended to help all entering the field further familiarise themselves with the concepts and principles of 4D printing technology, while the second volume focuses on a top-down approach to modelling and designing 4D printing applications. Overall, readers may find the text useful for identifying related research and business opportunities.

The first volume begins with an introduction to 4D printing, highlighting the contents of the book and their significance. Then, 11 chapters deal with modelling, fabrication and other aspects of various 4D-printed structures. These include the soft robots made from dielectric elastomers, especially the systems having high bending actuation, the light-responsive structures, including their potential applications in encryption, anti-counterfeiting, self-healing and photo-controlled microfluidics, the low-voltage electroactive polymers fabricated by the technology based on direct ink writing, and the formulation composition and chemistry of stimuli-responsive hydrogels. Further, they present the specifics of 4D bioprinting, the approaches for 4D printing at the microscale and the design of suitable inks, different soft materials for 4D printing from hydrogels to nanocomposites, 4D printing of natural fibre composite changing shape by hygromorphing, the functionalised 4D-printed sensor systems for human–device interfaces, the origami-inspired 4D printing, and the successful approaches to achieving reversible transformations of 4D-printed structures. The last chapter discusses the considerations for closing the gap between research and industrial applications.

The second volume overviews recent techniques and tools for 4D printing design and then, in 14 chapters, presents selected examples from various areas in depth. These include 4D printing of electro-induced shape memory polymers, modelling using the Abaqus software and via machine learning, 4D-printed pneumatic soft actuators, structures with tunable mechanical properties, shape memory polymer, 4D textiles, closed-loop control of 4D-printed hydrogel soft robots, the hierarchical motion of 4D-printed structures using the temperature memory effect, manufacturing highly elastic skin integrated with twisted and coiled polymer muscles, multi-material 4D printing simulation using a Rhinoceros 3D Grasshopper plugin, origami-inspired tunable radio frequency and wireless 4D structures and modules, shape-reversible 4D printing aided by shape memory alloys, and variable stiffness 4D printing.

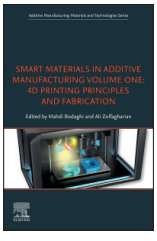

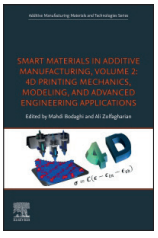

Editors: Mahdi Bodaghi, Ali Zolfagharian

Publisher: Elsevier
1st ed., June 2022
ISBN: 978-0-12-824082-3 & 978-0-323-95430-3
482 & 464 pages
Softcover
Available also as an eBook

Interdisciplinary Research for Printing and Packaging

Editors: Pengfei Zhao, Zhuangzhi Ye, Min Xu, Li Yang, Linghao Zhang, Shu Yan

Publisher: Springer
1st ed., April 2022
ISBN: 978-9811916724
557 pages, 364 images
Hardcover
Also as an eBook

This volume includes a selection of about 80 peer-reviewed papers from the 2021 12th China Academic Conference on Printing and Packaging held in Beijing, China. The topics cover colour science, image processing, reproduction quality, material properties, machinery, printed electronics, 3D printing, and more. The papers deal, for example, with colour-matching functions, structural colours, denoising methods, a halftone blind watermark, a flexible tactile sensor, mechanical properties of honeycomb paperboard, an edible ink based on chlorophyll and chitosan, thermal expansion microcapsules, a sound-absorbing ink, and smart storage location optimisation.

Sustainability for 3D Printing

Editors: Kamalpreet Sandhu, Sunpreet Singh, Chander Prakash, Karupppasamy Subburaj, Seeram Ramakrishna

Publisher: Springer
1st ed., September 2021
ISBN: 978-3030752347
205 pages, 68 images
Hardcover
Also as an eBook

As a part of the Springer Tracts in Additive Manufacturing series, this new book focuses on transforming different types of waste into 3D-printable materials appropriate for design and engineering applications. It reviews the practical examples with the corresponding models, machine tools and processing routes. Also, it deals with the life cycle assessment and evaluation of sustainability and eco-friendliness

FIRST 7.0
Flexographic Image Reproduction Specifications & Tolerances

The anniversary edition of this comprehensive guide for the flexographic industry, first published in 1997, reflects the changes in referenced methods and standards implemented during the past five years since the sixth edition and also brings improvements in the structure of the text. The Communication and Implementation section, which presents the methods for press optimisation, fingerprinting and characterisation, as well as process control and improvement, includes the updates based on CGATS TR 012-2020, the current version of the technical report prepared by the Committee for Graphic Arts Technologies Standards and registered with ANSI, the American National Standards Institute. The completely rewritten Design section with eight chapters introducing the relevant terms and concepts, type and design elements, digital photography, graphic arts software, document structure, file formats, usage and handing over to prepress can be downloaded for free. The updated Prepress and Print sections are followed by the new Measurement and Verification section, which collects information on barcodes, process control test elements, instrumentation, ink room procedures and testing, and ink trapping. The end part provides a glossary, index and eight appendices with contacts, extensively updated references, targets, 2D codes and guides to creating tone scale, process control of spot colours, understanding opacity and The Optimal Method for colour calibration.

Publisher:
Flexographic Technical Association, Inc.
7th ed., October 2022
ISBN: 978-1-735-28936-6
866 pages
Hardcover
Available also as an eBook

Industry 4.0 in Small and Medium-Sized Enterprises (SMEs)
Opportunities, Challenges, and Solutions

In twelve chapters, this new book introduces the Fourth Industrial Revolution in the context of small and medium-sized enterprises and discusses various related aspects as well as opportunities and issues in different areas. While some authors focus on the situation in India, some deal with the topic in general. One case study analyses technology gaps in the Mysore Printers Cluster with about 250 enterprises, identifying training requirements and proposing an action plan to create an attractive opportunity in the Industry 4.0 market. The last chapter deals with the Education 4.0 concept, the essential skills and competencies, and the related changing role of academics.

Editors: Ketan Kotecha, Satish Kumar, Arunkumar Bongale, R. Suresh

Publisher: CRC Press
1st ed., March 2022
ISBN: 978-1-03-206131-3
216 pages, 66 images
Hardcover
Available also as an eBook

Print Culture, Agency, and Regionality in the Hand Press Period

This book is published in the established New Directions in Book History series, reassessing and building upon the early work to advance the knowledge by employing advanced methods and exploring the subjects not studied before. The introductory chapter of the presented collection of essays establishes the historical context and defines the book's key concepts. The remaining chapters are organised into four parts. Three chapters of the first one present the printers of Yorkshire, including the career of York's first female printer, Alice Broad, between 1661 and 1680. The second part deals with circulation and networks, describing the Newcastle book trade and the circulation of chapbooks – the small books sold by peddlers – in early nineteenth-century Northumberland. The third part discusses the Scottish print trade in the late 16th century and compares the regional newspapers and directories in Liverpool and Glasgow two hundred years later. The last part focuses on the lack of letters that limited printing of foreign languages and the rise of jobbing printing in the 19th century connected with sans serif typography. The book is concluded with the afterword essay.

Editors: Rachel Stenner, Kaley Kramer, Adam James Smith

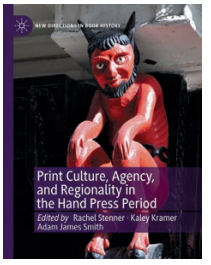

Publisher: Palgrave Macmillan
1st ed., April 2022
ISBN: 978-3-030-88054-5
294 pages, 18 images
Hardcover
Available also as an eBook

Visual Research
An Introduction to Research Methods in Graphic Design

The original edition of this book was written by Russell Bestley and Ian Noble and published in 2005, with the second edition from 2011 and the third one from 2016. The individual chapters introduce the need for design research and critical thinking, the fundamental design principles, approaches to analysis and proposition, the role of visual comparisons, bringing theory to practice, identifying the audience and the right message, considerations related to the production process and materials, and the process of synthesis. The main content is complemented by Ellen Lupton's foreword and the appendices with recommended reading and index. The current edition features several new case studies; their total number increased to 19. Also, it includes a Manifesto for Higher Learning in Design based on the text by Andrew Howard in Design Observer, 2013, and a new chapter collecting in alphabetical order the key concepts to facilitate the application of presented tools and methods in both print and on-screen design.

Authors: Russell Bestley, Paul McNeil

Publisher: Bloomsbury Visual Arts
4th ed., September 2022
ISBN: 978-1-350-16056-9
240 pages, 200 images
Softcover
Available also as an eBook

of the resulting feedstock and final products. The topics include laser additive manufacturing, fused deposition modelling, biomaterials printing and utilisation of agricultural waste, 3D-printed concrete and improving its strength, a material-driven design approach, and supply chain management. Considering the importance of the topic, the text would deserve more careful proofreading or at least spell checking, as illustrated by the book highlights on the Springer website: "This is is focused".

The Printing and the Printers of The Book of Common Prayer 1549–1561

Author: Peter W. M. Blayney

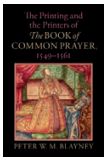

Publisher: Cambridge University Press
1st ed., January 2022
ISBN: 978-1108837415
278 pages, Hardcover
Also as an eBook

The author brings a deep insight into the genesis of the important prayer book based on a thorough examination of its printed copies, correctly identifying the editions of 1549, 1552 and 1559 versions and documenting cooperation between the two teams of printers producing the first two editions of 1559, with title pages probably finished on the same day.

Abstract Pattern Illustrations for Textile Printing

Authors: K. Murugesh Babu, M. Selvadass, Megha Shisodiya, Abera Kechi Kabish

Publisher: Springer
1st ed., November 2021
ISBN: 978-9811659744
283 pages, 251 images
Hardcover
Also as an eBook

This volume presents a selection of 250 designs suitable for textile surface printing and different types of fabrics, highlighting the importance of colour and colour combinations.

IoT-enabled Smart Healthcare Systems, Services and Applications

Editors: Shalli Rani, Maheswar Rajagopal, Neeraj Kumar, Syed Hassan Ahmed Shah

Publisher: Wiley
1st ed., January 2022
ISBN: 978-1119816799
256 pages
Hardcover
Also as an eBook

The scope of this new book encompasses different fields, which is reflected in the backgrounds of its over 30 contributors. The text reviews emerging technologies in smart healthcare, i.e. artificial intelligence, the Internet of Things, blockchain, 3D printing and 5G technology, and their applications. It introduces the fundamental concepts, practical implementation and use cases, as well as current limitations, future directions and related challenges, such as security and privacy issues in smart healthcare systems using the Internet of Things.

Natural Polymers
Perspectives and Applications for a Green Approach

Editors: Jissy Jacob, Fernando Gomes, Józef T. Haponiuk, Nandakumar Kalarikkal, Sabu Thomas

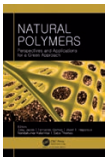

Publisher: Apple Academic Press
1st ed., March 2022
ISBN: 978-1771889605
336 pages, Hardcover
Also as an eBook

About 30 mostly Indian contributors of this new book present natural polymers like biodegradable, biocompatible, nontoxic, and also economical and readily available alternatives to synthetic polymers, thus being attractive for many applications. Among other topics, the text reviews chitosan biopolymer and its composites for 3D printing and nanocomposite flexible films based on cellulose acetate and TiO_2 for photochromic applications.

Flexible Supercapacitors
Materials and Applications

This new book, with almost 30 contributors, all except one affiliated in China, reviews the recent extensive research on flexible supercapacitors as energy storage devices essential for the development of flexible electronics in general. The topics cover flexible asymmetric supercapacitors, stretchable supercapacitors, flexible fibre-shaped supercapacitors, flexible supercapacitors based on ternary metal oxide nanostructures, transition metal oxide-based electrode materials for supercapacitors, and 3D nanoarray flexible electrodes for supercapacitors, including those based on self-supported metal oxide array materials. One chapter is dedicated to printed flexible supercapacitors. It presents the structure and elements of devices, printable materials for supercapacitors, namely carbon-based materials, electrolytes and flexible substrates, printing methods for fabrication of flexible supercapacitors, which include inkjet printing, screen printing, transfer printing and 3D printing, the possibility of integration with flexible/wearable electronics, and also the restrictions implied by required rheological properties. The next chapter deals with printing flexible on-chip micro-supercapacitors, including the printable materials for electrodes, current collectors and electrolytes, as well as inkjet printing, spray printing and screen printing as suitable fabrication techniques. The last chapter summarises the recent advances in flexible micro-supercapacitors.

Editors: Guozhen Shen, Zheng Lou, Di Chen

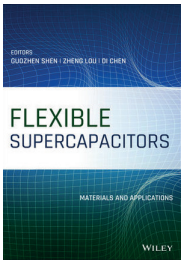

Publisher: Wiley
1st ed., April 2022
ISBN: 978-1-119-50616-4
336 pages
Hardcover
Available also as an eBook

Smart 3D Nanoprinting
Fundamentals, Materials, and Applications

In this new book, almost 50 contributors review in 16 chapters the emerging field of 3D printing at the nanoscale. The applications range from 3D nanoprinting in the aero and automobile industries to biomedical and health-care applications, including oral health care, to 3D-printed nanosensors and batteries, up to the evolution of 4D printing. The text presents various additive manufacturing methods and suitable nanomaterials, including 3D printing of hybrid nanocomposites, 2D nanomaterials, shape memory alloys, and metal alloys. Further, it discusses the impact of fused deposition modelling and nanofillers on the shape memory properties of polyurethane and the evaluation of dimensional inaccuracy in 3D-printed products.

Editors: Ajit Behera, Tuan Anh Nguyen, Ram K. Gupta

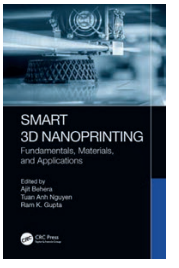

Publisher: CRC Press
1st ed., August 2022
ISBN: 978-1-03-203861-2
341 pages, 110 images
Hardcover
Available also as an eBook

Bookshelf

Academic dissertations

Reliable Classification in Digital and Physical Worlds Under Active Adversaries and Prior Ambiguity

Doctoral thesis – Summary

Author:
Olga Taran

Speciality field:
Computer Science – Physical Objects Authentication

Supervisor:
Slava Voloshynovskiy

Defended:
9 June 2021, University of Geneva, Faculty of Science, Computer Science Department
Geneva, Switzerland

Contact:
taran.olga@gmail.com

The topic of this thesis is of high importance due to the growing use of artificial intelligence and machine learning in various applications, accompanied by a rising threat of adversarial attacks. In particular, the presented research was focused on the security of printable graphical codes, especially their reliable authentication on smartphones to prevent counterfeiting and piracy. The proposed defence mechanism employs a key-based multi-channel randomisation in a specific transform domain. In addition, the study considered the lack of labelled training data and the occurrence of adversarial examples designed to trick machine-learning models.

The introductory chapter of the dissertation briefly overviews anti-counterfeiting technologies and concepts, including authentication, track and trace options and physical unclonable functions, especially the printable graphical codes and their security. The main content is organised into three chapters, each presenting the background, methods, results and their discussion. The strategy for the classification robust to the adversarial attacks comprises creating an information advantage of the defender over the attacker by using the secret key and applying randomised perturbations to more channels with the following aggregation. The method was tested on the general classification of natural images. The results show high efficiency against three selected attacks, two of which are gradient-based. Further study was focused on the possibilities of semi-supervised classification. The text describes the formulation of a variational information bottleneck for two types of priors on the latent space of the classifier – the hand-crafted and learnable ones. Finally, the work discusses the authentication and clonability aspects of printable graphical codes used as copy-detection patterns. Attention is also paid to the quality and accuracy of produced machine-learning fakes influenced by different factors, including the printing equipment and size of basic elements.

Further reading:
DOI: 10.13097/archive-ouverte/unige:152982

On the Appearance of Translucent Objects: Perception and Assessment by Human Observers

Doctoral thesis – Summary

Author:
Davit Gigilashvili

Speciality field:
Computer Science and Vision Science

Supervisors:
Jon Yngve Hardeberg
Marius Pedersen
Jean-Baptiste Thomas

This thesis contributes to the knowledge of how appearance is perceived and assessed and its relationship with the corresponding material and object properties. Among the significant appearance attributes, translucency was the main focus of the research. The aim was to identify the links between the physical and the perceptual properties, essential for relevant characterisation and applicable in various fields where translucency plays an important role, from 3D printing to visual arts. The research hypotheses were defined after observation of the process of assessment material appearance in general and then experimentally tested. Besides translucency as a material property, the work considered the effect of geometric properties because they inherently contribute to the perception of translucent objects. Other experiments were focused on digital stimuli and the extent to which they can emulate real-world experience. The study included selected image features possibly related to translucency. All findings were analysed in the context of state-of-the-art knowledge and its advancement.

Defended:
24 June 2021,
Norwegian University of Science and Technology, Faculty of Information Technology and Electrical Engineering, Department of Computer Science
Gjøvik, Norway

Contact:
davit.gigilashvili@ntnu.no

Further reading:
https://hdl.handle.net/11250/2757506

After the introduction and the background on appearance, its attributes, measurement, modelling and perception, the dissertation summarises the contributions presented in ten manuscripts (appended in Part II). The next chapter discusses in depth the answers to research questions. These begin with describing observers' behaviour when assessing appearance and the factors facilitating this process. The next group includes the factors affecting translucency constancy, translucency contributing to glossiness perception, the shape of the object impacting the perceived magnitude of translucency and detection of translucency differences, with the latter also depending on the magnitude of the subsurface scattering. Further sections describe the differences in appearance assessment between physical objects and displayed images together with the significance of the direct interaction with the objects, the presence of caustics and image blur as cues for judging the material translucency, and the possibility of using the luminance histograms for prediction of apparent gloss and translucency. In addition, the obstacles to advancing translucency perception research are outlined, as well as the knowledge status and future perspectives in this area. The discussion also points out the implications for prospective studies and highlights further findings and the identified limitations.

Doctoral thesis – Summary

Author:
Liwen Zhang

Speciality field:
Polymer Science, Nanomaterials and Advanced Manufacturing

Supervisors:
Cyrille Boyer
Yun Hau Ng

Degree conferral:
17 March 2022,
The University of New South Wales, School of Chemical Engineering
Sydney, Australia

Contact:
liwen.zhang@uq.edu.au

Metalloporphyrin Based Photocatalysts for PET-RAFT Polymerization and Applications

The research within this thesis contributes to the development of reversible-deactivation radical polymerisation and its applications in 3D printing. The focus was on the reversible addition–fragmentation chain-transfer polymerisation with photoinduced electron/energy transfer. The particular aim was to enable effective polymerisation mediation under far-red light irradiation, eliminate the side effects of oxygen, and address the poor recycling stability by developing a new metalloporphyrin-based photocatalyst.

The dissertation reviews the relevant background, going from reversible-deactivation radical polymerisation in general to polymerisations mediated using homogeneous or heterogeneous photocatalysts to utilising metal–organic frameworks as (photo)catalysts. The experimental part describes the catalytic use of oxygen in the radical photopolymerisation of acrylate and acrylamide monomers mediated by zinc (II) (2,3,7,8,12,13,17,18-octaethyl-5,10,15,20-tetraphenylporphyrin) under irradion at $\lambda = 690$ nm (3 mW/cm^2), resulting in well-defined polymers with low dispersity thanks to excellent control and end-group fidelity. This is marked as an oxygen paradox because the photopolymerisation of the proposed system can be controlled in time not only by light but also by the presence of oxygen, serving as a co-catalyst alongside a tertiary aliphatic amine instead of its typical inhibitory effect. Besides detailing the methods and results, the work discusses the proposed mechanism. Next, four porphyrinic zirconium metal–organic frameworks were synthesised, characterised and successfully tested as heterogeneous photocatalysts under different wavelengths, also demonstrating oxygen tolerance and temporal control. The work discusses the effect of their size and surface area on polymerisation rates and shows the possibility of separating, recycling and using these photocatalysts for up to five independent polymerisations. The proposed systems were processed by stereolithography controlled by visible light in an open-air environment. Finally, porphyrinic metal–organic frameworks in the form of 2D nanosheets were used as multidimensional photocatalysts for functional materials. Their application in stereolithographic 3D printing yielded well-defined objects with improved mechanical properties. In addition, they exhibited effective antimicrobial photodynamic activity.

Further reading:
DOI: 10.26190/unsworks/24182

Events

Electronic Imaging 2023

San Francisco, California, USA
15–19 January 2023

After two years, when this IS&T International Symposium was held online, the 2023 edition returns to the in-person format. The plenary speakers are Anima Anandkumar, who introduces the use of Fourier neural operators for solving partial differential equations, Eric Chan and Paul M. Hubel with a lecture on 'Embedded gain maps for adaptive display of high dynamic range images' and Andrew B. Watson presenting the so-called Pyramid of Visibility, a structural description of human visual sensitivity, with its benefits for display engineering. In 2023, the symposium comprises 18 technical conferences. Their list includes a new one, High Performance Computing for Imaging. Its focus is on research topics that converge high-performance computing and imaging research. The Imaging for XR workshop takes place on the last day. Its programme features invited speakers and a panel on the visual quality of XR displays. The IS&T EI Conference Proceedings are open access.

SPIE Events

Photonics West 2023

SPIE. PHOTONICS WEST

San Francisco, California, USA
28 January – 2 February 2023

This established, large-scale event again offers thousands of presentations, several tens of which deal with printing. Their topics include, for example, a novel dry multi-material 3D printing technology for flexible hybrid electronics, sensors and energy devices, additive nanomanufacturing of electronics with high electrical and mechanical performance, digital printing of photonic devices by inkjet and aerosol-jet printing, example applications of planar- and continuous, roll-based transfer printing for scalable heterogeneous integration, generation of photonic nanojets using 3D microstructures printed by two-photon polymerisation, 3D-printed milli-fluidic passive mixers for rapid and low-cost point-of-care analysis of biofluids, and accuracy evaluation of a new 3D photogrammetric position measurement system for 6D printing.

Smart Structures / Nondestructive Evaluation 2023

SPIE. SMART STRUCTURES+ NONDESTRUCTIVE EVALUATION

Long Beach, California, USA
12–16 March 2023

The papers presenting various applications of printing are also included in the programme of this SPIE event, such as those dealing with the fabrication of different types of electrodes by inkjet printing, a stretchable resistive heater textile enhanced using printed electronic coatings, inkjet and 3D printing of structurally coloured photonic colloidal glasses, and in-situ monitoring of composite materials additive manufacturing process, to name a few.

Packaging, Labelling and Printing Events by EasyFairs

EASYFAIRS Visit the future

In the first months of 2023, two EasyFairs events – Packaging Innovations and Empack – are co-located in Birmingham, UK (15–16 February) and accompanied by the Contract Pack & Fulfilment event. A month later, on 14–16 March, Sign & Print Expo 2023 takes place in Gorinchem, The Netherlands, covering the visual communication chain from the creative design to possibilities in recycling and circularity of a product.

VISIGRAPP 2023
18th International Joint Conference on Computer Vision, Imaging and Computer Graphics Theory and Applications

Lisbon, Portugal
19–21 February 2023

This established event again offers an intensive schedule planned into up to seven tracks. The keynote lectures announced for the 2023 edition deal with the synergy between multidimensional projections and machine learning (Alexandru Telea), the data-centric computer vision (Liang Zheng), the design of haptic interfaces (Vincent Hayward), and the research towards adaptive 3D user interfaces (Ferran Argelaguet).

High Security Printing EMEA

Abu Dhabi, UAE
7–9 March 2023

This Reconnaissance event also returns to the in-person format and keeps the proven schedule with seminars on the first day followed by two conference days.

INGEDE Symposium 2023

Munich, Germany
8 March 2023

This event is held in a hybrid format and can be participated online or in person. The focal point is the lack of quality raw material for the recycling paper industry. The sessions deal with the availability and supply of paper for recycling, the impact of packaging regulations and trends, the changes in recycling flows, the projects focused on certification and circular economy, and new solutions and developments in the field of paper recycling.

ICE Europe 2023

Munich, Germany
14–16 March 2023

The 13th International Converting Exhibition showcases solutions for management, measurement, printing, coating and laminating, and other processes. It is co-located with CCE International, the 6th International Exhibition for the Corrugated and Folding Carton Industry.

FESPA Digital Printing 2023

São Paulo, Brazil
20–23 March 2023

The calendar of Fespa events also seems to stabilise after the disturbances due to the pandemic. The first exhibition in 2023 takes place in South America.

InPrint Munich Conference 2023

Munich, Germany
21–23 March 2023

The InPrint Munich technical conference focuses on industrial printing solutions for packaging and manufacturing. Hosted by Werner Zapka, it offers each day about a dozen presentations on recent developments and new trends.

innoLAE 2023
Innovations in Large-Area Electronics

Cambridge, UK
21–23 February 2023

Returning to the in-person format for its 9th edition, this event offers two short supporting courses focused on dry and wet processing technologies on the first day and then two conference days with oral and poster presentations accompanied by the exhibition. The announced keynote speakers are Juha Virtanen, focusing on technical challenges for wearable patient monitoring sensors intended for use inside hospitals, Sebastian Meier, presenting design opportunities enabled by printed organic solar cells, and Natalie Stingelin, discussing the materials for flexible electronics, especially the use of multicomponent systems prepared by blending polymeric insulators with organic semiconductors in different devices that include organic field-effect transistors, organic solar cells and organic electrochemical transistors. The technical programme is scheduled into two parallel tracks with sessions dedicated to manufacturing, high-performance materials, bioelectronics, novel devices, systems and applications, sustainability and energy efficiency.

LOPEC 2023

Munich, Germany
28 February – 2 March 2023

Traditionally, the schedule of this event focused on printed electronics comprises short courses and presentations in business, technical and scientific conference tracks, as well as the accompanying two-day exhibition. For the current edition, the topics of the plenary lectures cover electrophoretic displays, smart tyres, the utilisation of spot robots for maintenance, unconventional materials and platforms for flexible and stretchable electronic devices, inkjet-printing technologies for the manufacturing of displays, innovation drivers for sustainable digital triggers, flexible electronics for human-centric health care, and the demand for mass-production of printed batteries. The sessions are mainly dedicated to various applications of printed electronics and the relevant materials and processes, including their upscaling.

TAGA 2023 Annual Technical Conference

Oklahoma City, Oklahoma, USA
12–15 March 2023

In 2023, the programme of this conference held by the Technical Association of the Graphic Arts begins with the keynote sessions. The announced presentations include ‘Sensory experiences: bringing printed designs to life’ by Kate Stone, ‘Where is the future of printing headed?’ by Volker Jansen, and ‘Process and workflow innovations in digital textile printing’ by Kerry Maguire King. The sessions on the next two days feature papers dealing with a wide range of topics, from the book printing history to web-based colour correction for social media content, from advanced colour management solutions to innovative processes and applications of printing, and more.

Journal of Print and Media Technology Research
A PEER-REVIEWED QUARTERLY

ISSN 2414-6250 (Online)
ISSN 2223-8905 (Print)
UDC 665

Call for papers

The Journal of Print and Media Technology Research is a peer-reviewed periodical, published quarterly by iarigai, the International Association of Research Organizations for the Information, Media and Graphic Arts Industries.

JPMTR is listed in Emerging Sources Citation Index, Scopus, DOAJ – Directory of Open Access Journals, Index Copernicus International, NSD – Norwegian Register for Scientific Journals, Series and Publishers.

Authors are invited to prepare and submit complete, previously unpublished and original works, which are not under review in any other journals and/or conferences.

The journal will consider for publication papers on fundamental and applied aspects of at least, but not limited to, the following topics:

- **Printing technology and related processes**
  Conventional and special printing; Packaging; Fuel cells, batteries, sensors and other printed functionality; Printing on biomaterials; Textile and fabric printing; Printed decorations; 3D printing; Material science; Process control
- **Premedia technology and processes**
  Colour reproduction and colour management; Image and reproduction quality; Image carriers (physical and virtual); Workflow and management
- **Emerging media and future trends**
  Media industry developments; Developing media communications value systems; Online and mobile media development; Cross-media publishing
- **Social impact**
  Environmental issues and sustainability; Consumer perception and media use; Social trends and their impact on media

Submissions for the journal are accepted at any time. If meeting the general criteria and ethic standards of scientific publishing, they will be rapidly forwarded to peer-review by experts of relevant scientific competence, carefully evaluated, selected and edited. Once accepted and edited, the papers will be published as soon as possible.

There is no entry or publishing fee for authors. Authors of accepted contributions will be asked to sign a Licensing agreement (CC-BY-NC 4.0).

Authors are asked to strictly follow the guidelines for preparation of a paper (see the abbreviated version on inside back cover of the journal).

Complete guidelines can be downloaded from: <http://iarigai.com/publications/journals/guidelines-for-authors/>
Papers not complying with the guidelines will be returned to authors for revision.

Submissions and queries should be directed to: journal@iarigai.org

Journal of Print and Media Technology Research
A PEER-REVIEWED QUARTERLY

Vol. 12, 2023
Prices and subscriptions

Since 2016, the journal is published in digital form; current and archive issues are available at: <https://iarigai.com/publications/journals/>.

Since 2020, the journal is published as "open access" publication, available free of charge for iarigai members, subscribers, authors, contributors and all other interested public users.

A print version is available on-demand. Please, find below the prices charged for the printed Journal, for four issues per year as well as for a single issue

Regular prices

Four issues, print JPMTR (on-demand)	400 EUR
Single issue, print JPMTR (on-demand)	100 EUR

Subscription prices

Annual subscription, four issues, print JPMTR (on-demand)	400 EUR

Prices for iarigai members

Four issues, print JPMTR (on-demand)	400 EUR
Single issue, print JPMTR (on-demand)	100 EUR

Place your order online at: <http://www.iarigai.org/publications/subscriptions-orders/>
Or send an e-mail order to: office@iarigai.org

Guidelines for authors

Authors are encouraged to submit complete, original and previously unpublished scientific or technical research works, which are not under reviews in any other journals and/or conferences. Significantly expanded and updated versions of conference presentations may also be considered for publication. In addition, the Journal will publish reviews as well as opinions and reflections in a special section.

Submissions for the journal are accepted at any time. If meeting the general criteria and ethical standards of the scientific publication, they will be rapidly forwarded to peer-review by experts of high scientific competence, carefully evaluated, and considered for selection. Once accepted by the Editorial Board, the papers will be edited and published as soon as possible.

When preparing a manuscript for JPMTR, please strictly comply with the journal guidelines. The Editorial Board retains the right to reject without comment or explanation manuscripts that are not prepared in accordance with these guidelines and/or if the appropriate level required for scientific publishing cannot be attained.

A – General

The text should be cohesive, logically organized, and thus easy to follow by someone with common knowledge in the field. Do not include information that is not relevant to your research question(s) stated in the introduction.

Only contributions submitted in English will be considered for publication. If English is not your native language, please arrange for the text to be reviewed by a technical editor with skills in English and scientific communications. Maintain a consistent style with regard to spelling (either UK or US English, but never both), punctuation, nomenclature, symbols etc. Make sure that you are using proper English scientific terms. Literal translations are often wrong. Terms that do not have a commonly known English translation should be explicitly defined in the manuscript. Acronyms and abbreviations used must also be explicitly defined. Generally, sentences should not be very long and their structure should be relatively simple, with the subject located close to its verb. Do not overuse passive constructions.

Do not copy substantial parts of your previous publications and do not submit the same manuscript to more than one journal at a time. Clearly distinguish your original results and ideas from those of other authors and from your earlier publications – provide citations whenever relevant.

For more details on ethics in scientific publication consult Guidelines, published by the Committee on Publication Ethics (COPE):
<https://publicationethics.org/resources/guidelines>

If it is necessary to use an illustration, diagram, etc. from an earlier publication, it is the author's responsibility to ensure that permission to reproduce such an illustration, diagram, etc. is obtained from the copyright holder. If a figure is copied, adapted or redrawn, the original source must be acknowledged.

Submitting the contribution to the Journal, the author(s) confirm that it has not been published previously, that it is not under consideration for publication elsewhere and – once accepted and published – it will be disseminated and make available to the public in accordance to the Creative Commons Attribution-NonCommercial 4.0 International Public License (CC-BY-NC 4.0), in English or in any other language. The publisher retains the right to publish the paper online and in print form, and to distribute and market the Journal containing the respective paper without any limitations.

B – Structure of the manuscript

Preliminary

Title: Should be concise and unambiguous, and must reflect the contents of the article. Information given in the title does not need to be repeated in the abstract (as they are always published jointly), although some overlap is unavoidable.

List of authors: I.e. all persons who contributed substantially to study planning, experimental work, data collection or interpretation of results and wrote or critically revised the manuscript and approved its final version. Enter full names (first and last), followed by the present address, as well as the E-mail addresses. Separately enter complete details of the corresponding author – full mailing address, telephone number, and E-mail. Editors will communicate only with the corresponding author.

Abstract: Should not exceed 500 words. Briefly explain why you conducted the research (background), what question(s) you answer (objectives), how you performed the research (methods), what you found (results: major data, relationships), and your interpretation and main consequences of your findings (discussion, conclusions). The abstract must reflect the content of the article, including all keywords, as for most readers it will be the major source of information about your research. Make sure that all the information given in the abstract also appears in the main body of the article.

Keywords: Include three to five relevant scientific terms that are not mentioned in the title. Keep the keywords specific. Avoid more general and/or descriptive terms, unless your research has strong interdisciplinary significance.

Scientific content

Introduction and background: Explain why it was necessary to carry out the research and the specific research question(s) you will answer. Start from more general issues and gradually focus on your research question(s). Describe relevant earlier research in the area and how your work is related to this.

Methods: Describe in detail how the research was carried out (e.g. study area, data collection, criteria, origin of analyzed material, sample size, number of measurements, equipment, data analysis, statistical methods and software used). All factors that could have affected the results need to be considered. Make sure that you comply with the ethical standards, with respect to the environmental protection, other authors and their published works, etc.

Results: Present the new results of your research (previously published data should not be included in this section). All tables and figures must be mentioned in the main body of the article, in the order in which they appear. Make sure that the statistical analysis is appropriate. Do not fabricate or distort any data, and do not exclude any important data; similarly, do not manipulate images to make a false impression on readers.

Discussion: Answer your research questions (stated at the end of the introduction) and compare your new results with published data, as objectively as possible. Discuss their limitations and highlight your main findings. At the end of Discussion or in a separate section, emphasize your major conclusions, pointing out scientific contribution and the practical significance of your study.

Conclusions: The main conclusions emerging from the study should be briefly presented or listed in this section, with the reference to the aims of the research and/or questions mentioned in the Introduction and elaborated in the Discussion.

Note: Some papers might require different structure of the scientific content. In such cases, however, it is necessary to clearly name and mark the appropriate sections, or to consult the editors. Sections from Introduction until the end of Conclusions must be numbered. Number the section titles consecutively as 1., 2., 3., ... while subsections should be hierarchically numbered as 2.1, 2.3, 3.4 etc. Only Arabic numerals will be accepted.

Acknowledgments: Place any acknowledgements at the end of your manuscript, after conclusions and before the list of literature references.

References: The list of sources referred to in the text should be collected in alphabetical order on at the end of the paper. Make sure that you have provided sources for all important information extracted from other publications. References should be given only to documents which any reader can reasonably be expected to be able to find in the open literature or on the web, and the reference should be complete, so that it is possible for the reader to locate the source without difficulty. The number of cited works should not be excessive – do not give many similar examples.

Responsibility for the accuracy of bibliographic citations lies entirely with the authors. Please use exclusively the Harvard Referencing System. For more information consult the fifth edition of the Guide to Referencing in the Harvard Style, used with consent of Anglia Ruskin University, released by ARU University Library, available at:
<https://library.aru.ac.uk/referencing/harvard.htm>

C – Technical requirements for text processing

For technical requirement related to your submission, i.e. page layout, formatting of the text, as well of graphic objects (images, charts, tables etc.) please see detailed instructions at:
<http://iarigai.com/publications/journals/guidelines-for-authors/>

D – Submission of the paper and further procedure

Before sending your paper, check once again that it corresponds to the requirements explicated above, with special regard to the ethical issues, structure of the paper as well as formatting.

Once completed, send your paper as an attachment to:
journal@iarigai.org

If necessary, compress the file before sending it. You will be acknowledged on the receipt within 48 hours, along with the code under which your submission will be processed.

The editors will check the manuscript and inform you whether it has to be updated regarding the structure and formatting. The corrected manuscript is expected within 15 days.

Your paper will be forwarded for anonymous evaluation by two experts of international reputation in your specific field. Their comments and remarks will be in due time disclosed to the author(s), with the request for changes, explanations or corrections (if any) as demanded by the referees.

After the updated version is approved by the reviewers, the Editorial Board will decide on the publishing of the paper. However, the Board retains the right to ask for a third independent opinion, or to definitely reject the contribution.

Printing and publishing of papers, once accepted by the Editorial Board, will be carried out at the earliest possible convenience.

4-2022

Journal of Print and Media Technology Research

A PEER-REVIEWED QUARTERLY

The journal is publishing contributions in the following fields of research

- Printing technology and related processes
- Premedia technology and processes
- Emerging media and future trends
- Social impacts

For details see the Mission statement inside

JPMTR is listed in

- Emerging Sources Citation Index
- Scopus
- DOAJ – Directory of Open Access Journals
- Index Copernicus International
- NSD – Norwegian Register for Scientific Journals, Series and Publishers

Submissions and inquiries

journal@iarigai.org

Subscriptions

office@iarigai.org

More information at

www.iarigai.org/publications/journal

Publisher

The International Association of Research Organizations
for the Information, Media and Graphic Arts Industries
Magdalenenstrasse 2
D-64288 Darmstadt
Germany